ELEVATED TEMPERATURE DEFORMATION MECHANISMS IN RAPIDLY SOLIDIFIED ALUMINIUM ALLOYS

by

SANTANU BANERJEE

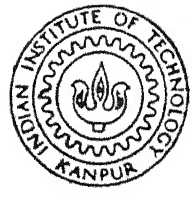

DEPARTMENT OF METALLURGICAL ENGINEERING

INDIAN INSTITUTE OF TECHNOLOGY KANPUR

MAY, 1993

ELEVATED TEMPERATURE DEFORMATION MECHANISMS IN RAPIDLY SOLIDIFIED ALUMINIUM ALLOYS

A Thesis Submitted
in Partial Fulfilment of the Requirements
for the Degree of
MASTER OF TECHNOLOGY

by

SANTANU BANERJEE

to the

DEPARTMENT OF METALLURGICAL ENGINEERING
INDIAN INSTITUTE OF TECHNOLOGY KANPUR

MAY, 1993

DEDICATED
TO

MY PARENTS
AND
FRIENDS

CERTIFICATE

this is to certify that the work "Elevated Temperature Deformation Mechanisms in Rapidly Solidified Aluminium Alloys" has been carried out by Mr. Santanu Banerjee under my supervision and that it has not been submitted elsewhere for a degree.

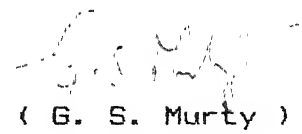

(G. S. Murty)
professor

Department of Metallurgical Engineering
Indian Institute of Technology
Kanpur

April , 1993

ACKNOWLEDGEMENT

I am extremely grateful to Dr. G. S. Murty for his invaluable guidance and enlightening discussions at various stages in this work. His continuous encouragement and suggestions throughout this study provided a pleasant academic environment.

Sincere thanks are due to Mr. B. K. Jain for his cooperation and technical help during the mechanical testing.

There is an adage at IIT Kanpur that the preparation of an M.Tech thesis is hardly an individual work. I cannot help saying that I could have never completed this thesis *on time* had my friends not rendered me all kinds of help and assistance voluntarily. I take this opportunity to thank Chhotu for providing me the graphics software and Govind for his help in getting the printouts. I am deeply indebted to Gourda, Tapasda,Niloyda and Pavitra who spent sleepless nights for typing this thesis.

SANTANU BANERJEE

CONTENTS

LIST OF TABLES

LIST OF FIGURES

ABSTRACT

The rapid solidification P/M route of processing Al alloys results in an ultra fine microstructure with intermetallic dispersoids. While some of these alloys exhibit high strain rate sensitivity in their high temperature deformation, lower rate sensitivity results in others. The flow mechanisms need to be identified in such alloys. Towards this purpose, the experimental constitutive equations have been assessed in four different alloys and compared with those of various mechanisms in this investigation. The requisite stress-strain rate data were generated by the differential strain rate test in the case of two alloys (Mn modified and Mo modified Al-Zn-Mg-Cu) and obtained from the literature for others (Al-4%Ti and Al-Fe-V-Si).

Out of the four alloys analyzed, Mn modified Al-Zn-Mg-Cu and Al-4%Ti showed high strain rate sensitivity (upto ≈ 0.45), while the other two alloys are of lower rate sensitivity (upto ≈ 0.2). The stress-strain rate relation of the former group was analyzed in terms of a constant threshold stress for a given temperature and grain size. The analysis is refined by incorporating the strain rate dependence of threshold stress, which fits better with the experimental data over the whole temperature and grain size range. The characteristic rate sensitivity (m) and the grain size exponent (p) for the threshold process are 0.1 and -3 respectively. The grain size exponent (p) and activation energy (Q) for the superplastic flow are 3 and 70-90 kJ/mole respectively.

The data of the lower m alloys (Al-Zn-Mg-Cu-Mo and Al-Fe-V-Si) were analyzed in terms of alternate mechanisms of superplasticity (m=0.5) and dislocation creep (m=0.2). The rate sensitivity values of the threshold process for superplastic flow are 0.05 (Al-Zn-Mg-Cu-Mo) and 0.11 (Al-Fe-V-Si). The grain size exponent (p) for the threshold process and the higher rate sensitivity mechanism (m=0.5) is observed to be negative in both the alloys. Such an observation is not consistent with those of superplastic flow mechanism in this regard.

CHAPTER I
INTRODUCTION

The continued rapid growth of the aerospace industry has provided the impetus for development of a new generation of aluminiam alloys. Traditionally Al alloys have been used in aircraft structures because of their high strength/weight ratio. However, in recent years, the ever increasing cost of raw materials, energy and manpower have challenged the research community to develop more cost effective materials. Moreover, the existing aerospace structural materials have been pushed to their operating limits with regard to stress, temperature and environment .

Al being basically a soft material, to achieve high level of strength at ambient and elevated temperature, it is necessary to have a high volume fraction of thermodynamically stable second phase uniformly distributed in the matrix on a fine scale. In such dispersion strengthened materials, high temperature strength is attained by the act of restricting and inhibiting the dislocation movements by the fine dispersoids. But the high level of solute required to achieve the high volume fraction of fine dispersoids makes it impossible to produce these alloys by conventional I/M practice which spells considerable segregation of alloying elements and associated course intermetallics owing to low solidification rate and low solubility. The rapid solidification technology followed by powder metallurgy (RST - P/M route) is the only alternative technique to overcome the above disadvantages of I/M for the production of such superior dispersion strengthened alloys usable in modern aerospace industries .

RST can produce very fine alloy powders with minimum micro segregation. Very high cooling rate (in the range 10^2 °C/sec to 10^5 °C/sec) achievable in RST expand the solubility of alloying elements well beyond the equilibrium levels and hence tremendous alloying flexibility is possible. Heavy transition elements like Fe, Mo, Cr etc. which have extremely low

solubility in Al can be introduced by taking advantage of this extended solute solubility in RST. The fine powders produced by RST are then compacted by P/M technique which offers finer and more homogeneous microstructure with reduced porosity and higher density and thus much better mechanical properties than those produced by conventional I/M route. Besides, cost advantage may be possible due to high materials utilization factor inherent in P/M processing .

This type of RST-PM route processed dispersion strengthened Al alloys have high strength and low ductility even at high temperature. Hence forming of such alloys is a problem due to inadequate ductility. But very fine submicron size grains stabilized by fine insoluble second phase dispersoids seem to suggest that superplastic properties might be found in them since the basic requirement of superplasticity is very fine stabilized grains resistant to high temperature growth and high forming temperature . The advantage of superplasticity is the very low flow stress required for high temperature forming and exceptionally large uniform ductility obtainable, without any adverse effect on the mechanical properties at low service temperatures. So if superplasticity is possible in these materials, then they can be formed readily.

This investigation is concerned with an assessment of elevated temperature deformation mechanisms in rapidly solidified Al alloys with fine grain size and intermetallic dispersions. Two RST-PM route processed 7075 series modified Al-Zn-Mg-Cu alloys have been studied. One is modified by the addition of Mn and another by Mo. Their stress - strain rate behaviour at high temperatures and the effect of various parameters such as temperature and grain size have been explored. Moreover, the stress - strain rate data of two other similar alloys (Al-4%Ti and Al-Fe-V-Si) from the literature have been analyzed from the viewpoint of providing further insight into the operative flow mechanisms at elevated temperatures. Needless to say that an understanding of the dependence of the flow stress on strain rate, temperature and grain size is of significance in optimizing the processing variables and in evaluating their performance in elevated temperature applications.

The layout of the thesis is as follows :

Chapter I presents a brief general introduction to this field of study and elucidates the need of pursuing such an investigation.

Chapter II mentions the recent trends in alloy designing and processing of Al alloys with special reference to the promising RST-PM route. It then sums up the progress hitherto made in understanding the mechanistic principles of elevated temperature deformation in the domains of superplasticity and dislocation creep of dispersion strengthened alloys.

Chapter III critically probes the role and scope of independent and interdependent interaction of flow mechanisms in elevated temperature deformation and illustrates their effect on the stress - strain rate behaviour of the material.

Chapter IV describes the experimental procedures adopted and the results of the experiments.

Chapter V discusses the significance of the experimental results. It further analyses and interprets the data from mechanistic viewpoint by evaluating the appropriate constitutive equations through curve fitting.

Chapter VI summerizes this work along with inferences based on the analysis done in the previous chapter.

CHAPTER II
LITERATURE SURVEY

2.1 MODERN TRENDS IN PROCESSING OF ALUMINIUM ALLOYS

2.1.1 New Class Of Aluminium Alloys

Aluminium alloys have been used in aircraft structures for a long time because of their high strength/weight ratio. In recent years, research and development in this area has been significantly accelerated by the emerging technology of powder metallurgy (P/M) processing which has distinct technical advantages over conventional ingot metallurgy (I/M) practice. P/M processed materials exhibit finer and more homogeneous microstructures than those obtained via I/M route and flexibility of alloying is enhanced. At full density mechanical property levels can exceed those of I/M materials. P/M alloy development has been extensive in three main categories of alloys :

(1) Moderately high temperature strength and corrosion resistant alloys

(2) Low density high modulus alloys

(3) Improved high temperature alloys

An example of the first category is the commercialization of X7091 alloy developed by Aluminium Company of America (ALCOA). This is based on the Al-Zn-Mg-Cu system but with Co addition. The Co forms fine dispersoids of the type Co_2Al_9 serving to refine the grain size. This alloy has better combination of strength, toughness and corrosion resistance than conventional X7000 series I/M alloys.

Alloying with Li can reduce density (ρ) by up to 15% with the added benefit of increased modulus (E) by up to 10% (a combined increase in E/ρ by up to 30%). These improvements over conventional Al alloys can result in considerable structural weight saving in aircraft industry. However, until recently, alloys based on the Al-Li system have received limited acceptance commercially due to problems related to melting, casting and

shortcomings in mechanical properties. In particular, ductility and fracture toughness values are low. P/M offers the possibility of eliminating some of the problems associated with these alloys. For example, the rapid rates of solidification associated with the atomization process can greatly reduce segregation and refine the grain size, thereby avoiding strain localization and hence improving ductility. It appears that compositions based on Al-Li-Cu-Mg-Zn will prove most effective for commercial applications.

Retention of high strength at elevated temperatures requires an alloy with a thermodynamically stable second phase dispersed in the matrix. Furthermore, to achieve the high level of strength at ambient and elevated temperatures, it is necessary to have a high volume fraction of the second phase uniformly distributed in the matrix on a fine scale. Of the available methods of strengthening the Al alloys like solid solution hardening, precipitation hardening and dispersion hardening, dispersion hardening is the most promising one. The high level of solute required to achieve the high volume fraction of fine dispersoids makes it impossible to produce these alloys by conventional I/M route. Low solidification rate of I/M results in substantial segregation of alloying elements and associated course intermetallics. P/M technique can be successfully used to produce these superior dispersion strengthened alloys. The rapid solidification process along with P/M route circumvents the above disadvantages of I/M .

P/M processed alloys based on the addition of transition metals like Fe, Ni, Co, Mo and rare earth elements like Ce to aluminium are prime contenders for application at elevated temperature. These elements are characterized by a moderate to high liquid solubility, low solid solubility and very low diffusivity in Al. The intermetallics (aluminides) based on these elements are therefore very stable thermodynamically and resistant to coarsening. There is considerable research activity in this area to develop P/M alloys for service in the range 230-340°C. A number of alloys are evaluated and the most promising compositions are based on the Al-Fe-Ce, Al-Fe-Co, Al-Fe-Mo and Al-Fe-Ni systems. The conventional 2XXX series alloys show a 24-40%

strength drop at 232°C and a 70-80% drop at 340°C whereas these new generation alloys exhibit up to 37% drop at 232°C and 43% at 340°C .

2.1.2 RAPID SOLIDIFICATION TECHNOLOGY (RST)

To get very fine alloy powders from RST, different elements are taken in solid form in requisite ratio, melted and the liquid is poured down. A jet of some inert gas (Argon, Helium etc.) disintegrates and atomizes the liquid alloy stream into tiny droplets which cool down very fast to form powders.

Unique structures, morphologies and metastable phases are associated with RST produced alloys which have several advantages over conventional ingot solidification. Foremost among these is the refinement of the microstructure with an accompanying improvement in mechanical properties. Time for coarsening during solidification is reduced resulting in finer secondary dendrite arm spacing and reduced microsegregation. Owing to the high cooling rates the solubility of the alloying elements is extended beyond the equilibrium levels and metastable phases are even possible. Utilizing this advantage, the heavy transition elements like Fe, Cr etc. which have extremely low solubility in Al can be introduced.

The extent of fineness of the microstructure is controlled by the cooling rate which is in the range of 10^2 °C/sec to 10^5 °C/sec depending on the atomization technique, average particle size and size distribution. During atomization, rapid heat loss to the surroundings causes a liquid metal droplet to undercool. A quantity of solid phase nucleates and grows rapidly into the undercooled melt. The average temperature of the droplet continues to decline for a short period until the rate of heat production exceeds the rate of heat removal and the solidification proceeds adiabatically. Grant [1] has correlated cooling rate with secondary dendritic arm spacing (DAS) and powder size. Mehrabian and Levi [2,3] studied heat flow during rapid solidification using Newtonian and non-Newtonian models and developed relationship

between atomization parameters, growth kinetics, interface velocity and undercooling.

2.1.3 CONSOLIDATION OF RST POWDERS

The particulates produced by the RST techniques ultimately have to be consolidated into useful forms. The steps involved in Al alloy particulate consolidation are

(a) Cold compaction
(b) Vacuum preheating and degassing
(c) Vacuum hot pressing
(d) Hot working and
(e) Heat treatment , if required

The atomized powders are cold compacted into billets by isostatic pressing at room temperature with pressure of approximately 414 Pa. The density of the green compacts is typically of the order of 80% of theoretical. Too high a green density can cause a too much reduction in porosity resulting in improper degassing. The green compacts are then canned in an Al container and sealed by welding leaving an evacuation tube in place. Next, the canned assembly is evacuated and heated simultaneously for degassing, which involves removal of moisture and other products of decomposition from the surface of the powder particles. If insufficiently degassed, when the material is exposed to high temperature either during the heat treatment or during application, the moisture and hydrogen released can cause blistering in the product. The pores reduce the ductility and the toughness of the material as they are sources of fracture initiation. On the other hand, too high a degassing temperature might coarsen the second phase causing drop in alloy strength. Hence, there is a need to optimize the degassing temperature for the alloy system under consideration. After a degassing cycle of 6-8 hours, the cans are sealed in vacuum.

The canned powder is then uniaxially hot pressed at approximately 714 MPa giving a full density product. In the case of Al alloys, it is necessary to impart considerable deformation (particle movement) in order to break down the tenacious oxide film on the surface of the powder particles and to establish good

bonding. The final step involves heat treatment where necessary. The dispersion strengthened high temperature Al alloys do not require any heat treatment.

An alternative processing route eliminates the vacuum hot pressing step where after degassing the cans are directly hot extruded with a sufficient reduction ratio to achieve full density.

2.1.4 MECHANICAL ALLOYING

A more recent development in the processing of Al alloys is mechanical alloying, where the elevated temperature strength retention properties are derived from the fine dispersoid of aluminides, carbides and oxides distributed in the microstructure. It is an excellent way of producing reasonably homogeneous powders from mixed elemental powders. Elemental powders are ball milled in a sealed attritor in the presence of a carbon bearing compound such as alcohol or stearic acid. The steel balls impelled by rotating paddles repeatedly impact the powders causing their cold welding. Cold welding is controlled by the amount and type of the carbon bearing agent used in the process. The oxide layer inherently present in the powder surface is fractured on impact. Oxides are dispersed into the material along with the carbon bearing compound. New oxide regenerates on the fresh surface and the process is repeated. The result is heavily cold worked powders of a homogeneous composition and uniform dispersion of submicron oxides and carbides.

At elevated temperature, materials show two types of deformation modes: superplasticity and dislocation creep. The superplastic deformation mechanism has a high value of strain rate sensitivity index, m, ($0.3 \leq m \leq 1.0$) whereas dislocation creep is weakly strain rate sensitive ($m \leq 0.25$). These two deformation mechanisms are discussed in sections 2.2 and 2.3.

2.2 SUPERPLASTICITY

Superplasticity is the property of a material to undergo large uniform plastic deformation at low stresses prior to failure. Elongation to failure in excess to 200% is usually indicative of superplasticity, although more than 6000% deformation has been reported in a few cases. Such a large plasticity is obtained owing to the suppression of localized plastic instability, i.e., necking. The three requisite conditions for superplastic deformation are very fine grains resistant against high temperature growth (typically <10 μm), high temperature (typically above 0.5 T_m) and low strain rate (in general, considerably lower than those for conventional hot working processes). A sound theoretical understanding of the dependence of the strain rate on temperature, grain size and flow stress is of significant use in optimization of these variables, so that the material can be deformed at the highest possible forming rates and still benefit from the exceptionally large, neck-free ductility associated with superplasticity.

2.2.1 MECHANICAL AND MICROSTRUCTURAL BEHAVIOUR OF SUPERPLASTIC MATERIALS

The typical stress-strain rate curve for superplastic deformation is sigmoidal in nature having three regions of different slopes as shown in Fig. 1.1. Though several plausible hypothesis have been proposed for the origin of superplasticity in fine grain materials, none has been found capable of accurately describing both the mechanical and microstructural features of superplastic deformation. Considering each of the regions, the strain rate of deformation at high temperature can be expressed in terms of stress and other variables by Dorn equation (which was originally developed for power law creep)

$$\dot{\varepsilon} = AD \left(\frac{G\,b}{k\,T}\right) \left(\frac{b}{d}\right)^{p} \left(\frac{\sigma}{G}\right)^{n} \qquad (2.1)$$

Where $\dot{\varepsilon}$ = Strain rate

σ = Flow stress

A = Dimensionless constant

D = Diffusivity

G = Shear modulus

b = Burger's vector

k = Boltzmann's constant

T = Temperature

d = Grain size

p = Grain size exponent

n = Stress exponent

Alternatively, equation (2.1) can be rewritten as

$$\dot{\varepsilon} = A' \frac{\sigma^{n}}{d^{p}} \exp(-Q/RT) \qquad (2.2)$$

Where A' = Constant

Q = Activation energy of the flow process

p, n and Q are characteristic of a certain micromechanism of deformation which can be found out by comparing the experimentally evaluated values of p, n and Q with those already established for various basic processes.

In a double logarithmic plot of stress vs. strain rate, the slope is the strain rate sensitivity index m

$$m = \frac{d \log \sigma}{d \log \dot{\varepsilon}} = \frac{1}{n} \qquad (2.3)$$

The characteristic values of m, n, p and Q for each region, as commonly found in the experiments, are shown here :

REGION I	REGION II	REGION III
	superplasticity	power law creep
m : 0.2	m : 0.5	m : 0.2
n : 5	n : 2	n : 5
p : 2 - 3	p : 2- 3	p : 0 - 1
Q : $Q_v - Q_{gb}$	Q : Q_{gb}	Q : Q_v

The characteristics of the three regions are discussed below.

2.2.1.1 REGION III

By far it has been identified that this region corresponds to power law creep, i.e., conventional recovery controlled dislocation creep. The strain rate sensitivity is around 0.2. Activation energy for flow is that for lattice diffusion. Strain is accumulated by the glide of dislocations inside the grains. Dislocation glide is resisted by various obstacles such as dispersoids, other immobile dislocations etc. Glide is therefore dependent on the rate at which the barriers are bypassed. At high temperatures, the thermal energy enables the dislocations to climb over the obstacles. The strain rate is therefore controlled by the rate at which the dislocations are available for glide. As a result of continued slip on a limited number of active slip systems, grains become elongated parallel to the tensile axis. Since the distance over which dislocations move between pinning points is small compared to the grain size. Lower the temperature and larger the grain size, more dominant is region III and it interferes with region II at lower $\dot{\varepsilon}$.

2.2.1.2 REGION II

At intermediate strain rate, the flow process is less well understood although there is agreement on the microstructural features associated with it. Strain is accumulated by the motion of individual or cluster of grains relative to each other by sliding and rolling. Grains are observed to change the neighbors and emerge at the free surface from the interior and vice versa. During the deformation the

grains remain equiaxed. Texture become less intense. Grain boundary sliding plays a significant role in this region. If grain boundary sliding were to occur in a completely rigid system of grains, then voids would develop in the microstructure. The holes or cavities would expand or contract as grains, moving in three dimensions, approached or receded from them. However many superplastic materials do not cavitate. Grain boundary sliding is therefore accommodated. Actually in course of rotation or sliding, a stress concentration develops. That stress concentration is relaxed accommodation mechanisms, such as diffusion and dislocation activity which result in physical rearrangement of matter. Microstructural studies have found only limited evidence of dislocation activity within the grains. In contrast, normal large-grain non-superplastic materials deformed under the same conditions of strain rate and temperature often show well defined microstructure. The fine grain size of superplastic materials coupled with low flow stress ensure that the equilibrium subgrain size is grater than the grain size [4] as subgrain size is proportional to applied stress. It might then be argued that the material is deforming by the conventional dislocation creep and that the dislocations are not observed as most of them are absorbed in the grain boundaries. However, the absence of dislocations within the grains may be also cited as evidence in support of superplastic flow accommodated solely by diffusion.

2.2.1.3 REGION I

This is the least understood region of all the three. There has been debate among the researchers about its mechanism. Until now, no single deformation mechanism has been identified which adequately corroborates all the mechanical and microstructural characteristics of this region. No dislocation activity is generally seen within the grains when deformed in this low strain rate range, which seems to suggest that diffusion flow controls the deformation. It is also supported by the fact that

at sufficiently low stresses, diffusion creep dominates over the dislocation creep since the stress is inadequate to initiate dislocation activity. The value of m in this range is not unique. Zn-22% Al surprisingly shows a very high m value approaching unity[35] in this region. But other than this, all the other alloys show a low m value of around 0.2 in the region I. From a high value in region II, the decrease in m value at low strain rates has been explained by various researchers in terms of

(a) a separate independent mechanism

(b) sequential interaction

(c) threshold stress for deformation

Each of these concepts will be critically discussed in chapter III.

2.2.2 FLOW MECHANISM IN REGION II

Grain boundary sliding has been identified to be playing a major role in region II, but it has to be accommodated by physical rearrangement of matter. The different accommodation mechanisms suggested in the literature for the steady state flow of this high m are as follows

(1) Diffusional flow

(2) Dislocation mechanism

2.2.2.1 DIFFUSIONAL FLOW

Nabarro and Herring developed a diffusional creep model considering stress directed vacancy migration through the lattice. But Coble suggested that at relatively lower homologous temperature and smaller grain sizes, the grain boundary diffusion dominates the lattice diffusion resulting in a mass transport through the grain boundaries. Generally both the Nabarro-Herring and Coble mechanisms, operating in parallel, contribute to diffusional creep. The effective creep rate is then described as

$$\dot{\varepsilon} = \frac{B\,\sigma\,\Omega}{d^2\,k\,T}\,D_{eff} \qquad (2.4)$$

Where B=14

and $$D_{eff} = D_l \left(\frac{\pi}{d} \frac{D_{gb}\,\delta_{gb}}{D_l} \right) \qquad (2.5)$$

with

D_{eff} = Effective diffusivity
D_l = Lattice diffusivity
D_{gb} = Grain boundary diffusivity
Ω = Atomic volume
δ_{gb} = Effective boundary width

It follows that greater the ratio of $\frac{D_{gb}}{D_l}$ and lower the value of d, more will be the extent of grain boundary diffusion.

But it is quite evident that pure diffusional flow (Nobarro-Herring and Coble mechanisms) is inadequate in giving rise to large plastic strain in a polycrystalline aggregate keeping the grain shape intact. Ashby and Verrall [5] developed a theory based on grain boundary sliding along with diffusional accommodation through the lattice as well as grain boundaries. A group of four regular hexagonal grains in a two dimensional model is considered. These grains through a neighbor switching event move from the initial state to the final one with an identical grain shape. In this process, the grains translate past each other by grain boundary sliding and accommodation strains. A constitutive equation based on this mechanism is derived which is similar to classical Nabarro-Herring-Coble equation but gives rise to a threshold stress for deformation (due to transient increase in grain boundary area) and a strain rate that is an order of magnitude faster.

2.2.2.2 DISLOCATION MECHANISM

According to Ball and Hutchison [6], a group of grain slides as a unit along same common direction. A grain, which does not have its boundary along the common sliding direction and is across the sliding path of the group, acts as an obstacle to the sliding process. This leads to stress concentration resulting in emission of dislocations from triple points of the blocking grain and the dislocations move to the opposite boundary until the back stress prevents the further activation of the source and sliding stops. The leading dislocation in the pile up then climbs into and along the grain boundary. This results in further sliding at a rate governed by the kinetics of dislocation climb along grain boundary to annihilation sites. Mukherjee [7,8] also developed a similar theory but the dislocations are assumed to emanate from ledge in the sliding boundary and the specific requirement of the movement of groups of grains is not necessary.

2.3 MECHANISM OF CREEP IN DISPERSION STRENGTHENED ALLOYS

In dispersion strengthened materials, strength from the particles arises due to the interaction of dislocations with the dispersoids. Plastic deformation by slip involves substantial movement of dislocations on the slip planes which is obstructed by the dispersoids and cause strengthening. Orowan [9] first developed a model for the yielding of dispersion strengthened materials. The dislocations bypass the incoherent impenetrable particles by bowing leaving behind loops around the particles. The dislocations then continue to glide till they encounter other particles. The critical shear stress required for a dislocation to loop around a particle was found to depend solely on the properties of the matrix and the spacing of the particles

$$\tau = \frac{G\,b}{l} \qquad (2.6)$$

Where

τ = critical shear stress

G = shear modulus of matrix

b = burgers vector of dislocations

l = interparticle spacing

Orowan proposed that the sum of the yield stress of matrix phase and the stress to bow dislocations between the particles is the yield stress of the dispersion strengthened alloys

$$\sigma_{ys} = \sigma_{matrix} + \frac{G\,b}{l} \qquad (2.7)$$

Orowan's original relationship has been modified by Martin [10] to account for the dislocation dipole effect, dislocation line tension and the mean planar spacing of particles of finite diameters. This more precise version is given below

$$\tau = \frac{0.81\ G\ b}{2\,\pi\,(1-\nu)^{1/2}} \quad \frac{\ln\,(2r_s/r_o)}{(h_s - 2\,r_s)} \qquad (2.8)$$

Where

$r_s = \sqrt{2/3}$ of particle radius

h_s = average center to center spacing of particle

r_o = dislocation core radius

Apart from strength due to particle strengthening at room temperature, strength also arises from grain size effect as per Hall-Petch relation. These two strengthening effects may be added at room temperature. But at higher temperature, grain size effect has the opposite contribution to the overall strength of the material since the amorphous grain boundary area becomes weaker when temperature is high. Moreover, the particle strengthening contribution also decreases as temperature is increased. As the expression of Orowan mechanism contains a term of matrix shear modulus(whose value naturally drops with increase in temperature), the temperature dependence of modulus must possibly contribute to strength loss at elevated temperatures.

But the experimental observations show that loss of strength is greater than that suggested by temperature compensated modulus. So the modulus variation can not alone account for the strength loss in dispersion strengthened alloys. Some other kind of dislocation particle interactions seem to take place at higher temperatures. In this regard, recovery mechanisms operative at high temperature are of interest. The thermal energy aids the climb of dislocations over particles providing additional freedom of motion to the dislocations. Several models have been proposed in relation to the climb of dislocations over the dispersoids at high temperature.

2.3.1 ANSELL WEERTMAN MODEL

The first quantitative model to describe the creep behavior in particle strengthened alloys was developed by Ansell and Weertman [11]. The model considers a simple behavior of dislocation loops left around the particles by the dislocations bypassing them in Orowan mechanism. The rate controlling process is the climb of dislocation loops over the second phase particles. The incoherent particle-matrix interface is supposed to be an efficient source and sink for vacancies and consequently a flux of vacancies can occur between a climbing dislocation and the interface to aid the climbing process. The creep rate is given by

$$\dot{\varepsilon} = 2\pi D_l \left(\frac{\lambda}{b}\right)^2 \left(\frac{G\,b}{k\,T}\right)\left(\frac{\sigma}{G}\right)^4 \qquad (2.9)$$

Where

D_l = lattice diffusively

λ = interparticle spacing

2.3.2 BROWN AND HAM MODEL OF LOCAL CLIMB

Brown and Ham [12] proposed that at elevated temperature, dislocations do not bypass the particles by Orowan bowing. Instead, the dislocations climb locally over the particles by increasing their length as shown in Fig. 2.2(a). The dislocation segments in between the particles bow out and the segments profiling the particles(i.e., touching the particles) climb over them. The energy required to increase the length of the dislocation, which in turn depends on the shape of the particles, determines the stress for *local climb*. For a cuboidal particle, the critical stress is given by

$$\tau = \frac{\tau_{or}}{\sqrt{2}} \qquad (2.10)$$

This model predicts a constant value modulus compensated strength, which is 70% of Orowan stress, over the whole high temperature range. But the ratio of the observed strength to Orowan strength, changes with temperature from 1.0 at 0.5 T_m to 0.5 at 0.95T_m (T_m being the melting point of the material on absolute scale). This model fails to account for the observed temperature variation the strength.

2.3.3 LAGNEBORG'S MODEL OF GENERAL CLIMB

The primary criticism leveled against the model of *local climb* is about the stability of the process. Langeborg [13] argued that the local climb involves sharp bends in the dislocation profile near the particle matrix interface. Such bends increase the line strength of the dislocation unnecessarily and is not feasible from dislocation line energy point of view. He proposed that the dislocations bypass the particles by *general climb* instead as shown in Fig 2.2(b).

For dispersion strengthened alloys, the creep rate vs. applied stress curve is very steep and stress exponent of creep rate,*n*, is unusually high(20 to 100 or sometimes even more

than 200), whereas that for pure metals and alloys is less than 10 (4 to 6 for pure metals and 6 to 9 for alloys). The activation energy is extremely high, 5 to 6 times for self diffusion of matrix atoms. But for climb controlled deformation mechanism involving diffusion of atoms, the activation energy should be given by that for self diffusion of matrix atoms. This behavior has been explained in terms of the threshold stress for deformation at high temperature. The possibility and quantification of threshold stress (σ_o)has been suggested by various workers as discussed in the previous models. Incorporation of threshold stress in the power law creep equation reduces the stress exponent to 4 and normalizes the activation energy to that for self diffusion

$$\varepsilon = AD_v \left(\frac{Gb}{kT}\right)\left(\frac{\sigma - \sigma_o}{G}\right)^n \qquad (2.11)$$

The threshold stress represents the stress below which no deformation occurs. By curve fitting, consistent sets of values for σ_o, A and n can be found which describe the creep data within a certain range of experimental conditions.

2.3.4 ARZT AND ASHBY'S MODEL FOR EVALUATION OF THRESHOLD STRESS

Arzt and Ashby [14] assumed the mechanism of local climb and that the climb does not occur over all particles indiscriminately, but only over a fraction of them depending on the stress applied. At a stress σ ($\sigma < \sigma_{or}$), the fraction of particles over which *climb is necessary* is

$$f_n = 1 - \frac{\sigma}{\sigma_{or}} \qquad (2.12)$$

At that stress, the fraction over which *climb is possible* energetically by increasing the line length of the dislocation is

$$f_p = \frac{2C}{\alpha}\frac{\sigma}{\sigma_{or}} \qquad (2.13)$$

Where $C = 0.84$ [15]

$$\alpha = \frac{d\,l}{d\,x}$$ (depends on particles shape)

The fraction f_n (climb necessary) and (climb possible) are plotted in Fig.2.3 as a function of applied stress. The point of intersection between these two gives the threshold stress for deformation. At stress below σ_o, the number of particles to be climbed are more than those possible, hence no deformation takes place. At stresses higher than σ_o , the situation is reverse.

The threshold stress is given by

$$\sigma_o = \frac{\alpha}{2C + \alpha}\sigma_{or} \qquad (2.14)$$

The values of α are dependent on particle morphology and vary from 1 to 2. σ_o accordingly varies from 0.38 to 0.56 which tallies with experimental observation. But this this theory does not account for the temperature dependence of σ_o.

2.3.5 ARZT AND WILKINSON'S THRESHOLD STRESS MODEL ON ATTRACTIVE INTERACTION BETWEEN DISLOCATIONS AND PARTICLES

On Transmission Electron Microscope weak beam study on super alloy, Arzt and Schroder [16] found that the dislocations, near many particles, were in a state of local climb, some segments of them clearly sticking to the surface of the particles. So they proposed the theory of attractive interaction between the particles and dislocations. Srolovitz [17] analyzed the effect of particle-matrix interface on dislocation behavior and postulated that the dislocation relaxes the part of its energy(line tension) when it comes in contact with the particle.

The attractive interaction between the dislocation and particle can be characterized by relaxation parameter k[18]. The smaller the value of k, greater is the relaxation of dislocation and larger is the detachment threshold stress given by

$$\tau_d = \tau_{or}\sqrt{1 - k^2} \qquad (2.15)$$

The stress required for the process of climb as a function of k

$$\tau_c = 0.4k^{3/2}\tau_{or} \qquad (2.16)$$

The variation of normalized τ_d and τ_c with relaxation parameter k is shown in Fig.2.2(b). When k < 0.94 the threshold stress is governed by detachment stress and when K > 0.94 the climb resistance dictates the stress. From the same figure it can also be noticed that for moderate relaxation, the threshold stress is 0.4 to 0.6 of Orowan stress.

As general climb is energetically more favorable and requires less threshold stress than that for local climb, it was not clear as to why local climb is assumed to occur in other models. The particular advantage of Arzt and Wilkinson's model [18] is its ability to substantiate the existence of sharp bends at the particle-matrix interface, i.e., local climb. But it cannot explain the temperature dependence of threshold stress.

2.3.6 ARZT'S NEW MODIFIED CREEP EQUATION FOR DISPERSION STRENGTHENED ALLOYS

Arzt and Rosler [19] have derived a new type of equation for all temperature ranges based on the model of attractive interaction between the dislocation and particle. The high values of stress exponent and activation energy can be explained by the model

$$\dot{\varepsilon} = \dot{\varepsilon}_o \exp(-E_d/kT) \qquad (2.17)$$

Where E_d is the activation energy for detachment process which has never been considered in calculations before. The energy required for detachment has been derived by Arzt and Rosler [19] and given by

$$E_d = G\, b^2 r \left[(1 - k)\ (1 - \frac{\sigma}{\sigma_d}) \right] \qquad (2.18)$$

The high values of E_d match with those of the activation energy obtained for dispersion strengthened alloys. Substituting for the frequency factor and activation energy in equation(2.17)

$$\frac{\dot{\varepsilon}}{D_v} = \frac{6\,\lambda\,\rho}{b} \exp \left[\frac{G\, b\ r^2 \left[(1 - k)\ (1 - \sigma/\sigma_d) \right]}{k\, T} \right] \qquad (2.19)$$

This modified model does overcome the drawbacks of previous models. The logarithmic nature of relation between strain rate and applied stress gives a high value of stress exponent and attributes the high activation energy to the energy required for the dislocation detachment. Moreover, it substantiates the temperature dependence of the stress.

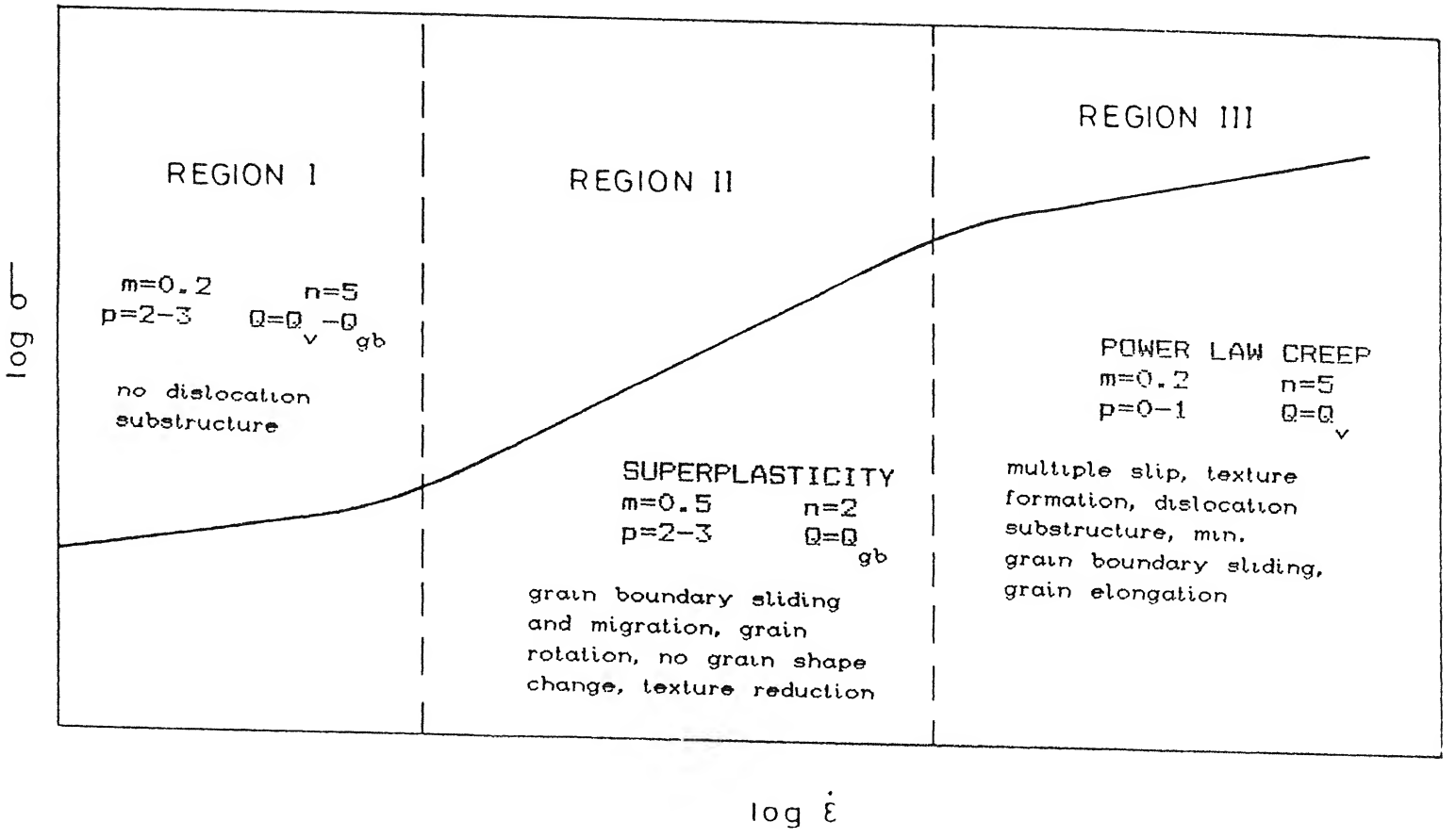

FIG. 2.1 : SCHEMATIC ILLUSTRATION OF THE STRAIN RATE DEPENDENCE OF FLOW STRESS IN SUPERPLASIC MATERIALS

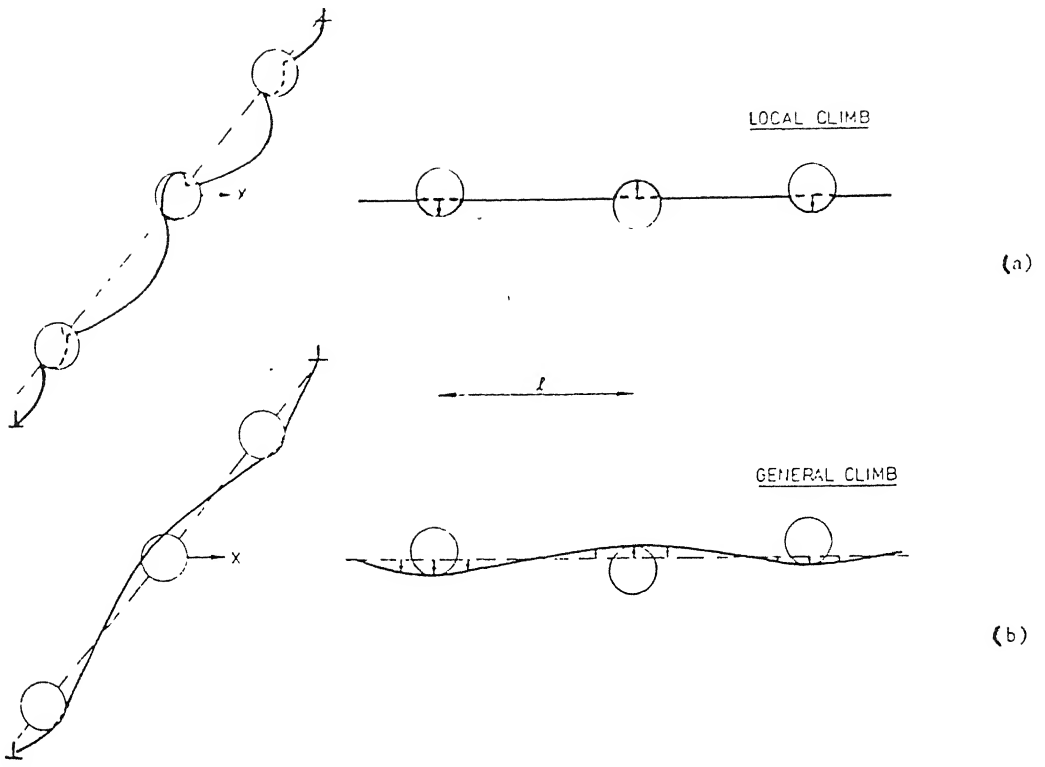

FIG. 2.2

Distinction between local climb and general climb of a dislocation bypassing particles

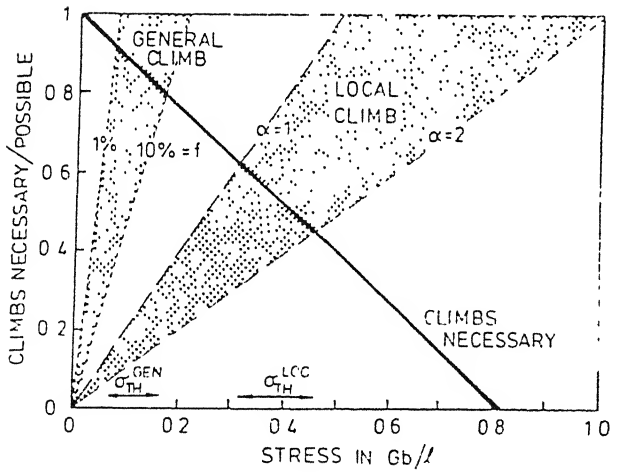

FIG. 2.3

Fraction of particles to be bypassed by climb (full line - "climbs necessary") and fraction of particles that can be bypassed (for different values of α) at a given shear stress. The intersection determines the threshold stress. f is the volume fraction of particles.

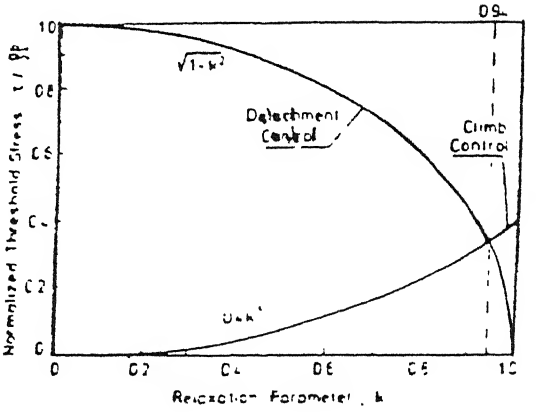

Fig. 2.4: the nomalized threshold stress for climb and for detachment vs. relaxation parameter k

CHAPTER III

CONSTITUTIVE EQUATIONS AND ANALYSIS OF MECHANISMS

3.1 INTRODUCTION

In the high temperature deformation, two or more processes may interact with each other and contribute towards the total flow rate. Suppose two stresses σ_1 and σ_2 drive two processes, 1 and 2, and cause flow rates $\dot{\varepsilon}_1$ and $\dot{\varepsilon}_2$ respectively. To illustrate the way total stress and strain rate should be related, the following constitutive relationships are assumed for the two processes

$$\text{Process 1 :} \qquad \dot{\varepsilon}_1 = k_1 \sigma_1^{n_1} \tag{3.1}$$

$$\text{Process 2 :} \qquad \dot{\varepsilon}_2 = k_2 \sigma_2^{n_2} \tag{3.2}$$

where n_1 and n_2 are stress exponents and hence characteristics of the two deformation mechanisms. k_1 and k_2 are constants for particular experimental conditions and depend on grain size, temperature and other physical variables.

Provided that no additional mechanism generates heat and otherwise dissipates energy, the total work done by the applied stress should equal the work done by the two processes. If σ be the total applied stress and $\dot{\varepsilon}$ be the total flow rate, then the rate of work done per unit volume is

$$\sigma \dot{\varepsilon} = \sigma_1 \dot{\varepsilon}_1 + \sigma_2 \dot{\varepsilon}_2 \tag{3.3}$$

If these two processes are *independent* (also called *parallel*) of each other, i.e., one can operate without the help of the other, each one experiences the full applied stress

$$\sigma = \sigma_1 = \sigma_2 \tag{3.4}$$

Substitution of equation (3.4) in (3.3) brings out that the total observed flow rate is the sum of the individual ones

$$\dot{\varepsilon} = \dot{\varepsilon}_1 + \dot{\varepsilon}_2 \qquad (3.5)$$

So equations (3.1) and (3.2) in (3.5) gives

$$\dot{\varepsilon} = k_1 \sigma^{n_1} + k_2 \sigma^{n_2} \qquad (3.6)$$

On the other hand, if the two processes are *interdependent* (also called *sequential* or *series*) ,i.e., the operation of one is the requisite condition for the continuation of the other, then preserving geometrical integrity of the specimen [20]

$$\dot{\varepsilon} = \dot{\varepsilon}_1 = \dot{\varepsilon}_2 \qquad (3.7)$$

Equations (3.3) and (3.7) are satisfied if

$$\sigma = \sigma_1 + \sigma_2 \qquad (3.8)$$

i.e., the applied stress is distributed between the two processes. Substitution of equations (3.1) and (3.2) in (3.8) gives

$$\sigma = \left(\frac{\dot{\varepsilon}}{k_1}\right)^{1/n_1} + \left(\frac{\dot{\varepsilon}}{k_2}\right)^{1/n_2} \qquad (3.9)$$

This can be simplified since $m = 1/n$

$$\sigma = K_1 \dot{\varepsilon}^{m_1} + K_2 \dot{\varepsilon}^{m_2} \qquad (3.10)$$

where K_1 and K_2 are two other related constants ; and m_1 m_2 are strain rate sensitivities of process 1 and 2.

The results of the *independent* and *interdependent*

interactions are illustrated in Fig. 3.1, where AA and BB represent the flow mechanisms. The thick continuous line is the resultant flow curve when the mechanisms are *independent* and broken line when they are *interdependent*.

The concept of independent and interdependent interactions can be considered to explain the typical sigmoidal $\sigma - \dot{\varepsilon}$ curve of superplasticity. The three regions, I, II and III, of different slopes suggest different types of interactions at each region. From a high value of m in region II, the reason for the decrease in m value at low strain rates has been a subject of debate since long and so there is a need to weigh and critically discuss the different possibilities. A clear understanding of the effect of the different physical variables like temperature, grain size etc. on the relative predominance of different regions, which in turn changes the slope of the $\sigma - \dot{\varepsilon}$ curve, is very much necessary. Moreover, the method of identification of the flow mechanisms, operative in different regions is also worth exploring.

3.2 INTERACTION OF INDEPENDENT AND INTERDEPENDENT FLOW MECHANISMS IN SUPERPLASTICITY

If the characteristic values of different parameters in equation (2.2) are known, then using these values of A, p, Q and n, the constitutive equation for a given deformation mechanism can be plotted in a double logarithmic graph of σ vs. $\dot{\varepsilon}$ which gives a straight line of slope m (= 1/n). In Fig. 3.2 AA and BB are flow mechanisms representing region III and region II constitutive equations. The two regions are separated by a center - line passing through the intersection of AA and BB. By far it can be said that these two mechanisms are independent since result of their independent interaction, represented by thick continuous line, completely tallies with region II to III transition portion of experimental $\sigma - \dot{\varepsilon}$ plot of any superplastic material. Had there been an interdependent interaction, the resultant plot would have looked like that presented by the thick dashed line.

Unlike the clarity in region II to III transition, the nature of region I mechanism and its interaction with region II mechanism have been the bone of contention for a long time. The three major possibilities, as suggested by various workers are

(1) A separate mechanism with independent interaction with region II

(2) An interdependent interaction with region II

(3) A threshold stress for deformation

3.2.1 AN INDEPENDENT MECHANISM FOR REGION I

If an independent mechanism exists in region I, then either it has an m value lower than that for region II mechanism (represented by BB in Fig. 3.3) as shown by CC, or it has an m value higher than that as shown by DD. In the former case, at region I, at any strain rate CC demands higher flow stress than BB which makes CC unfavourable to BB. The resultant of independent interaction between BB and CC is shown by the dashed line whose slope decreases continuously with the increase in strain rate. In region II it exhibits a slope charactreristic of CC rather than that of BB II which is unreasonable since it is BB that corresponds to region II. So the possibility of any independent mechanism in region I having lower slope than region II mechanism can be quite conclusively ruled out.

On the other hand, when the independent mechanism in region I (DD) has a higher slope than that for region II (BB), the resultant curve is shown by the thick solid line. This possibility justifies the experimental findings for Zn - 22% Al [21] where region I has slope approaching 1.0 which is greater than the m value of region II and it was identified to be Nabarro - Herring creep mechanism. But other than Zn - 22% Al, all the other superplastic alloys exhibit a smaller slope in region I.

3.2.2 AN INTERDEPENDENT MECHANISM FOR REGION I

In Fig. 3.4, BB and CC are region I and II mechanisms respectively. The resultant of series interaction between BB and CC is shown by thick solid line. As per equation (3.10), the constitutive equation for such an interaction occurring both in region I and II is

$$\sigma = K_1 \dot{\varepsilon}^{m_1} + K_2 \dot{\varepsilon}^{m_2} \qquad (3.11)$$

The resulting $\sigma - \dot{\varepsilon}$ plot has a low m value in region I (corresponding to CC) and a high m value in region II (corresponding to BB). This trend is similar to the experimental observations of most of the superplastic materials (other than Zn - 22% Al) as discussed in the previous section).

3.2.3 THRESHOLD STRESS FOR SUPERPLASTIC FLOW

A threshold stress, σ_o, fixed stress which may vary with the physical variables like temperature or grain size, but independent of applied stress and strain rate. The applied stress must exceed the threshold stress before the deformation can occur. Thus it can be represented by a horizontal line in $\sigma - \dot{\varepsilon}$ plot, as shown by CC in Fig. 3.5 . The resultant curve, shown as thick solid line, has a constitutive equation

$$\sigma = \sigma_o + K_2 \dot{\varepsilon}^{m} \qquad (3.12)$$

It is to be noted here that incorporation of a threshold stress for deformation tantamounts to nothing but a special case of series interaction where one process is just strain rate independent. The overall $\sigma - \dot{\varepsilon}$ plot exhibits an increasing slop with increasing strain rate and it is divided into

regions I and II on the basis of m value. The same constitutive equation (3.12) is thus valid for both the regions. The resultant curve corroborates the experimentally observed σ - $\dot{\varepsilon}$ curves of most of the superplastic alloys (other than Zn - 22% Al).

3.3 EFFECT OF THE MAGNITUDE OF THRESHOLD STRESS ON STRESS - STRAIN RATE BEHAVIOR

When a threshold stress is operative, the slope of log σ - log $\dot{\varepsilon}$ curve, m, drops asymptotically towards zero as applied stress approaches the threshold stress in low strain rate ranges. Only at high strain rate, when σ is very as compared to σ_o, m can approach the value characteristic of the superplastic region. Under this condition, region II appears as a transition stage between two low m regions, one arising from the threshold stress σ_o and the other from region III. Then the peak value of m in region II is dependent on the magnitude of σ_o on one hand and on the onset of region III on the other. The effects of the magnitude of σ_o on the shape of σ - $\dot{\varepsilon}$ curve and m - $\dot{\varepsilon}$ curve are illustrated in Fig. 3.6 and 3.7 respectively.

Murty et al. [22, 23] have worked on fine grained dispersion strengthened Al alloys and have observed that σ_o drops exponentially with rise in temperature and varies inversely with grain size. They have proposed an empirical relation of the following type to incorporate the effects of temperature and grain size on σ_o

$$\sigma_o = Ad^p \exp(Q/RT) \qquad (3.13)$$

where p is grain size exponent with a typical value of -1.

They have observed a cross-over of σ_o plots of different grain sizes at a given temperature, as shown in Fig. 3.8. The observation of a positive grain size exponent in region II and a negative one in region I can be reasoned out on the basis of equation (3.13). The σ - $\dot{\varepsilon}$ plots are shown for two grain sizes

d_1 and d_2 ($d_1 > d_2$). The dashed lines show the shape of the curves had there been no threshold stress, whereas solid lines show the shape of the curves for the existence of σ_o. For a positive value of p in region II mechanism, curve for d_2 falls below that for d_1 in region II. But according to equation (3.13), threshold stress (σ_o'') for finer grain d_2 is more than that for d_1 (σ_o'). Hence in the low strain rate range, the curve for d_2 is flatter than that for d_1 and the two curves may even cross over if σ_o'' is sufficiently large compared to σ_o'. Thus it appears that region I has a negative grain size exponent, which is the manifestation of the physical process involved.

3.4 EVALUATION OF THRESHOLD STRESS

As discussed in section 3.1.3, one of the ways of interpreting existence of region I is by incorporating a threshold stress σ_o for superplastic deformation. When there is a threshold stress, a part of the applied stress, σ, is required for surmounting the barrier for the flow mechanism and the remaining part, σ_{eff}, activates the flow process. Thus

$$\sigma_{eff} = \sigma - \sigma_o \qquad (3.14)$$

Now substituting equation (3.14) in the Dorn equation (2.1), the constitutive equation for region I and II can be rewritten as

$$\dot{\varepsilon} = AD\left[\frac{Gb}{kT}\right]\left[\frac{b}{d}\right]^p\left[\frac{\sigma - \sigma_o}{G}\right]^n \qquad (3.15)$$

$$\sigma - \sigma_o = \dot{\varepsilon}^{1/n}\, G\left[\frac{1}{AD}\left(\frac{kT}{Gb}\right)\left(\frac{d}{b}\right)^p\right]^{1/n} \qquad (3.16)$$

It can be written as

$$\sigma = \sigma_o + K \dot{\varepsilon}^m \qquad (3.17)$$

where

$$K = G \left[\frac{1}{AD} \left(\frac{kT}{Gb} \right) \left(\frac{d}{b} \right)^p \right]^m \qquad (3.18)$$

K is a constant which depends on physical variables like temperature and grain size.

For a certain deformation mechanism, there is a characteristic m value which is greater than or equal to the experimentally observed maximum m value in region II. A double linear plot of applied stress σ vs. $\dot{\varepsilon}^m$ with the characteristic value of m will show a linear trend of experimental points. The best fit straight line through the experimental points will have a slope of K and an intercept of σ_o. It must be noted that the proper choice of m is very crucial here. In fact several σ vs. $\dot{\varepsilon}$ plots can be generated for a series of m values and the one (greater than or equal to the experimentally observed maximum m value in region II) which shows a best linear fit of experimental points, can be chosen as the characteristic m for the concerned case.

3.5 VALIDITY OF THE CONSTANT THRESHOLD STRESS CONCEPT

Murty et al. [22, 23] have worked extensively on the fine grain dispersion strengthened Al alloys. They found the maximum m value to be around 0.45 for Mn modified Al-Zn-Mg-Cu and Al- 4% Ti alloys [22, 23], whereas the typical m value for region II mechanism, as reported in the literature, is 0.5. They selected this typical value of m = 0.5 as the characteristic one which is quite reasonable in all aspects. But on plotting σ vs. $\dot{\varepsilon}^{0.5}$, there were deviations from linear trends in the low strain rate range in some cases. As the choice of characteristic m value is reasonable, the validity of the constitutive equation (3.18), on the basis of which their analysis was done, may be questionable. The fact that the deviation from linearity in such

plots increases with the decrease in strain rate, seems to suggest that the threshold stress σ_o, which has been assumed constant, may be dependent on strain rate. Considering the strain rate dependence of threshold stress

$$\sigma_o = K_1 \dot{\varepsilon}^{m_1} \qquad (3.19)$$

where m_1 is characteristic of the threshold process for deformation. Substitution of equation (3.19) in equation (3.12) results in

$$\sigma = K_1 \dot{\varepsilon}^{m_1} + K_2 \dot{\varepsilon}^{m_2} \qquad (3.20)$$

This is the typical constitutive equation for interdependent interaction of two flow mechanisms. Accordingly these observations on superplastic behaviour need to be considered in the light of the possibility of the strain rate dependence of threshold stress as given in equation (3.20). The effect of the magnitude of m_1 on the shape of the $\sigma - \dot{\varepsilon}$ plot is illustrated in Fig. 3.9 along with the situation of a constant threshold stress ($m_1 = 0$) and when there is no threshold stress at all ($K_1 = 0$). It can be observed that at a given strain rate, higher the value of m_1, less is the value of the threshold stress.

3.6 POSSIBILITY OF m = 1 FOR REGION II MECHANISM

Although the typical m value characteristic of region II is generally taken as 0.5, region II mechanism may as well be imagined to have an m value as high as unity (e.g. Ashby - Verral model [5]). But attaining such a high value of m in the experimental observations may be eclipsed by high magnitude of the threshold stress on one hand and by the early onset of low m region III on the other. Then the observed maximum m value may be lower than unity because of these two interfering effects. Keeping this possibility in mind, data analysis needs to be done

as discussed in section 3.4 with m = 1.

3.7 EFFECT OF GRAIN SIZE AND TEMPERATURE ON THE ONSET OF REGION III

The common observation that the transition from region II to region III is delayed as the grain size becomes finer and temperature increases, can be rationalized as follows. As the grain size decreases, the stress - strain rate curve AA of region III (shown in Fig. 3.10) is nearly independent of grain size ($p \cong 0 - 1$ for region III) whereas region II curve BB shifts downwards as the flow stress in region II decreases strongly with the decrease in grain size ($p \cong 2 - 3$ for region II). Accordingly their point of intersection shifts to higher strain rate with the decrease in grain size.

The temperature effect on the onset of region III has been illustrated in Fig. 3.11. When the temperature increases, both the lines AA and BB shift downwards because the flow stress decreases for both the processes with the increase in temperature. Their point of intersection representing region II to III transition is shifted to higher strain rate.

3.8 POSSIBILITY OF AN INDEPENDENT FLOW MECHANISM AT LOW STRAIN RATES

If the threshold stress for the superplastic flow is very high, then there is a possibility that the independent flow mechanism of region III may manifest itself at low strain rates as shown in Fig. 3.12. Regions II and III mechanisms being mutually independent, the resultant stress - strain rate curve would be as shown by the dashed line. It is to be noted here that unless the interaction between region III and region I curves takes place within the experimentally measurable strain rate range, it will not be possible to have an independent flow mechanism of this type at low strain rate range.

3.9 DISTINCTION BETWEEN DISLOCATION CREEP AND SUPERPLASTIC FLOW MECHANISMS

An m value of 0.3 may be used to distinguish between superplasticity and conventional plasticity. In rapidly solidified Al alloys with fine grain microstructure and a high volume fraction of intermetallic dispersoids, there is the possibility of superplastic flow on one hand and recovery controlled creep on the other. So when such a material shows a low maximum m value , ambiguity arises in deciding whether it is due to normal dislocation creep or due to the suppression of high m value region II by high magnitude of threshold stress and early onset of region III. A low m value does not necessarily signify a low characteristic m value of the operative flow mechanism. Murty et al. [24] worked on RST/PM route processed Al-Fe-V-Si alloys which had submicron size grains stabilized by fine dispersoids. Although the maximum m value was found to be only around 0.2, their analysis was based on a superplastic flow (m = 0.5) with a high threshold stress. Sherby et al. [25] have questioned the validity of this analysis based on superplastic flow mechanism when the observed maximum m value is so low. Instead, they have considered an analysis based on dislocation creep mechanism with n=8.

3.10 OBJECTIVE OF PRESENT STUDY

From the above analysis of the stress - strain rate behaviour of superplastic materials, it is clear that there are various possibilities in the identification and mode of interaction of different deformation mechanisms particularly in region I. Previous works in the field of fine grained dispersion strengthened alloys have interpreted the region I in terms of a threshold stress for superplastic deformation. In view of the deviations in the experimental data from predictions basd on for

this type of interpretation in some cases, there is a need to critically assess the operative mechanisms. Furthermore in some of the alloys with fine grains and dispersoid, it is not clear whether the operative mechanisms at elevated temperatures is that of superplasticity or dislocation creep with a threshold stress. The present study is aimed at exploring the type of interaction between possible flow processes and nature of constitutive equations for regions I and II of superplastic materials and distinguishing the operative mechanisms between superplasticity and dislocation creep in materials exhibiting lower rate sensitivity.

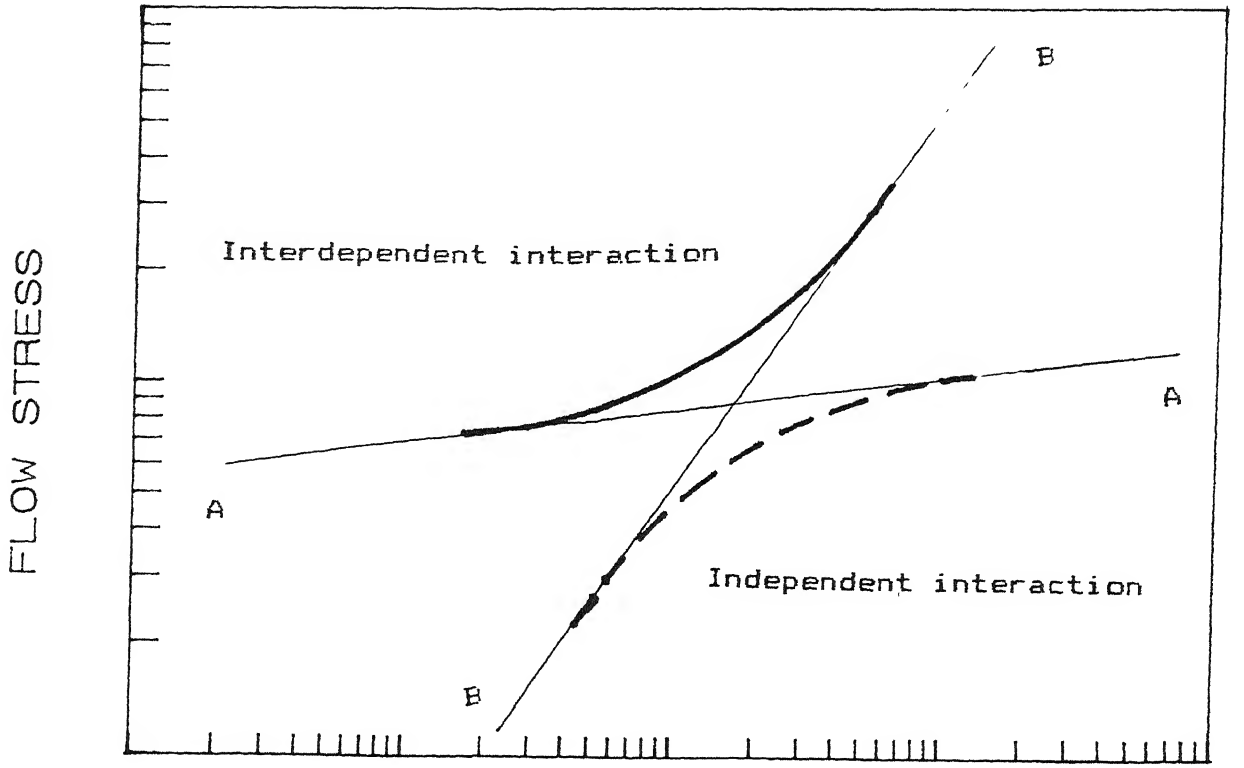

Fig. 3.1: Result of independent and interdependent interaction between flow mechanisms

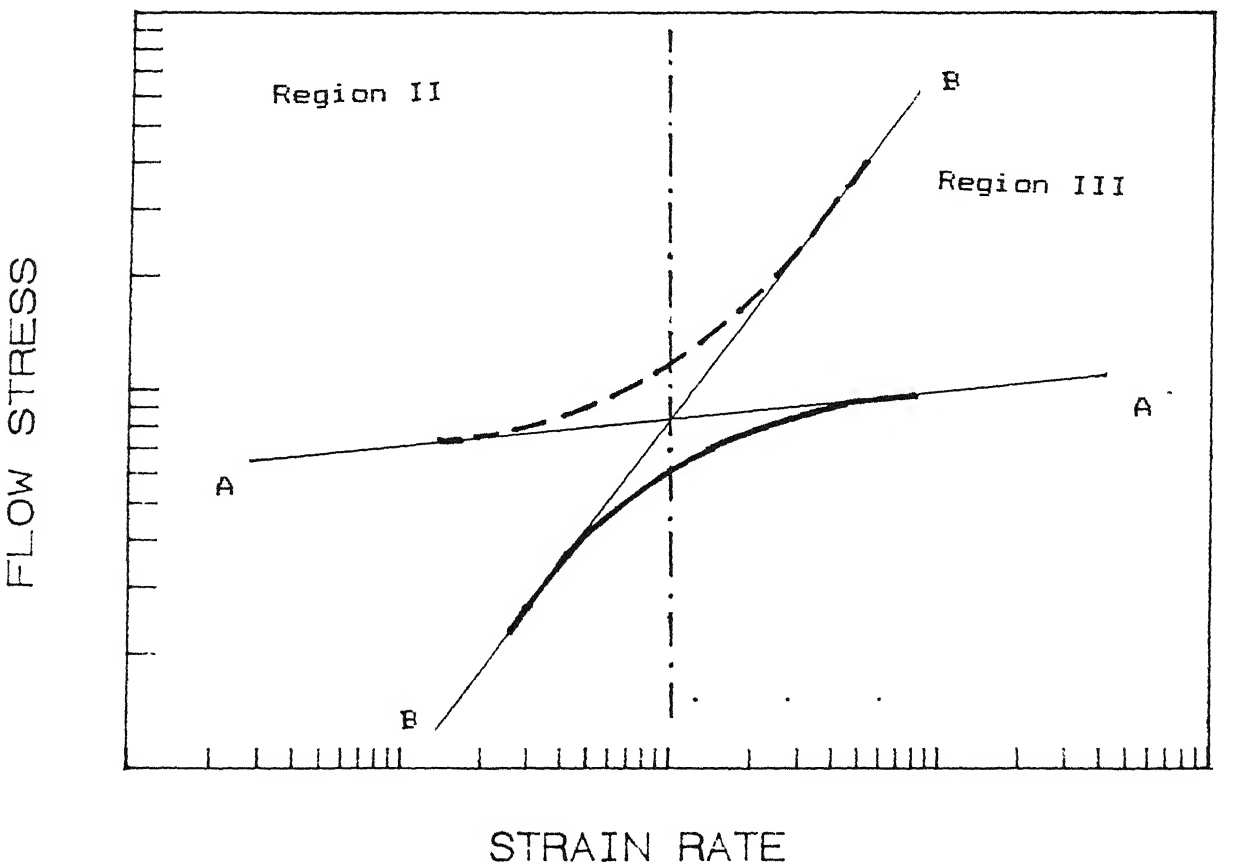

Fig. 3.2: Independent and interdependent interactions of region II and III flow mechanisms in superplasticity

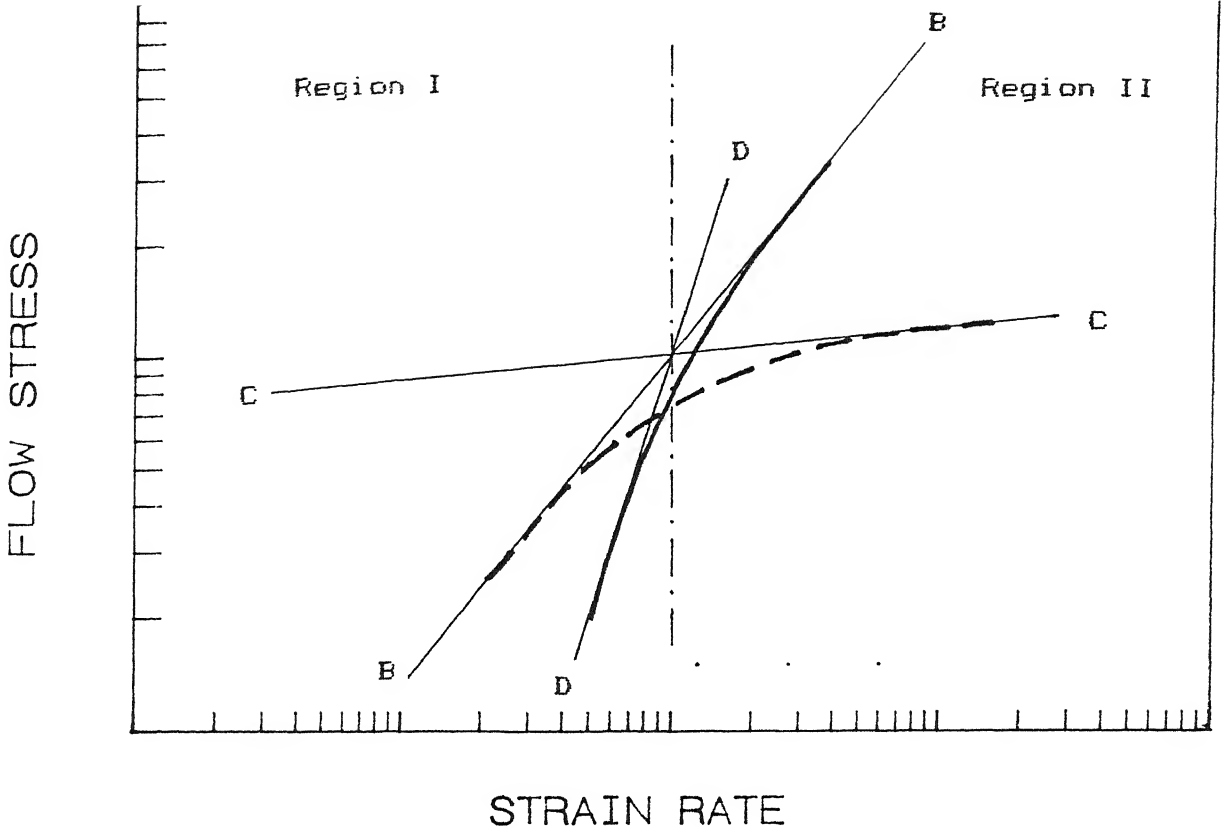

Fig. 3.3: Independent interaction of region I and II mechanisms

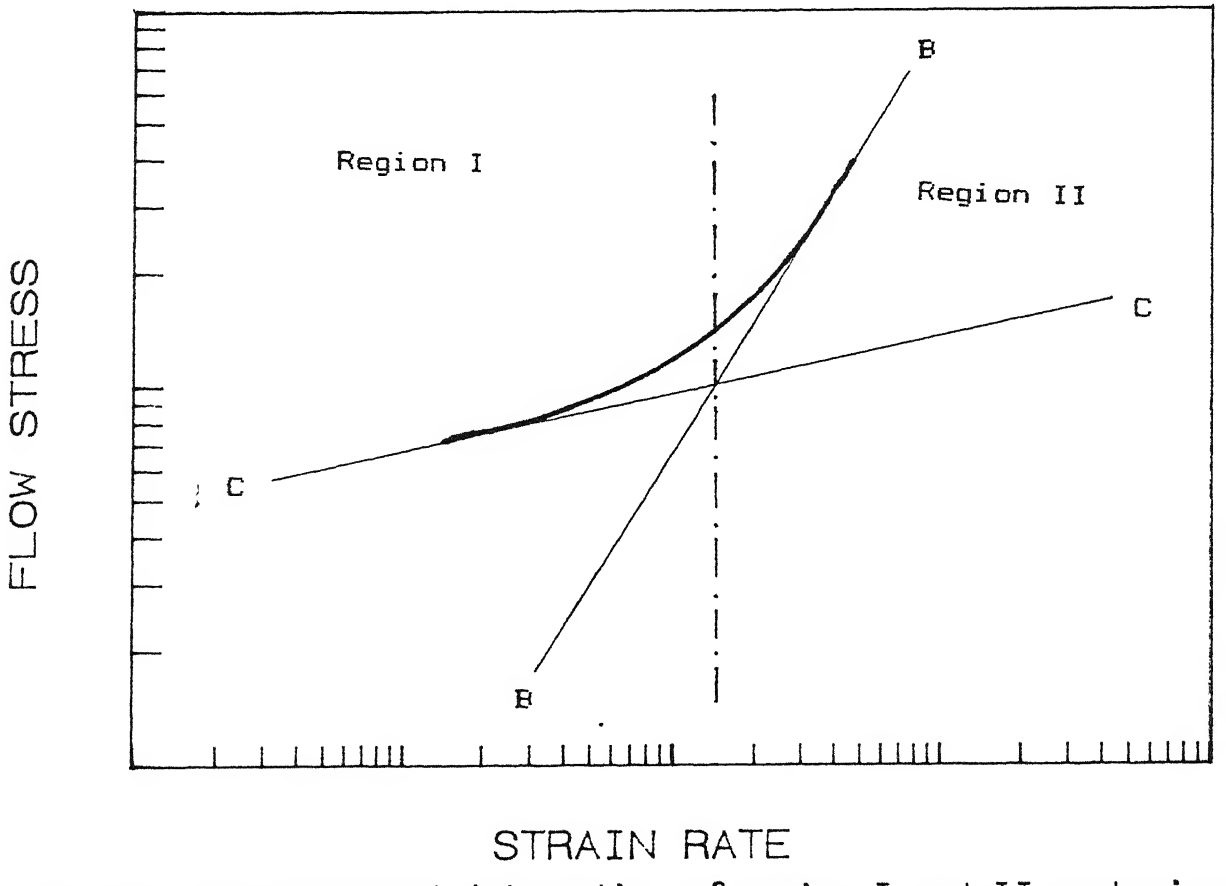

Fig. 3.4: Interdependent interaction of region I and II mechanisms

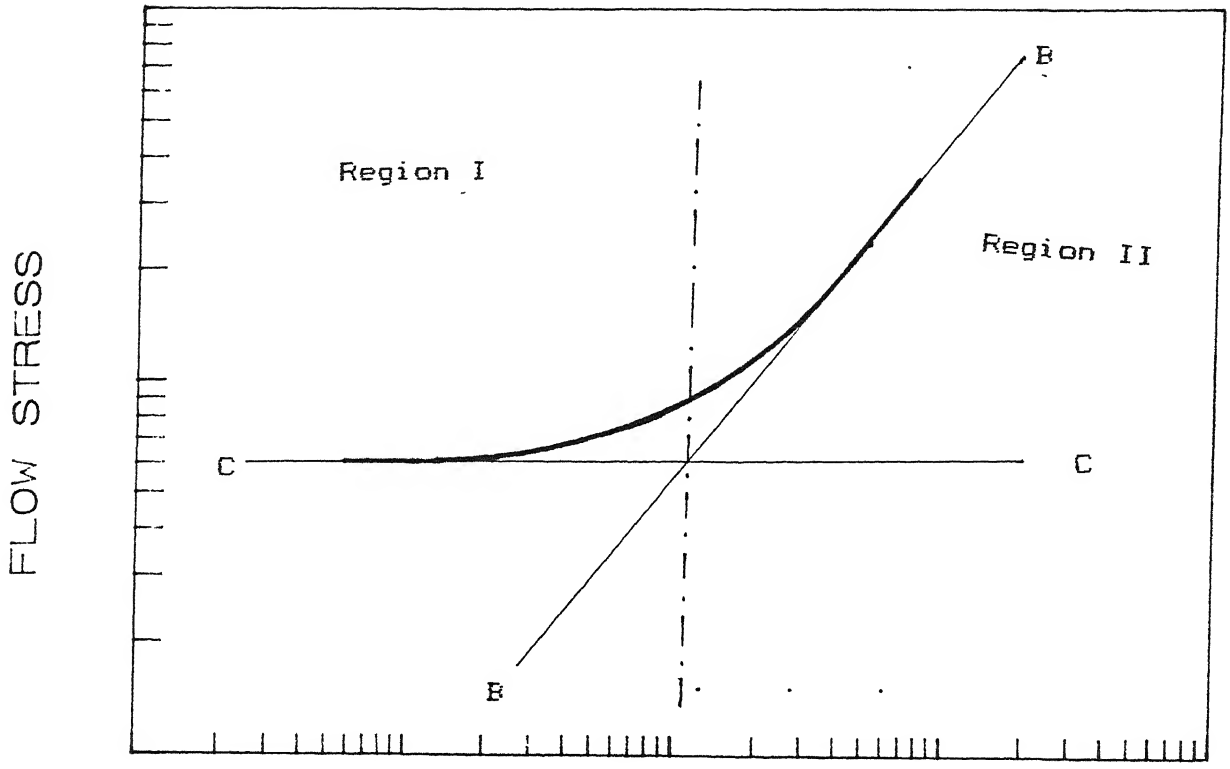

Fig. 3.5: A threshold stress for superplastic deformation

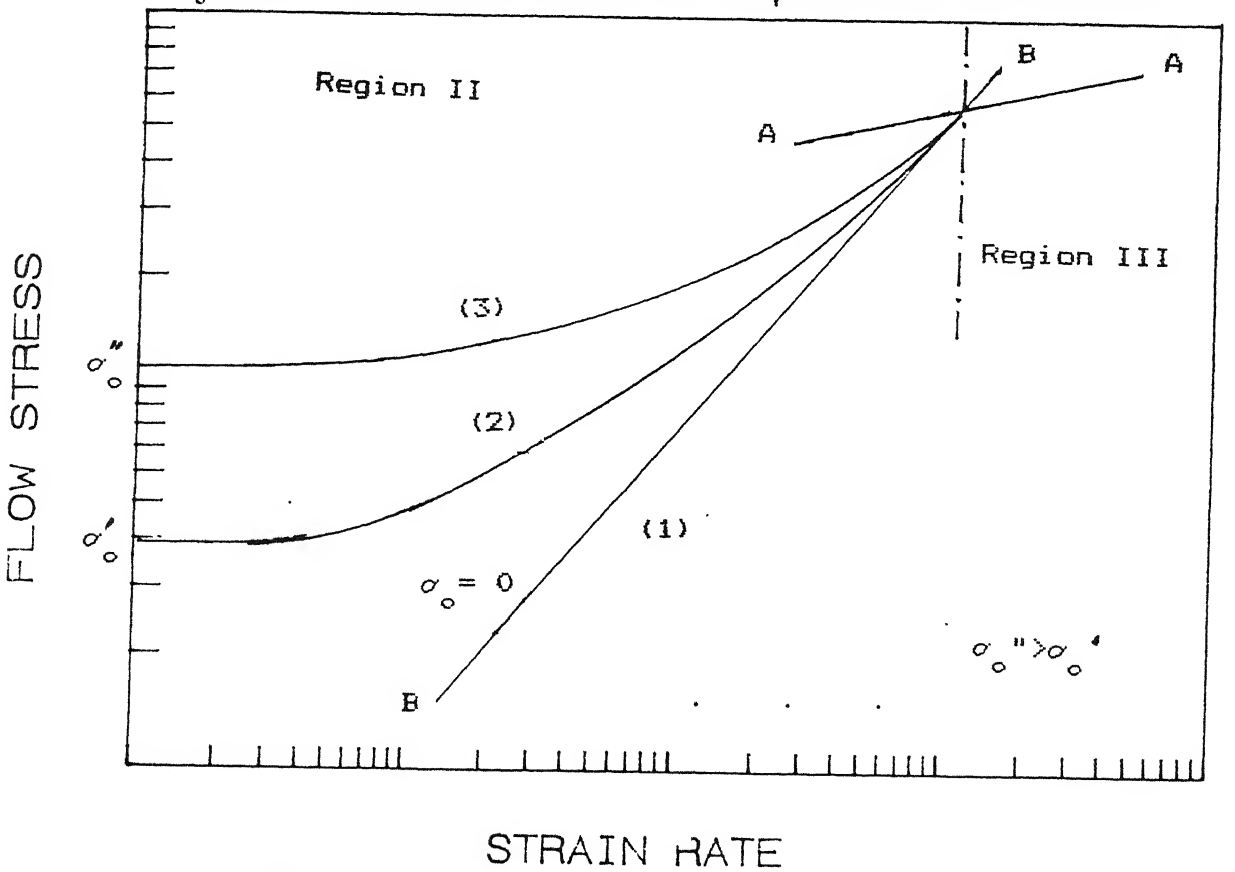

Fig. 3.6: Effect of the magnitude of threshold stress on the stress-strain rate behaviour of superplastic materials

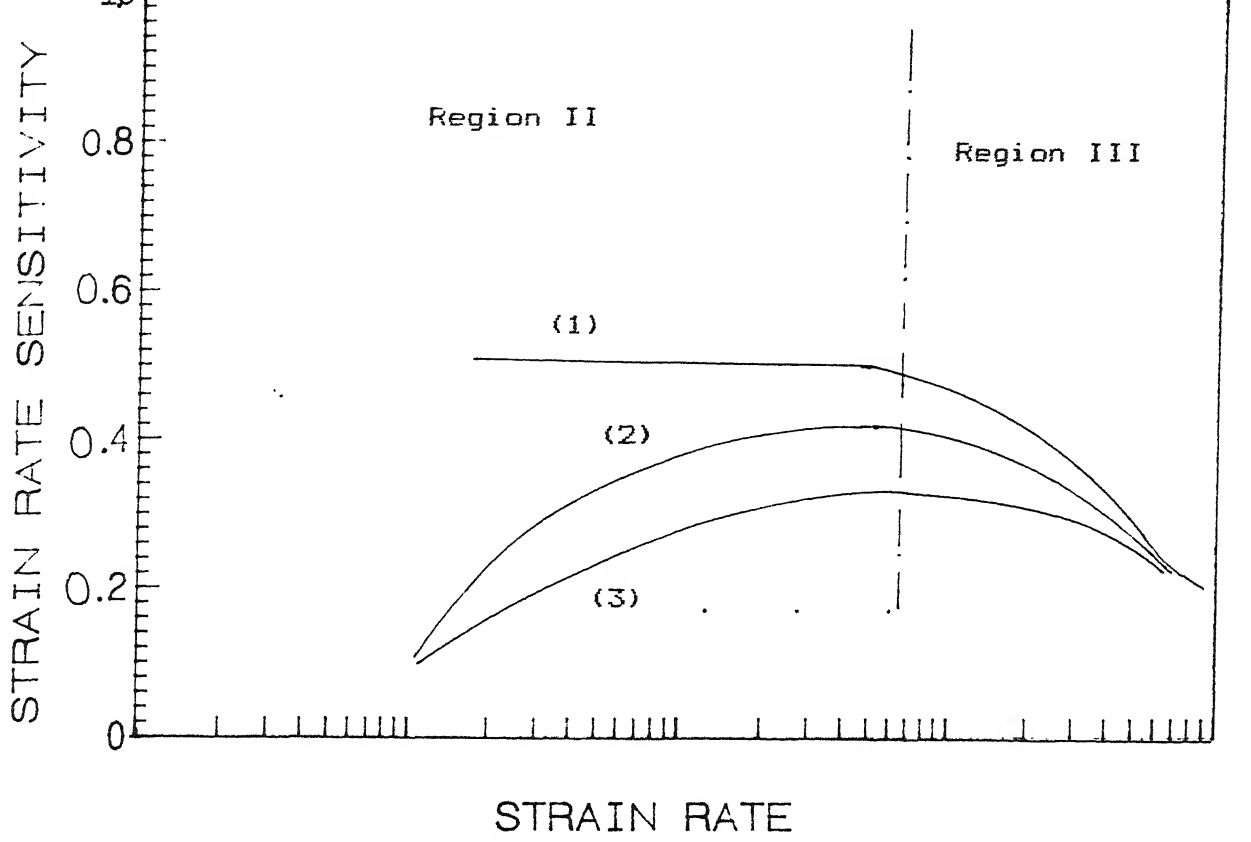

Fig. 3.7: Effect of the magnitude of threshold stress on the apparent strain rate sensitivity of superplastic materials

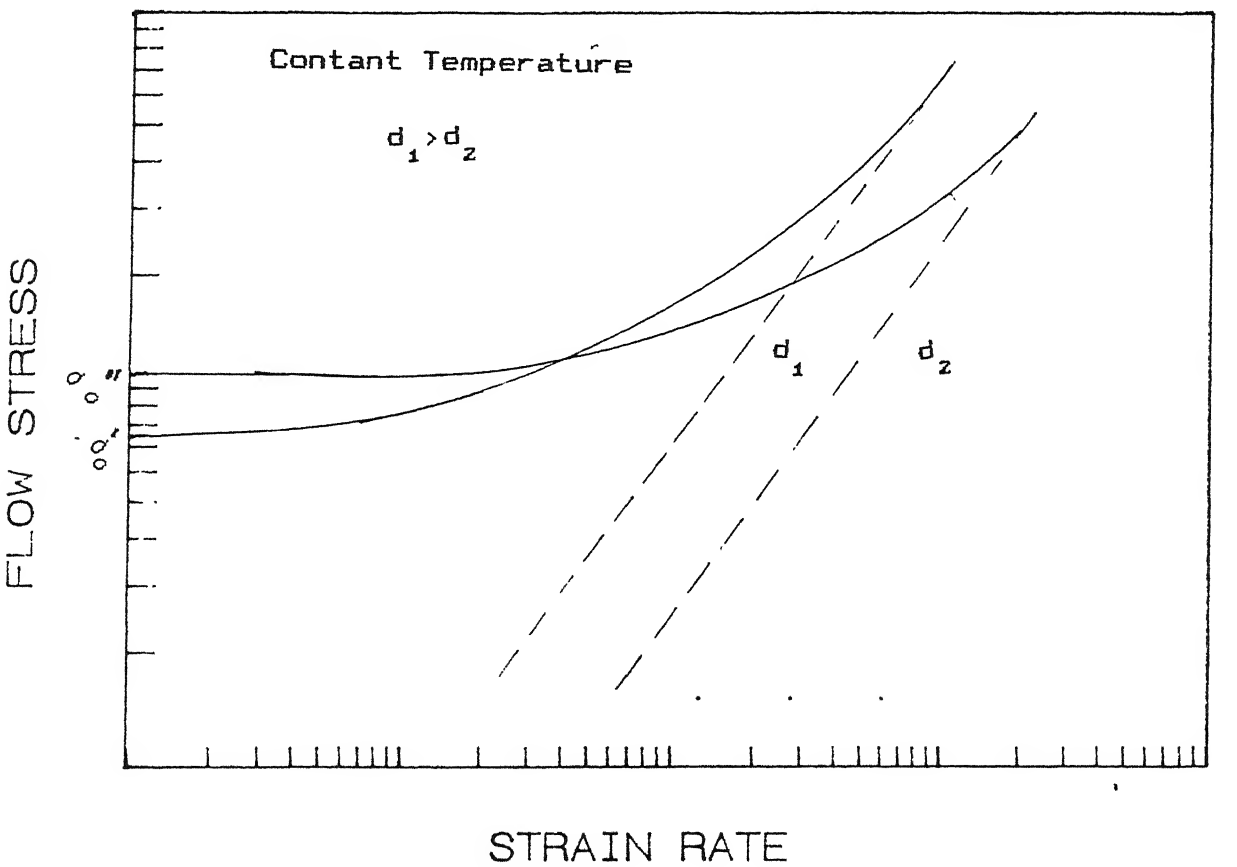

Fig. 3.8: Cross-over of stress-strain rate plots at a given temperature due to the grain size dependence of threshold stress

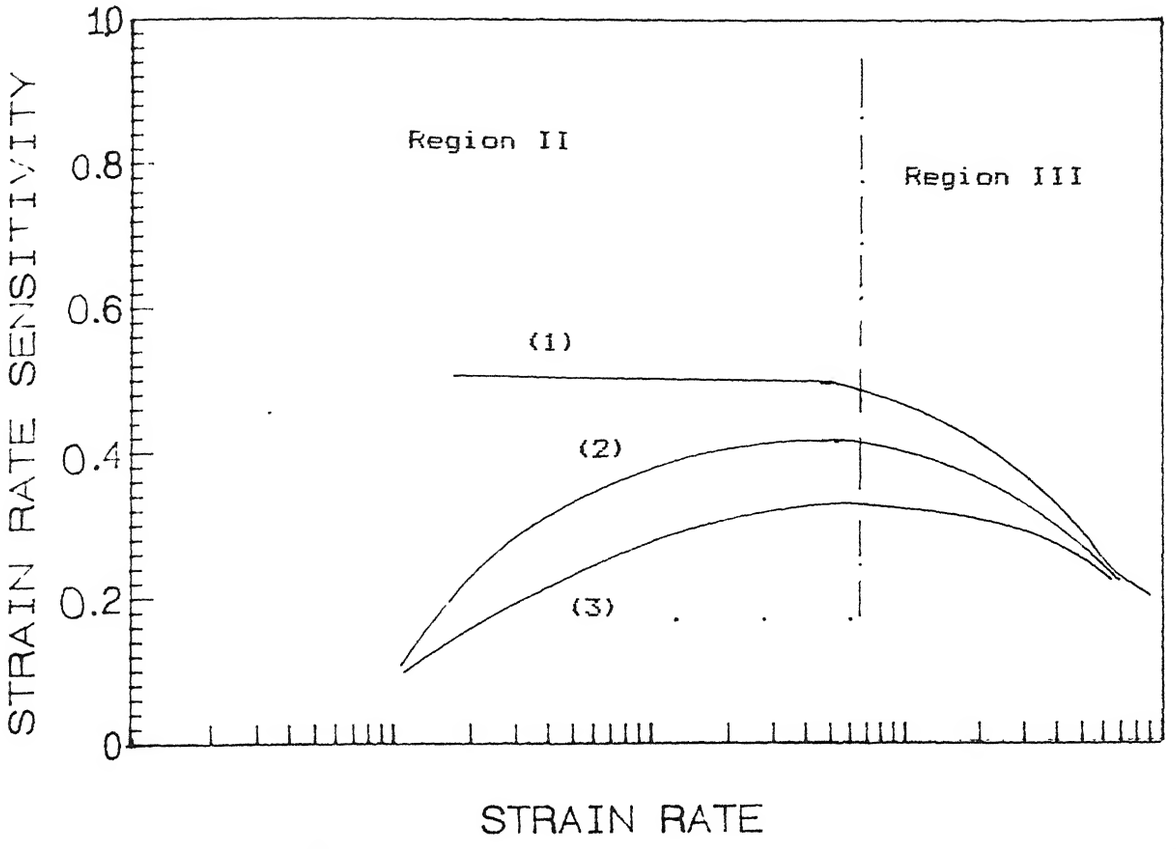

Fig. 3.7: Effect of the magnitude of threshold stress on the apparent strain rate sensitivity of superplastic materials

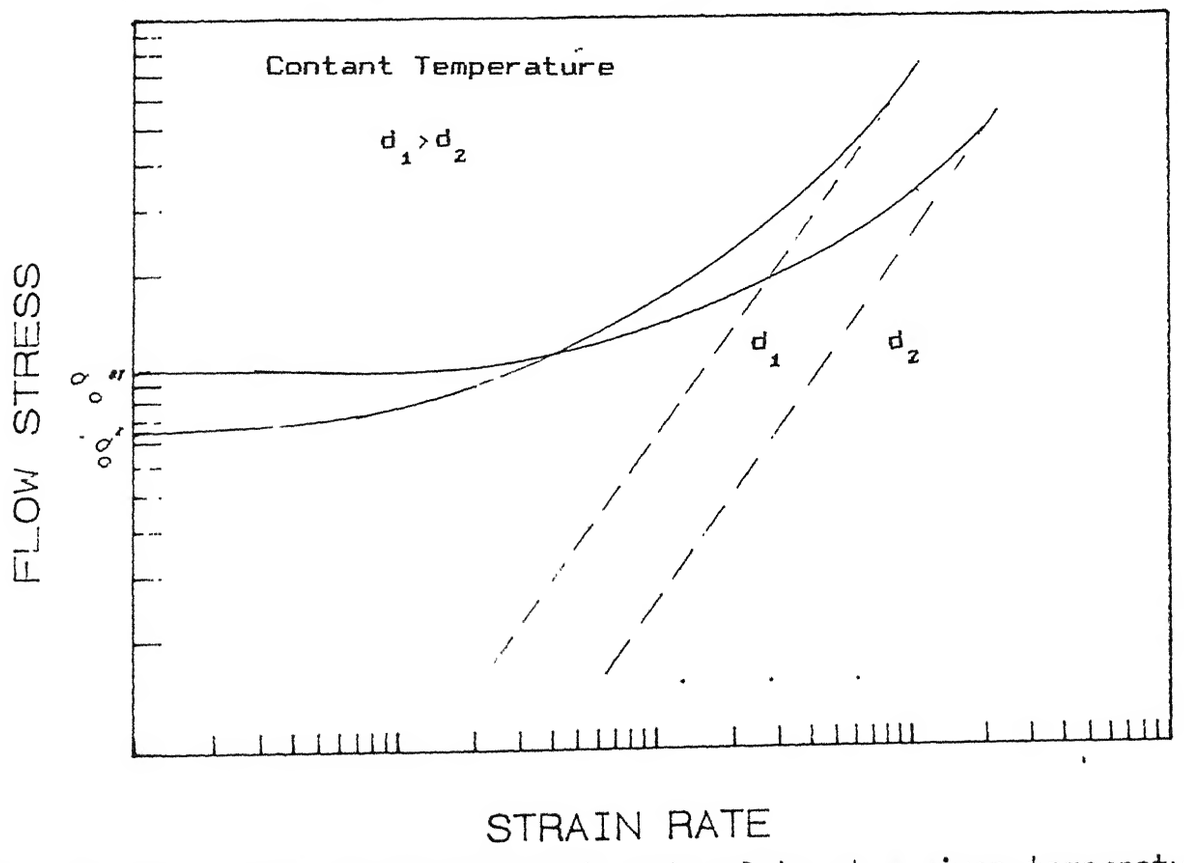

Fig. 3.8: Cross-over of stress-strain rate plots at a given temperature due to the grain size dependence of threshold stress

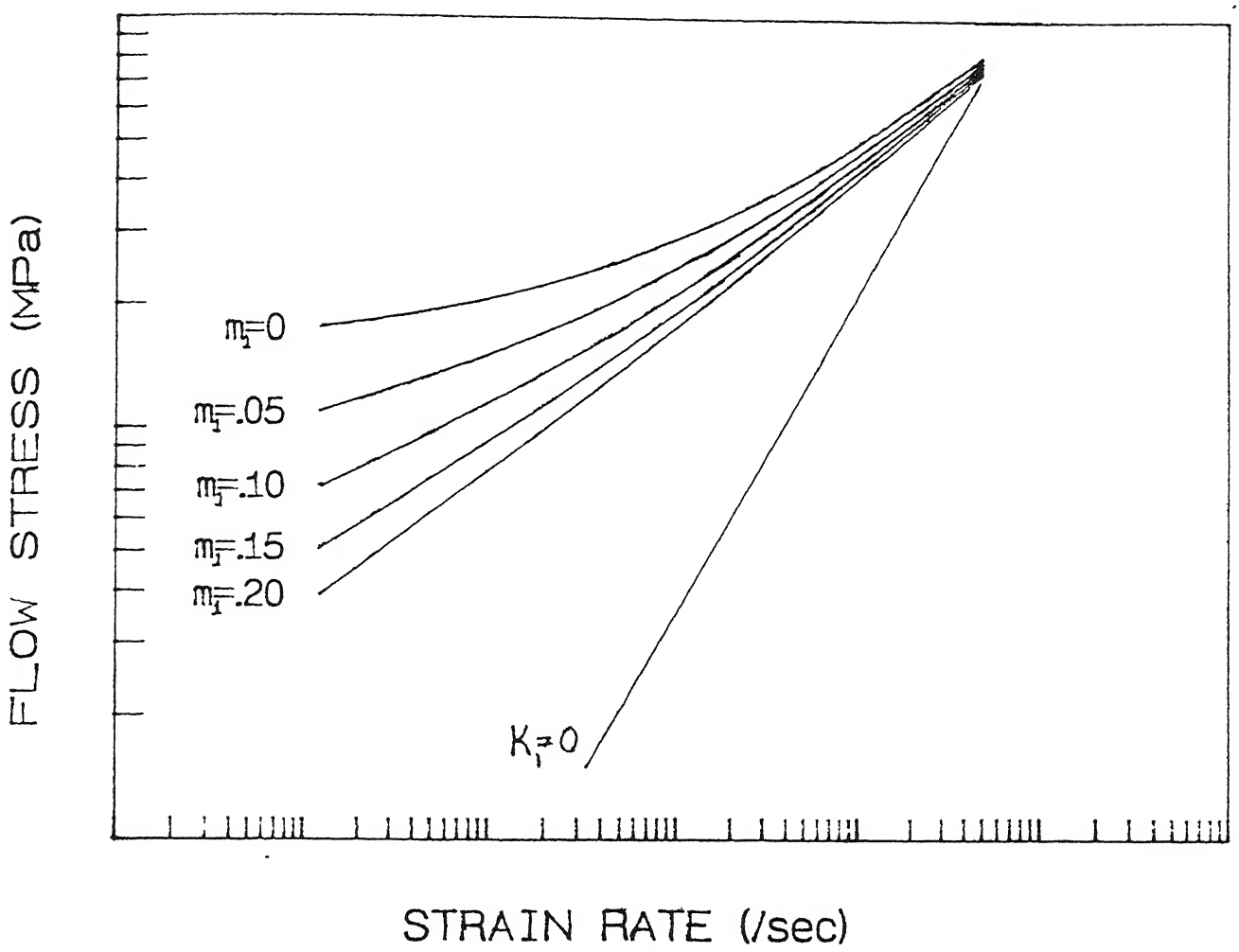

Fig. 3.9 : Effect of strain rate dependent threshold stress on $\sigma - \dot{\varepsilon}$ behaviour with various values of m_1 (m_2=0.5)

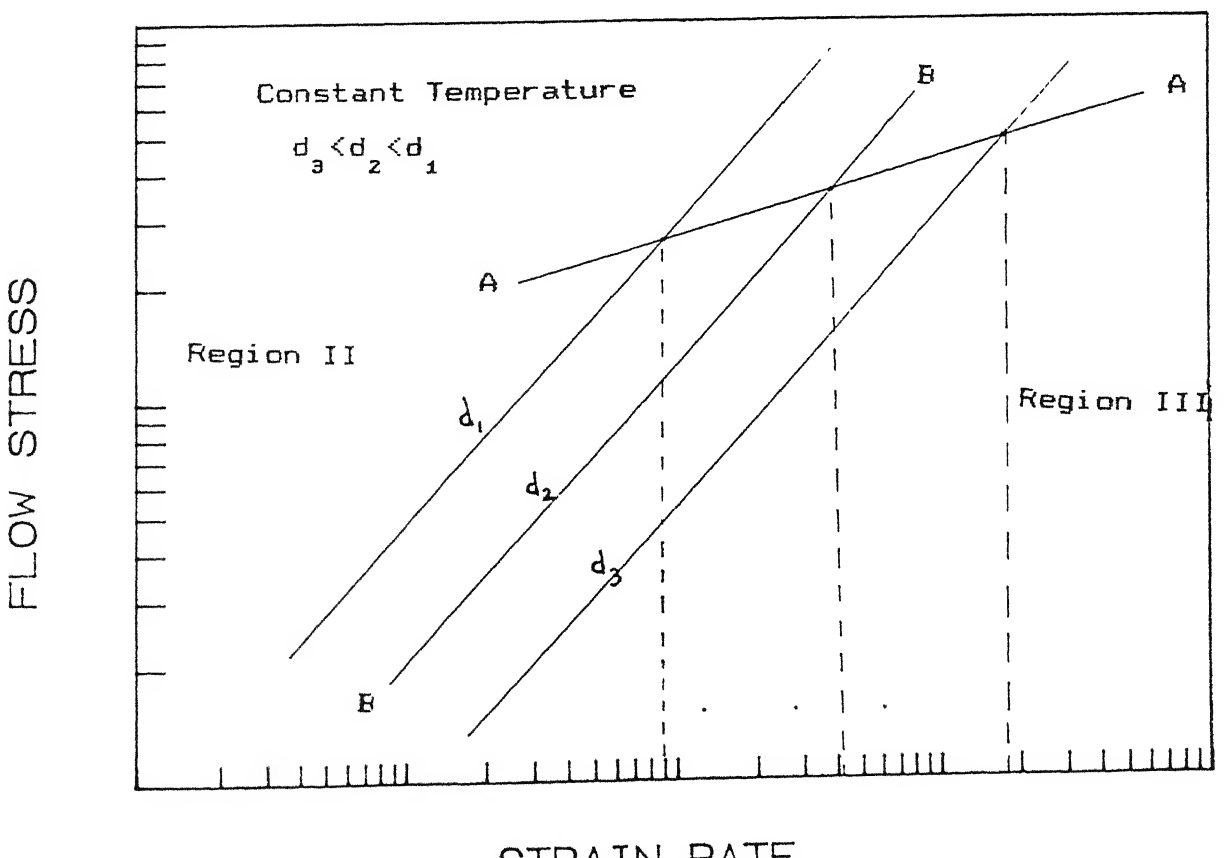

Fig 3.10: Effect of grain size on region II to III transition

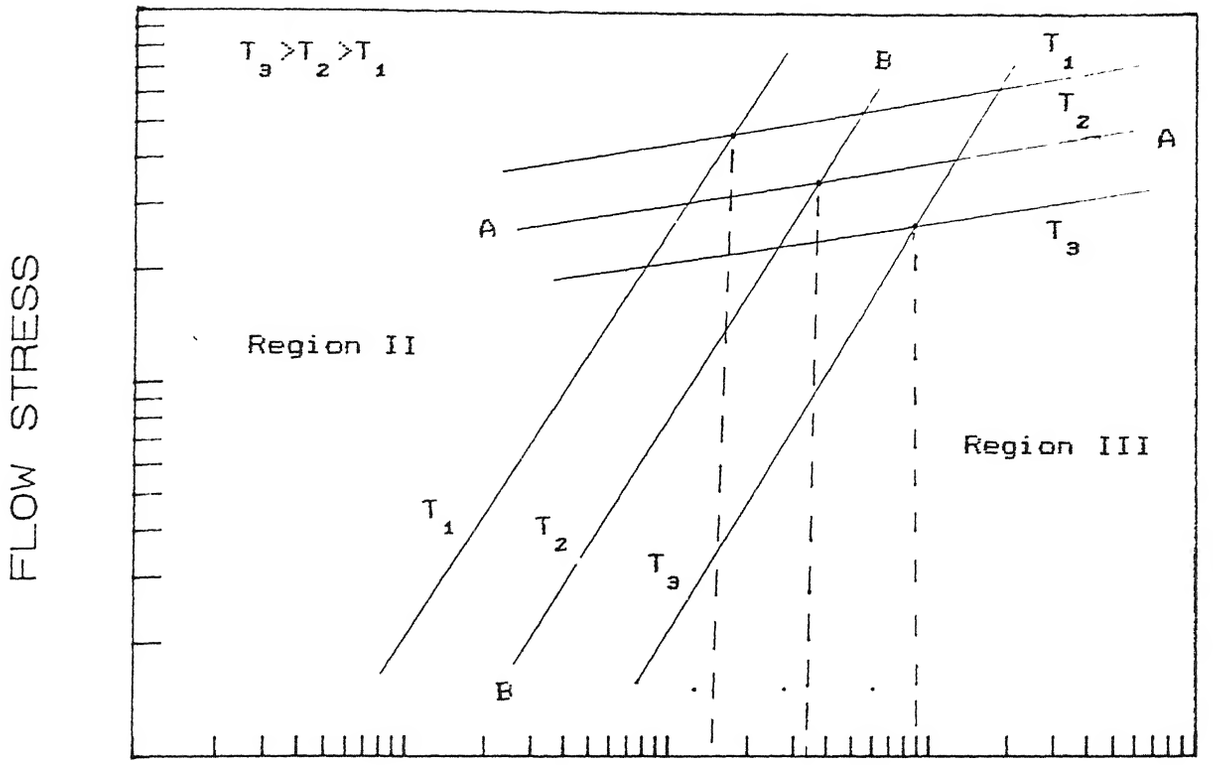

Fig. 3.11: Effect of temperature on region II to III transition

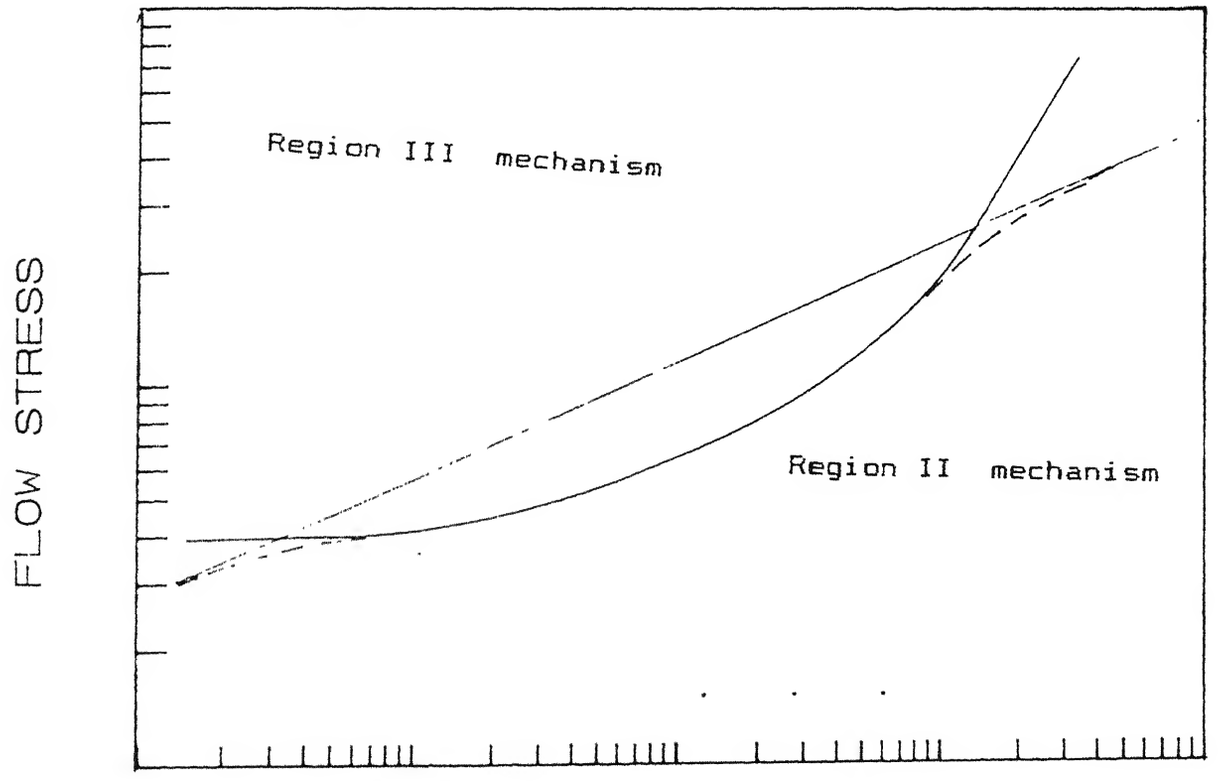

Fig. 3.12: Possibility of independent flow mechanism at low strain rates due to the interference of region III flow process

CHAPTER IV
EXPERIMENTAL PROCEDURE AND RESULTS

4.1 MATERIALS

Both the 7075 series modified Al alloys (Al-Zn-Mg-Cu plus modifier), i.e.,Mn and Mo modified ones were available in the form of cylindrical rods of approximately 15mmΦ x 30cm dimensions. The processing method for such RST/PM route processed Al alloys was discusscd in section 2.1.2 and 2.1.3. The typical microstructure of such alloys consists of very fine grains with both precipitates and dispersoids in the Al matrix. The different alloying elements, e.g., Zn, Mg, Cu give the precipitates whereas the modifier (some heavy transitional element like Mo, Mn, V etc) forms the insoluble intermetallic phase which imparts high temperature strength to the material and stabilizes the fine grains against coarsening at high temperatures. The data were also considered from the literature for two other alloys, Al-4% Ti [23] and Al-Fe-V-Si [24] for reanalysis. The compositional and the microstructural details of all these four alloys are given below.

4.1.1 Al-Zn-Mg-Cu-Mn ALLOY

The composition of the alloy is cited from the previous work of Murty et.al [22]

Table 4.1

Composition of Al-Zn-Mg-Cu alloy

Element	Zn	Mg	Cu	Mn	Cr	Fe	Al
Weight %	6.48	2.77	1.95	3.87	0.21	0.16	balance

The microstructure consists of fine intermetallic dispersoids of $MnAl_6$ with a volume fraction of 0.15. These grain sizes were developed by coarsening the alloy at 520 °C for two

different time periods of 120 hours and 263 hours. Their grain sizes are [22] d = 0.7±0.2μm (Mn as received), d = 1.3±0.4μm (Mn-120Hr) and d = 2.5±0.7μm (Mn-263hr)

4.1.2 Al-4% Ti ALLOY

The stress strain rate data of this alloy were obtained from the earlier work [23] in the temp range of 525 to 625°C. Out of the three types of samples of different grain sizes, one is mechanically alloyed and the other two are RST/PM route processed. These samples have around 10 volume percent of fine submicron size Al_3Ti intermetallic dispersoids in their microstructure. In addition, the mechanically alloyed one has approximately 4 volume percent of even finer Al_2O_3 and Al_4C_3 dispersoids (<0.1 μm). These details are summarized below.

Table 4.2
Particulars of Al-4% Ti alloy

Alloy code	Processing	Dispersoid	Grain Size (μm)
AM-4C	Mechanically alloyed	Al_3Ti + Al_4C_3 +Al_2O_3	1.0±0.28
AT-4	RST/PM	Al_3Ti	1.6±0.45
AT-4C	RST/PM	Al_3Ti	2.6±0.74

4.1.3 Al-Zn-Mn-Cu-Mo ALLOY

The insoluble dispersoid phase is identified to be $MoAl_{12}$ with a BCC structure and lattice parameter of 7.581 Å (the details of the X-ray diffraction study are given in section 4.2). Samples with three different grain sizes were developed by annealing the received samples at 500°C for 120 hours and 500 hours. These are named as Mo-as received, Mo-120hr and Mo-500hr.

The composition of both the modified Al-Zn-Mg-Cu alloys were designed with the purpose of having the same volume fraction of dispersoids, around 0.15. Although the actual chemical composition of the Mo modified alloy is not available, the Mo content can be estimated on the basis of the above consideration. The Mo content estimated thus is 4.08 volume percent and the rest of the composition is similar to the Mn modified alloy.

4.1.4 Al-Fe-V-Si ALLOY

The stress strain rate data for this alloy were taken from the literature [24] in the temperature range of 475-575 ^{o}C. Here the three types of samples have different chemical composition, different volume fraction of intermetallic phase and different grain sizes. But in all the three samples the fine intermetallic dispersoids that stabilize the structure is a complex $Al_{12}(FeV)_3Si$ phase. The relevant details of the alloy are tabulated below [24].

Table 4.3

Particulars of Al-Fe-V-Si alloy

Alloy code	Composition(wt%) Fe	V	Si	Al	Dispersoid Volume %	Grain Size (μm)	Dispersoid dia (μm)
11C	5.95	1.00	1.02	bal	16	.72±.24	.15±.06
486C	8.75	1.60	1.60	bal	26	.44±.09	.14±.04
480C	11.61	1.38	2.23	bal	36	.40±.09	.08±.03

4.2 X-RAY DIFFRACTION

X-ray diffraction was made use of in identifying the second phase of the Mo modified Al-Zn-Mg-Cu alloy. The sample, in the shape of a disc, was annealed at 500^{o}C for 5 hours to dissolve all the precipitates other than the insoluble dispersoid phase which is to be identified and then quenched. X-ray

Table 4.4

X-ray diffraction data

λ = 1.54056 Å (Cu K_α)

V = 30 KV

Scanning speed = 0.6°/min (in 2θ)

Counts per min = 10K

Time constant = 10 sec

Observed values			Values from ASTM data card for $MoAl_{12}$			
Line no.	2θ	d = $\lambda/2\sin\theta$	I/I_o	d	I/I_o	hkl
1	16.5	5.368	100	5.361	100	110
2	29.0	3.076	42	3.095	33	211
3	37.6	2.390	79	2.397	86	310
4	41.1	2.194	28	2.189	38	222
5	44.7	2.026	82	2.026	71	321
6	48.0	1.894	16	1.8954	11	400
7	51.0	1.789	12	1.7870	6	330
8	59.8	1.545	9	1.5476	9	422
9	62.4	1.487	9	1.4868	13	510
10	72.7	1.299	15	1.3002	13	530
11	75.2	1.262	10	1.2636	6	442
12	77.6	1.230	21	1.2299	15	532

diffraction spectrum was recorded using a Cu target. To locate the position of the major diffraction peaks, at first a rapid scan (3°/min) was made from 0° to 150° 2θ values. In the second step slow scanning (0.6°/min) was done near the peaks in order to get more accurate 2θ values for the peak positions.

After the solutionising and quenching treatment, there are only two phases in the microstructure, viz., the insoluble intermetallic phase and the aluminium solid solution matrix with the other alloying elements Zn, Mg and Cu. The peaks of the Al solid solution are nearly at the same angles as those of pure Al, since the lattice parameter of the Al solid solution is only slightly different from that of pure Al. Only the peaks other than those of Al solid solution were indexed. The 2θ values of the peaks were compared with those of the probable intermetallic compounds from the ASTM data cards and the phase was identified to be the binary compound $MoAl_{12}$, which has a BCC structure with lattice parameter of 7.581 Å. The observed 2θ and intensity values and those from ASTM data card are shown in table 4.4.

4.3 DIFFERENTIAL STRAIN RATE TEST

Differential strain rate test under compression was carried out in a 10 ton MTS 810 machine in order to obtain the stress strain rate data for Mn and Mo modified alloys in the temperature range of 450-550 C. A cylindrical split furnace was used for this high temperature testing. The diameter and length of compression specimens of Al-Zn-Mg-Cu-Mn alloy are 7mm and 11mm and those for Al-Zn-Mg-Cu-Mo are 9mm and 12mm. To achieve the step change in cross head velocity the machine was set in single cycle mode and a certain rate was fixed. the load versus displacement data are recorded. Then the cross head measurement was arrested by pressing the *hold* button, a new rate was set, the *hold* button was released and the load vs. displacement corresponding to this new cross head velocity is recorded. Starting with a cross head velocity of 4.14^{-4}mm/sec, the speed is successively increased to the next higher level in a step of 2.5 upto a maximum of 1.56mm/sec. the strain rate sensitivity, m, was calculated by the

relation

$$m = \frac{\ln(P_2/P_1)}{\ln(V_2/V_1)} \qquad (4.1)$$

Where P_1 and P_2 are steady state loads corresponding to cross head speeds V_1 and V_2 respectively. From the load Vs. displacement data the true stress vs true strain rate and m vs true strain rate data were calculated making use of a computer program (given in the appendix A). A new specimen was used for each test temperature. At each cross head speed, the test was continued till the steady state was reached and only after attaining that, the cross head speed was changed to the next higher one. The strain given at each cross head speed was about 2-3%.

4.4 RESULTS OF MECHANICAL TESTING

The behavior of the four alloys considered (including the two alloys, data for which have been taken from literature) can be classified into two distinct types. Two alloys, Mn modified Al-Zn-Mg-Cu and Al-4% Ti exhibit high values of m upto around 0.45 which is a clear indication of superplastic behavior, where as the other two alloys Al-Fe-V-Si and Al-Zn-Mg-Cu-Mo exhibit rather low values of m upto 0.23. Accordingly their behavior is grouped into higher and lower strain rate sensitivity types.

4.4.1 ALLOYS SHOWING HIGHER STRAIN RATE SENSITIVITY

The specimens of Mn modified Al-Zn-Mg-Cu alloy with different grain sizes were tested at temperatures, 400°C,450°C and 500°C in the strain rate range of 10^{-5} to 10^{-1} /sec. Their σ-$\dot{\varepsilon}$ plots and the corresponding m vs $\dot{\varepsilon}$ plots are shown in Figs 4.1 to 4.6. A little strain softening was observed only at the highest

TABLE 4.5(a)

MAXIMUM m VALUES FOR THE Mn MODIFIED Al-Zn-Mg-Cu ALLOY

Sample code	Grain Size (μm)	Test Temperature (°C)		
		400	450	500
Mn-as received	0.7	0.27	0.32	0.37
Mn-120 hr	1.3	0.25	0.32	0.41
Mn-263 hr	2.5	0.25	0.31	0.40

TABLE4.5(b)

MAXIMUM m VALUES FOR Al-4%Ti [23]

Sample code	Grain size (μm)	Test temp (°C)			
		605	575	550	525
AM-4C (Mech. alloyed)	1.0	0.21	0.17	--	0.13
AT-4	1.6	0.36	0.31	0.22	--
AT-4C	2.6	0.45	0.35	--	0.28

Table 4.6(a)

MAXIMUM m VALUES FOR Mo MODIFIED Al-Zn-Mg-Cu

Sample code	Test Temperature (°C)			
	400	450	500	550
Mo-as received	0.11	0.10	0.16	0.21
Mo-120 hr	0.15	0.11	0.16	0.22
Mo-500 hr	0.18	0.15	0.18	0.23

Table 4.6(b)

MAXIMUM m VALUES FOR Al-Fe-V-Si [24]

Sample code	Grain size (μm)	Volume pct.	Test Temperature (°C)		
			400	450	500
480C	0.40	36	0.11	0.13	0.16
486C	0.44	26	0.11	0.13	0.17
11C	0.72	16	0.10	0.14	0.15

temperature of testing, 500°C, which might be due to dynamic recrystallisation. The σ-$\dot{\varepsilon}$ plots for various grain sizes at 500°C are compared in Fig 4.7. The maximum m value for each sample is tabulated in table 4.5(a).

For the Al-4% Ti alloy, stress-strain rate data have been taken from the literature [23]. The σ-$\dot{\varepsilon}$ plots are shown in Fig 4.8 to 4.10. The σ-$\dot{\varepsilon}$ plots at 605°C for different grain sizes are compared in Fig 4.11 to illustrate the effect of grain size on the shape of stress-strain rate behavior. Their maximum m values are shown in table 4.5(b).

4.4.2 ALLOY SHOWING LOWER STRAIN RATE SENSITIVITY

As regards to the Mo modified Al-Zn-Mg-Cu alloy, Three types of samples of varying grain sizes, Mo-as received, Mo-120hr and Mo-500hr, were tested at 400,450,500 and 550°C. The σ-$\dot{\varepsilon}$ plots and the corresponding m-$\dot{\varepsilon}$ plots are shown in Fig 4.2 to 4.17. Comparative σ-$\dot{\varepsilon}$ plots at 500°C for various grain sizes are shown in Fig 4.18. The observed maximum m values for various samples are given in table 4.6(b)

Where as the previous three alloys have same volume fraction of dispersoid phase but different grain sizes, the Al-Fe-V-Si alloys are of three different compositions with different dispersoid content as well as grain sizes. The stress-strain rate data were taken from the literature [24] and the various plots are shown in Fig 4.19 to 4.21. At 575°C, the σ-$\dot{\varepsilon}$ curves are compared in Fig 4.22. The maximum m values for various samples are listed in table 4.6(b).

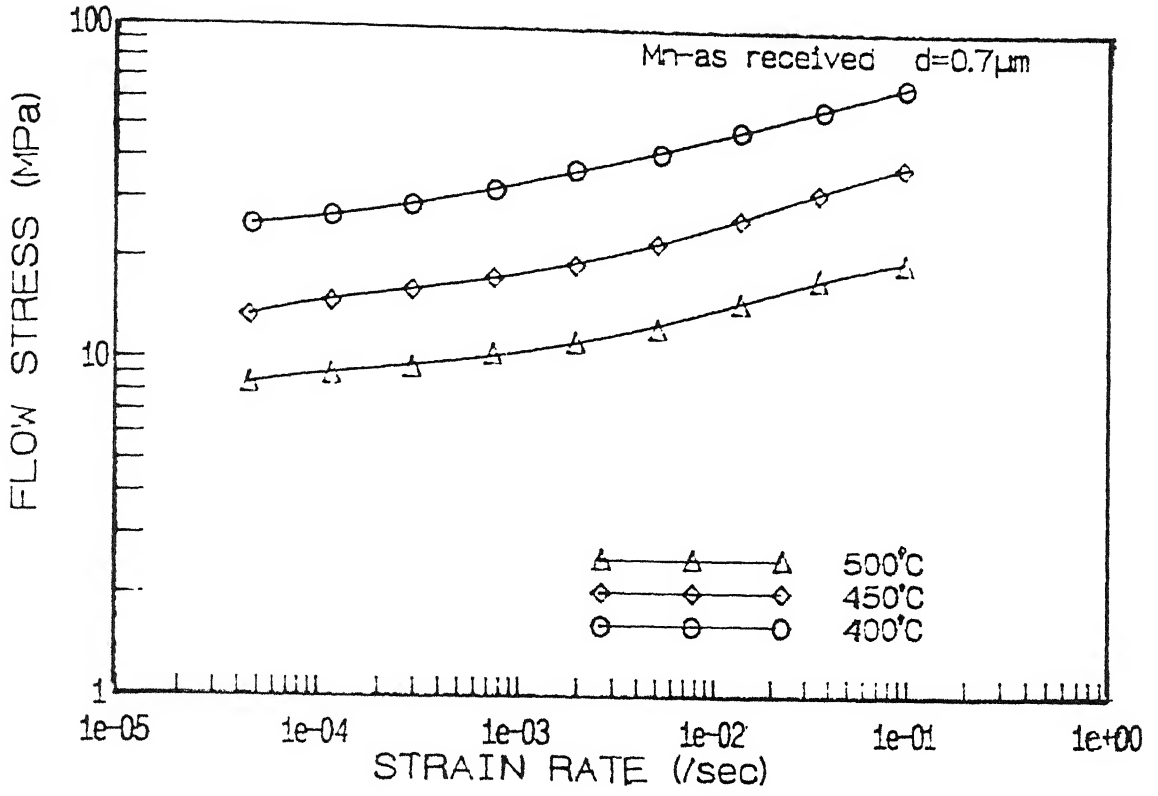

Fig. 4.1 : σ-$\dot{\varepsilon}$ behaviour of Mn modified alloy in as received condition

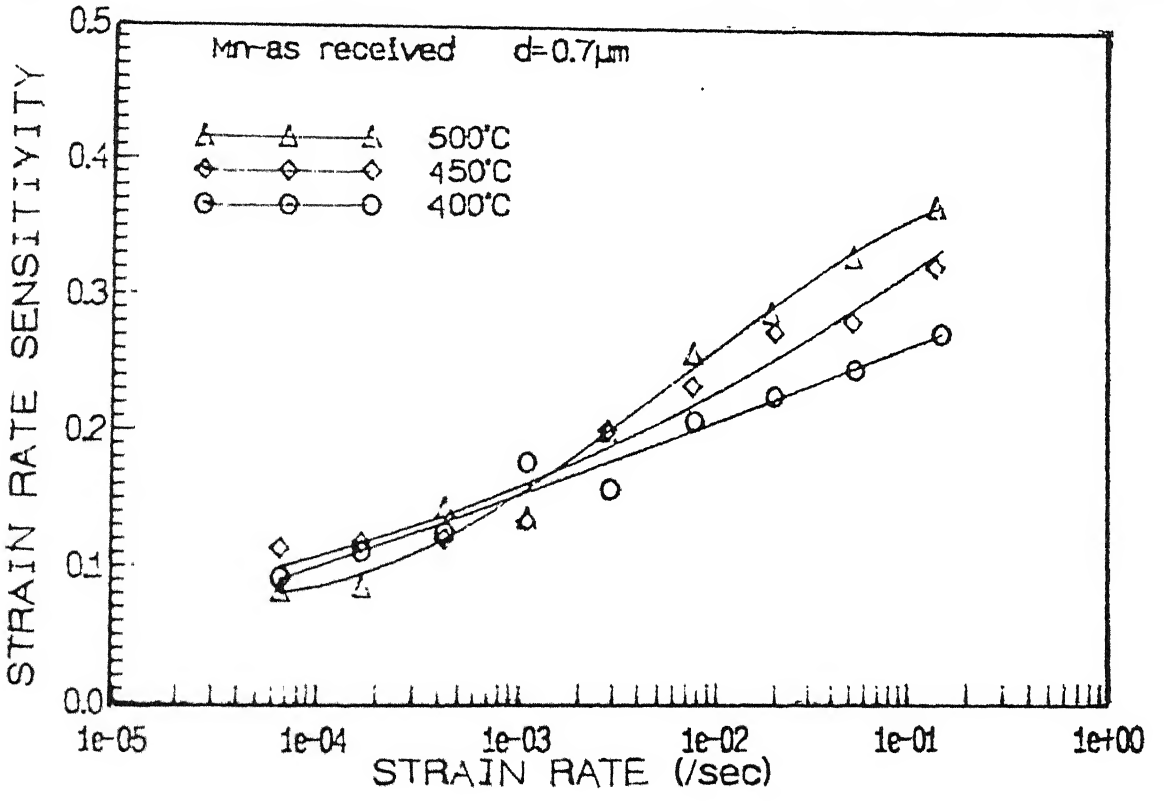

Fig. 4.2 : m-$\dot{\varepsilon}$ behaviour of Mn modified alloy in as received condition

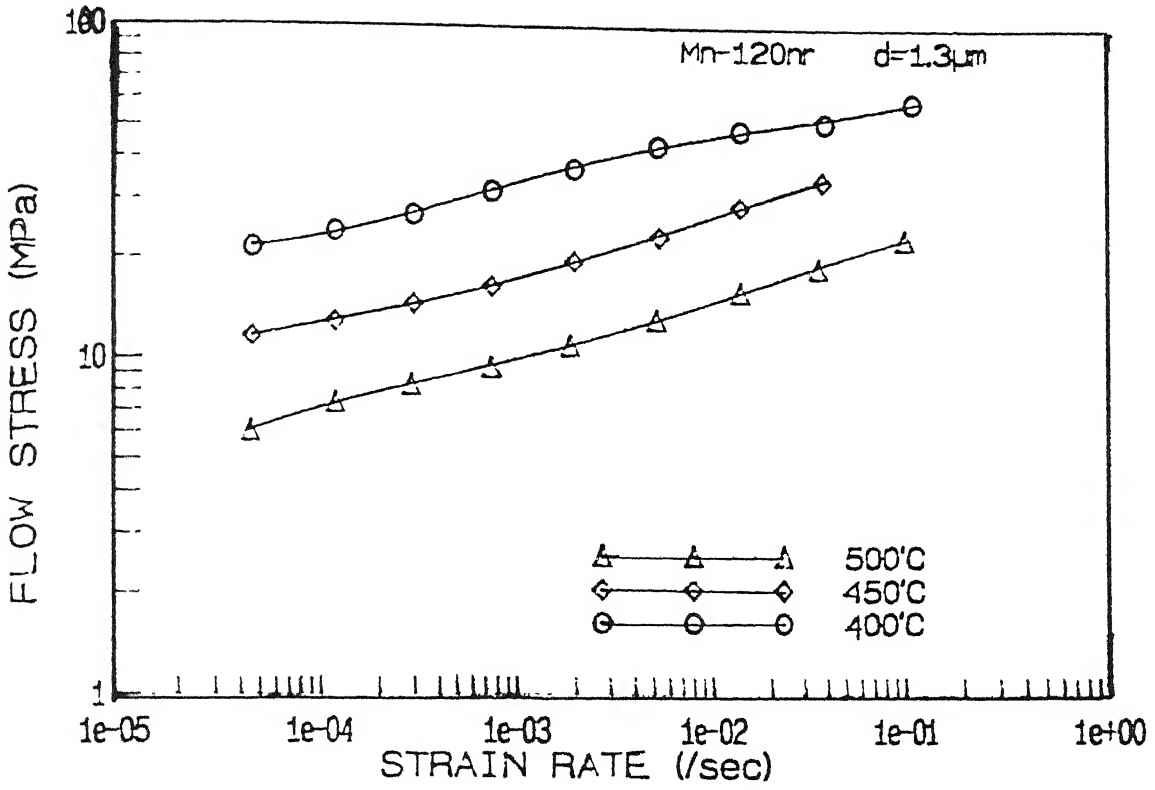

Fig. 4.3 : σ-$\dot{\varepsilon}$ behaviour of Mn modified alloy after 120hr annealing

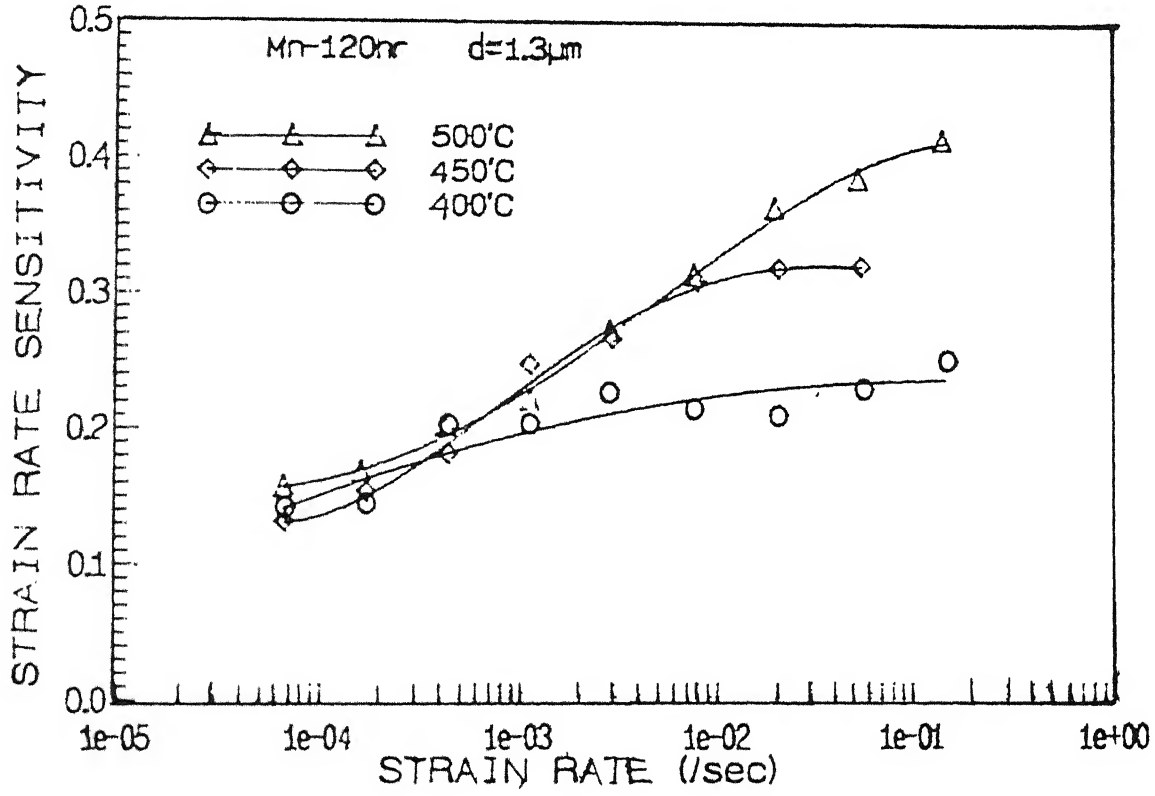

Fig. 4.4 : m-$\dot{\varepsilon}$ behaviour of Mn modified alloy after 120hr annealing

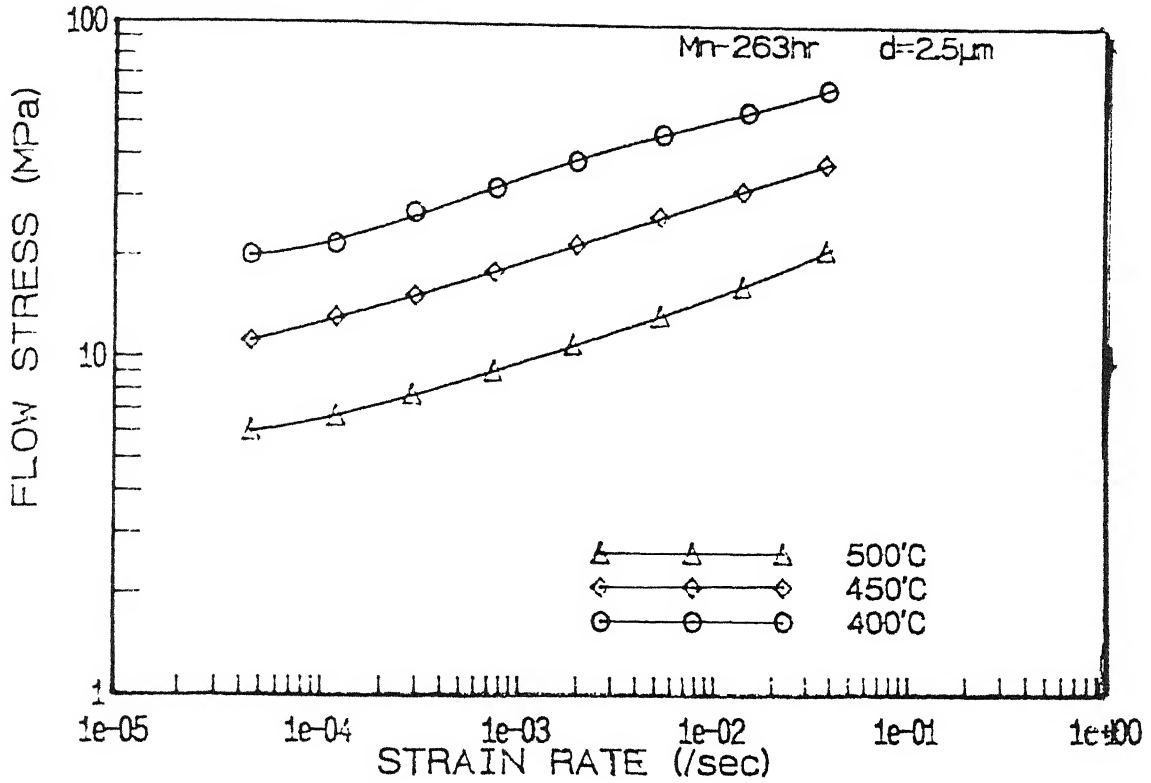

Fig. 4.5 : σ-$\dot{\varepsilon}$ behaviour of Mn modified alloy after 263hr annealing

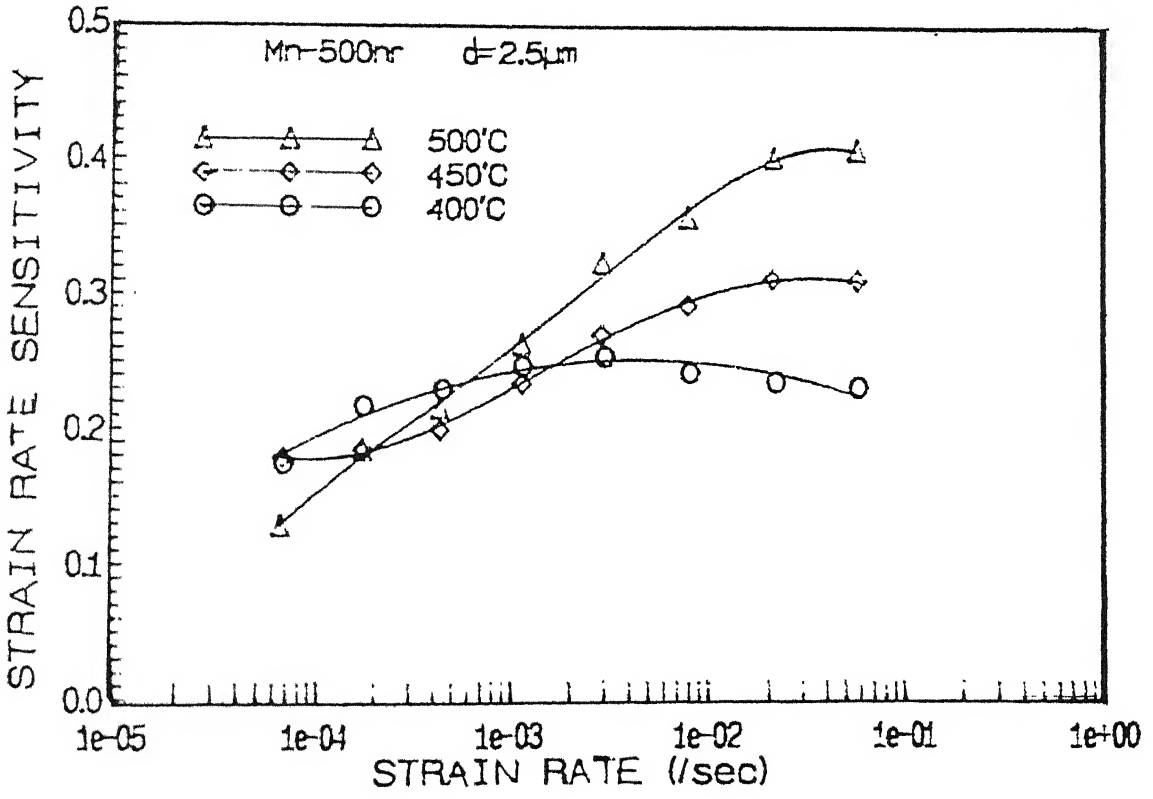

Fig. 4.6 : m-$\dot{\varepsilon}$ behaviour of Mn modified alloy after 263hr annealing

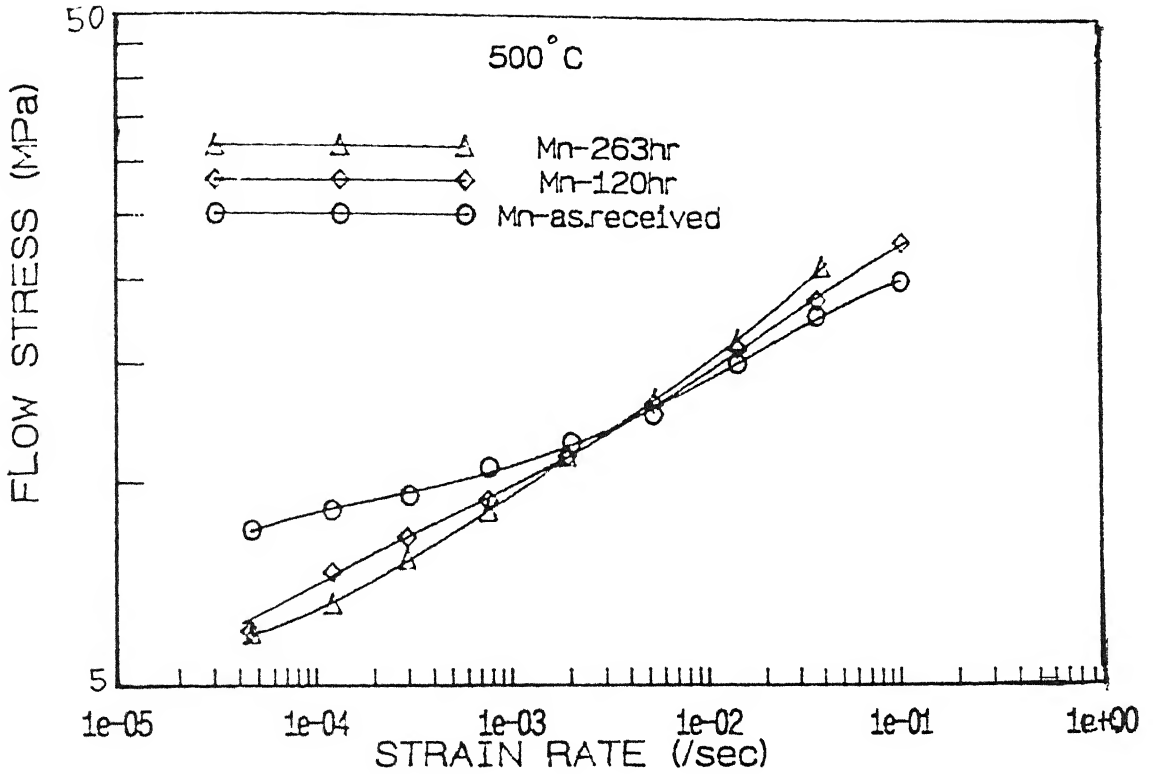

Fig. 4.7 : Comparison of σ-$\dot{\varepsilon}$ behaviour of Mn modified alloys at 500°C

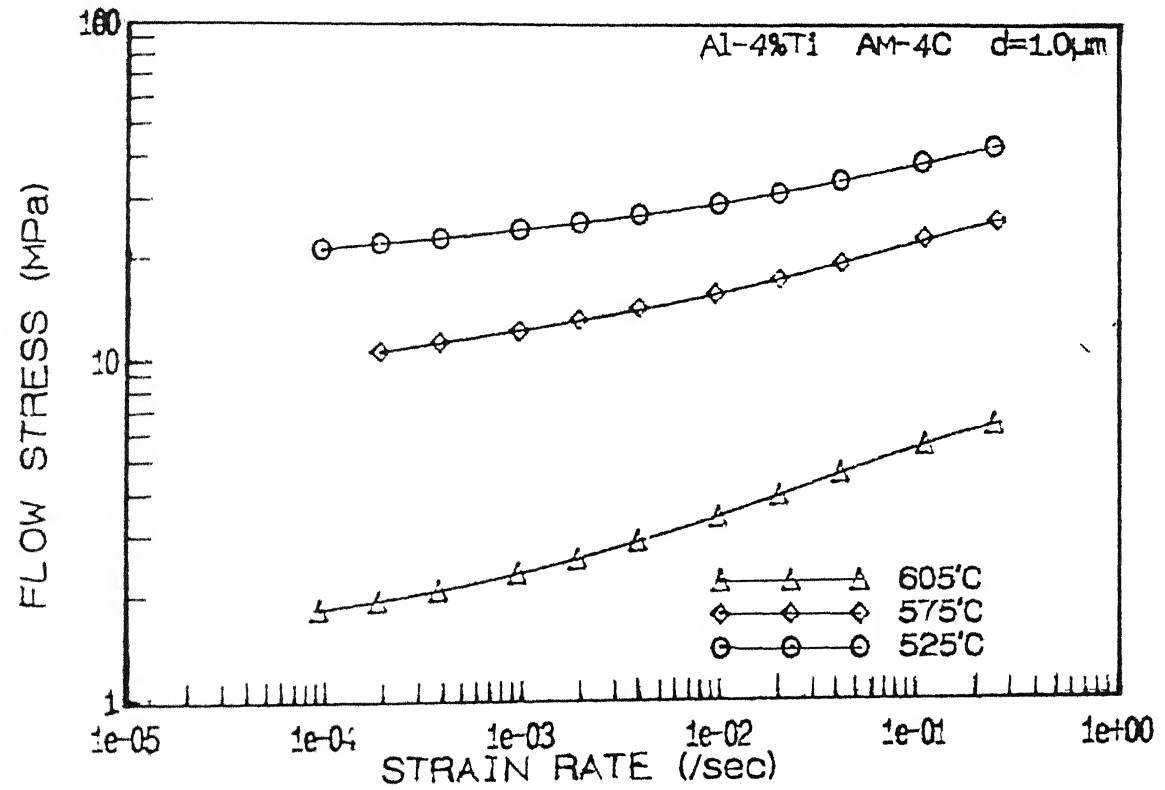

Fig. 4.8 : σ-$\dot{\varepsilon}$ behaviour of Al-4%Ti alloy (mechanically alloyed) with d=1.0μm

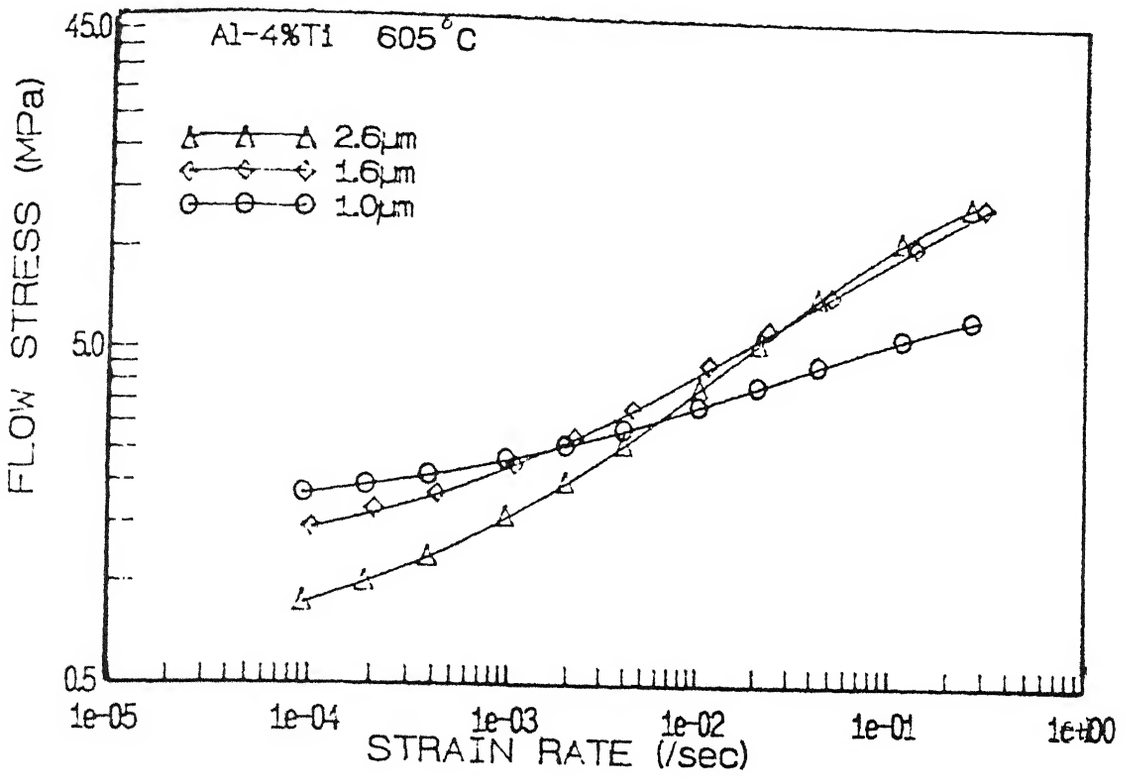

Fig. 4.11 : Comparison of σ-$\dot{\varepsilon}$ behaviour of Al-4%Ti alloys at 605 °C

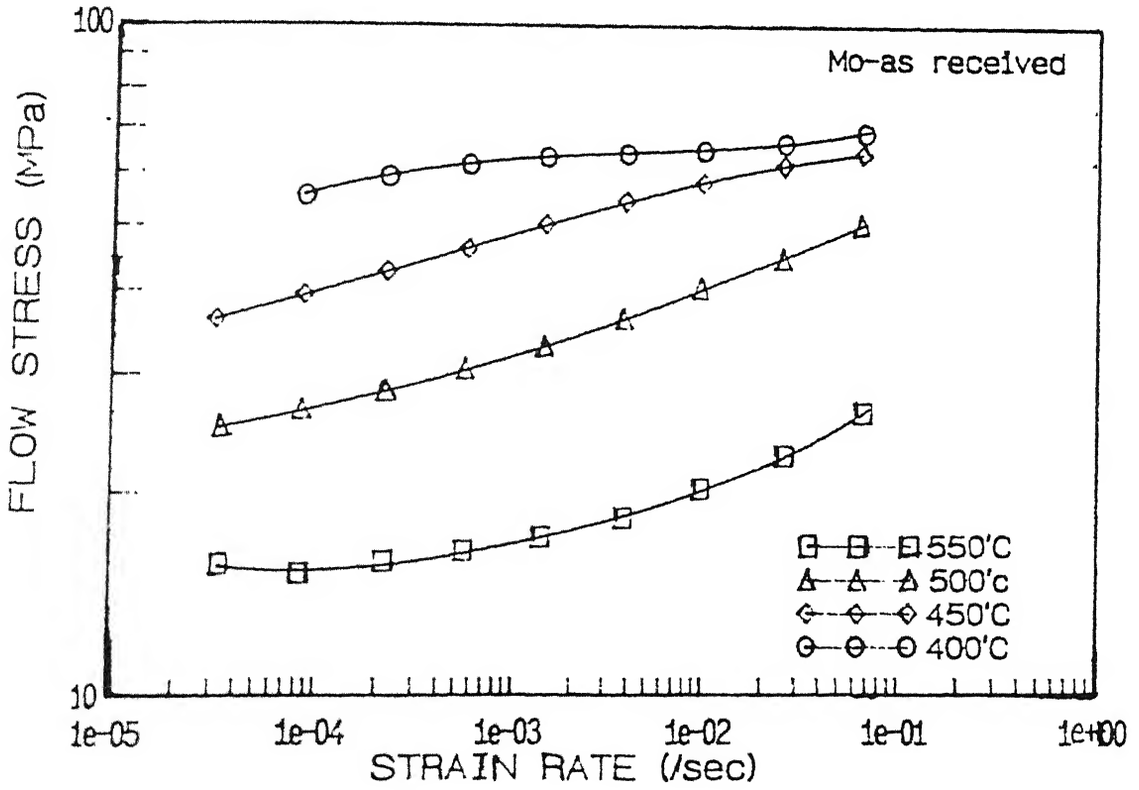

Fig. 4.12 : σ-$\dot{\varepsilon}$ behaviour of Mo modified alloy in as received condition

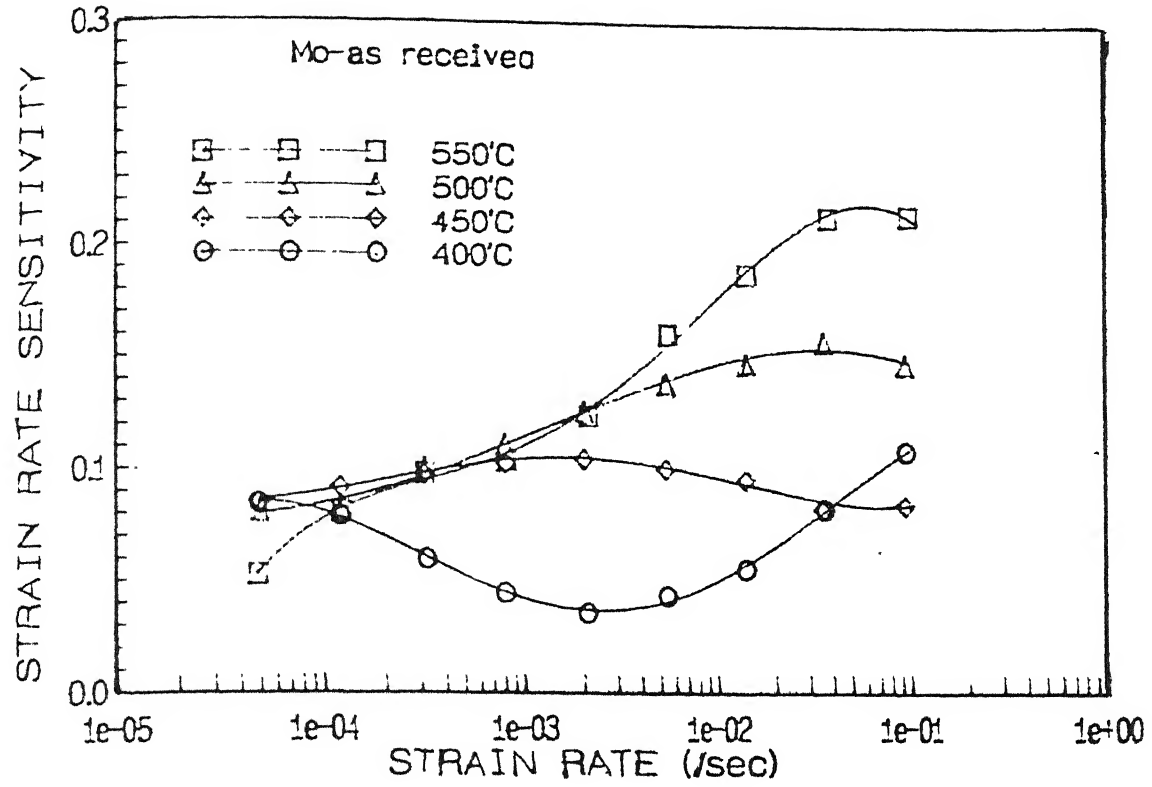

Fig.4.13 : m-$\dot{\varepsilon}$ behaviour of Mo modified alloy in as received condition

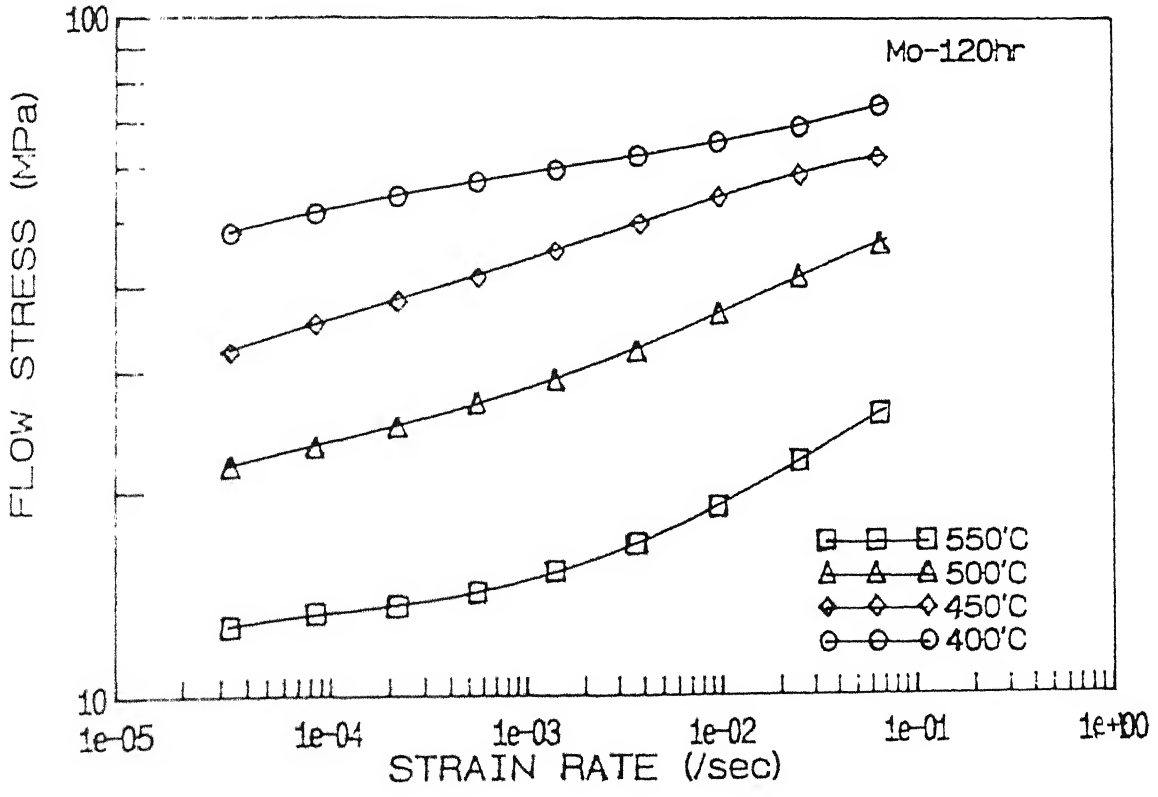

Fig.4.14 : σ-$\dot{\varepsilon}$ behaviour of Mo modified alloy after 120 hr annealing

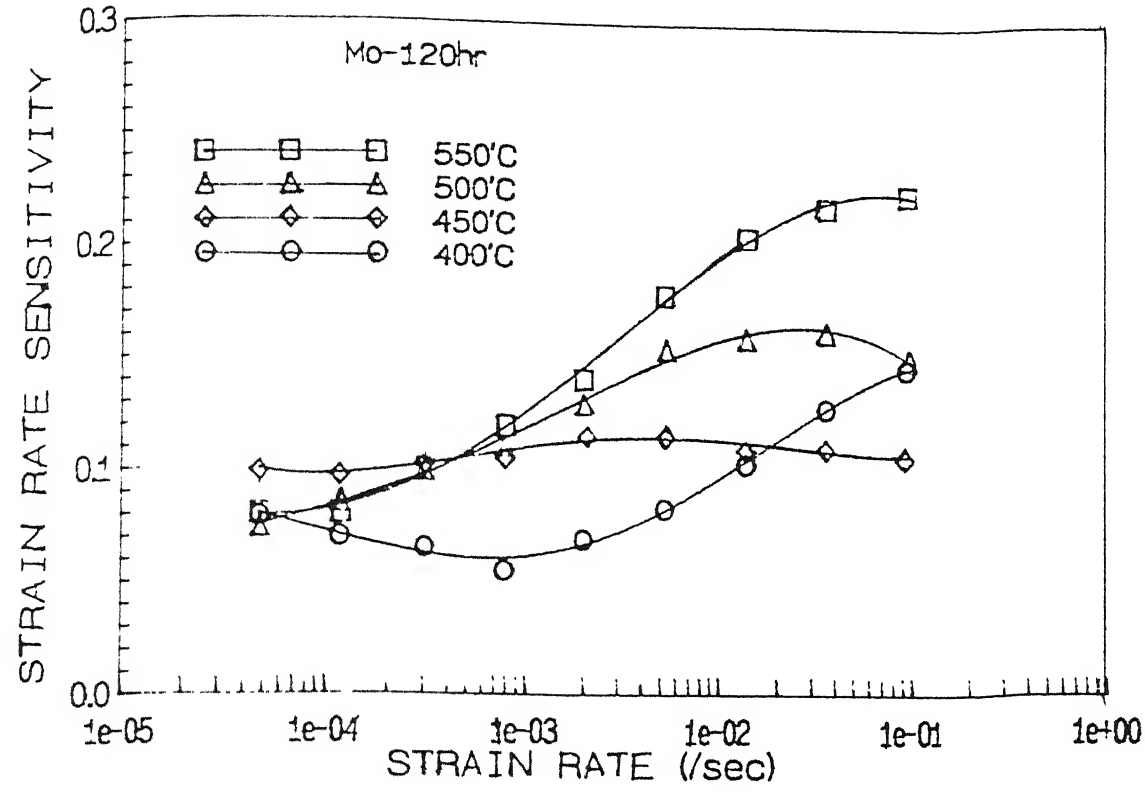

Fig.4.15 : m-$\dot{\varepsilon}$ behaviour of Mo modified alloy after 120hr annealing

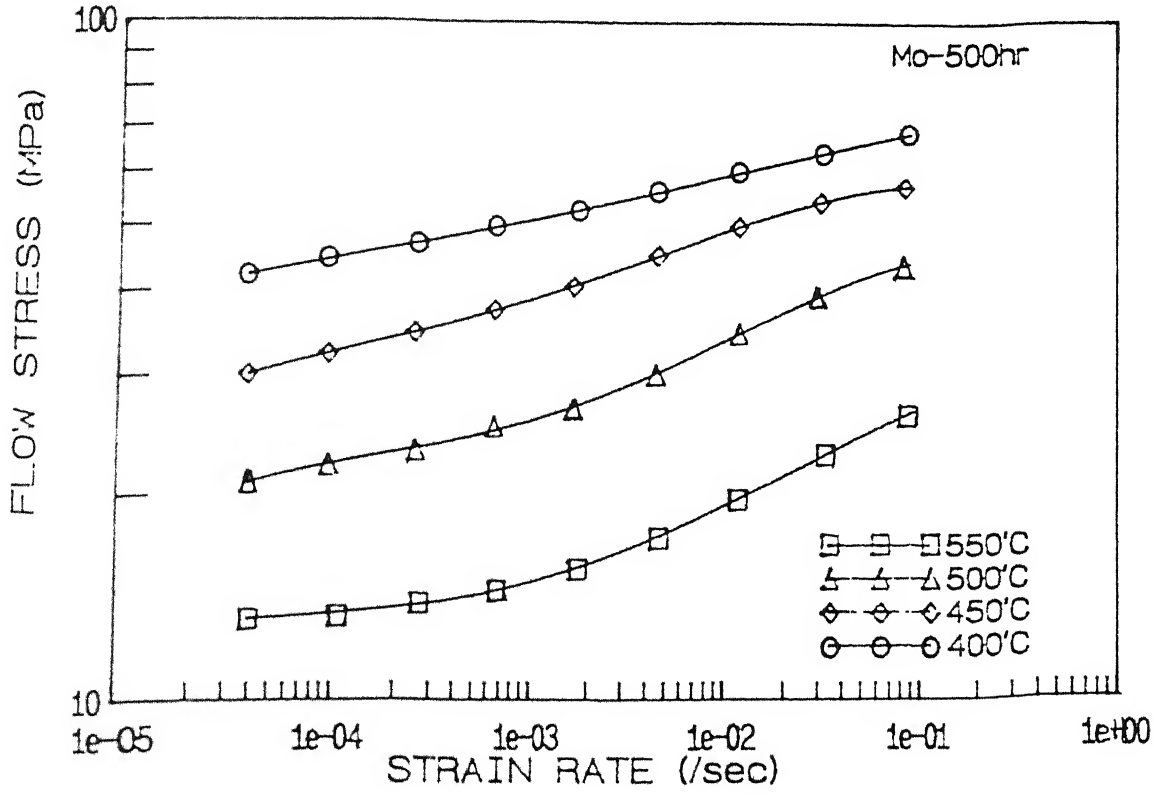

Fig.4.16 : σ-$\dot{\varepsilon}$ behaviour of Mo modified alloy after 500 hr annealing

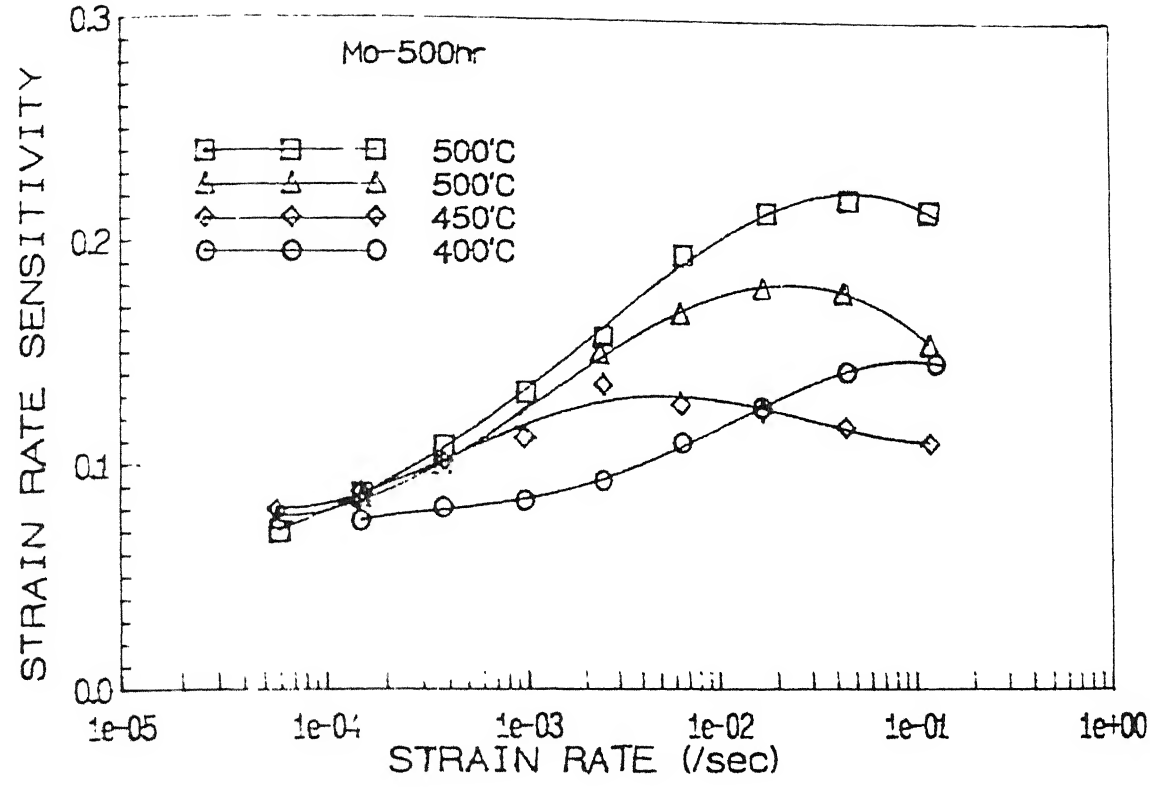

Fig. 4.17 : m-$\dot{\varepsilon}$ behaviour of Mo modified alloy after 500hr annealing

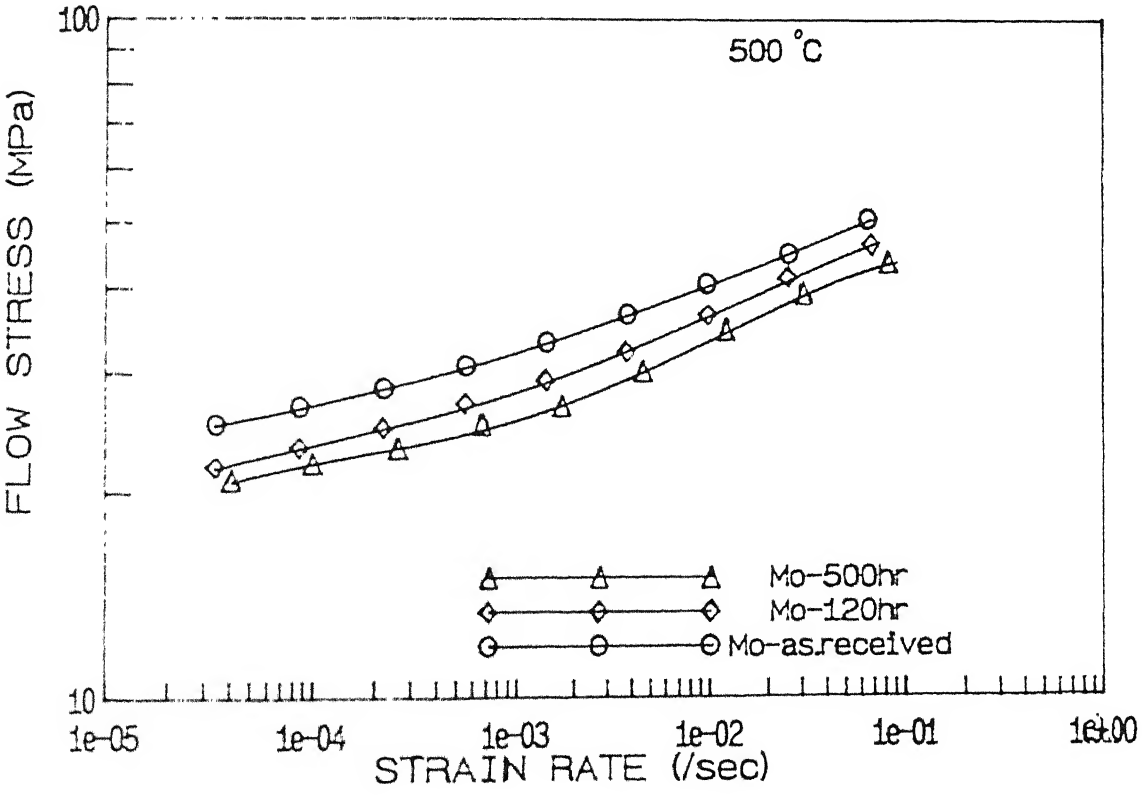

Fig. 4.18 : Comparison of σ-$\dot{\varepsilon}$ behaviour of Mo modified alloys at 500 °C

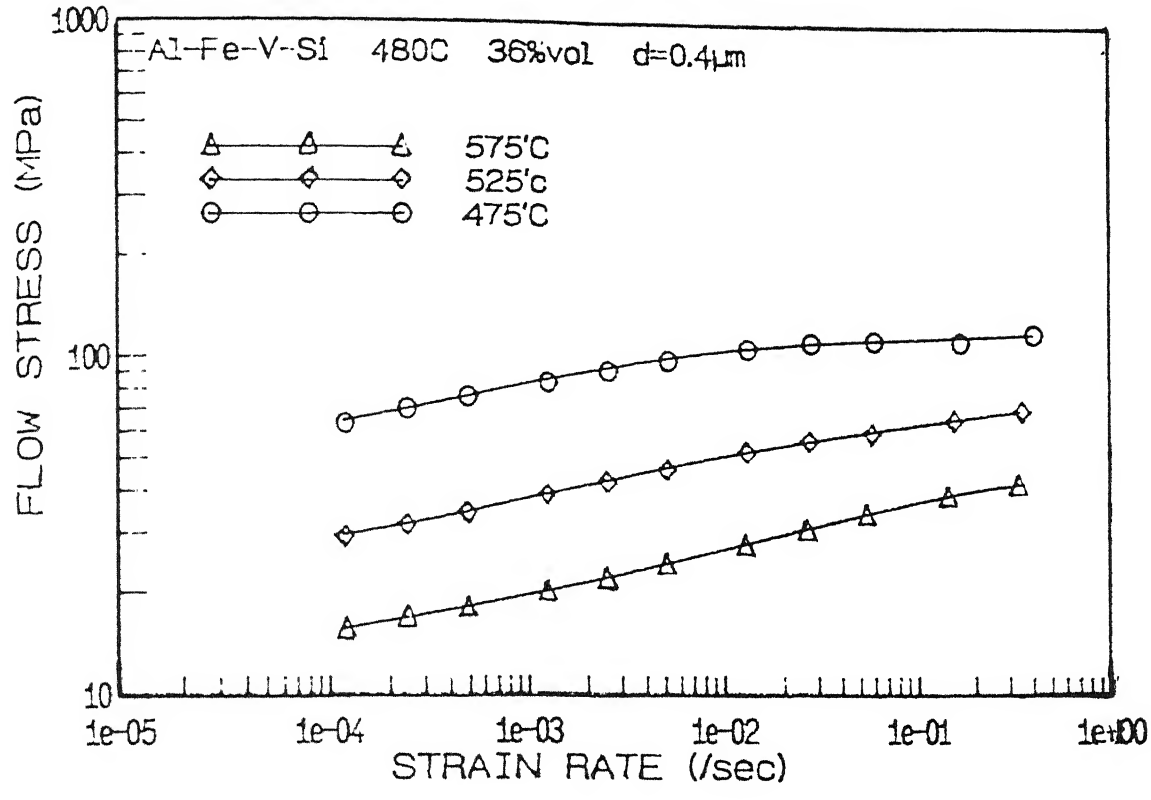

Fig. 4.19 : σ-$\dot{\varepsilon}$ behaviour of Al-Fe-V-Si alloy with 36%vol dispersoid and d=0.4µm

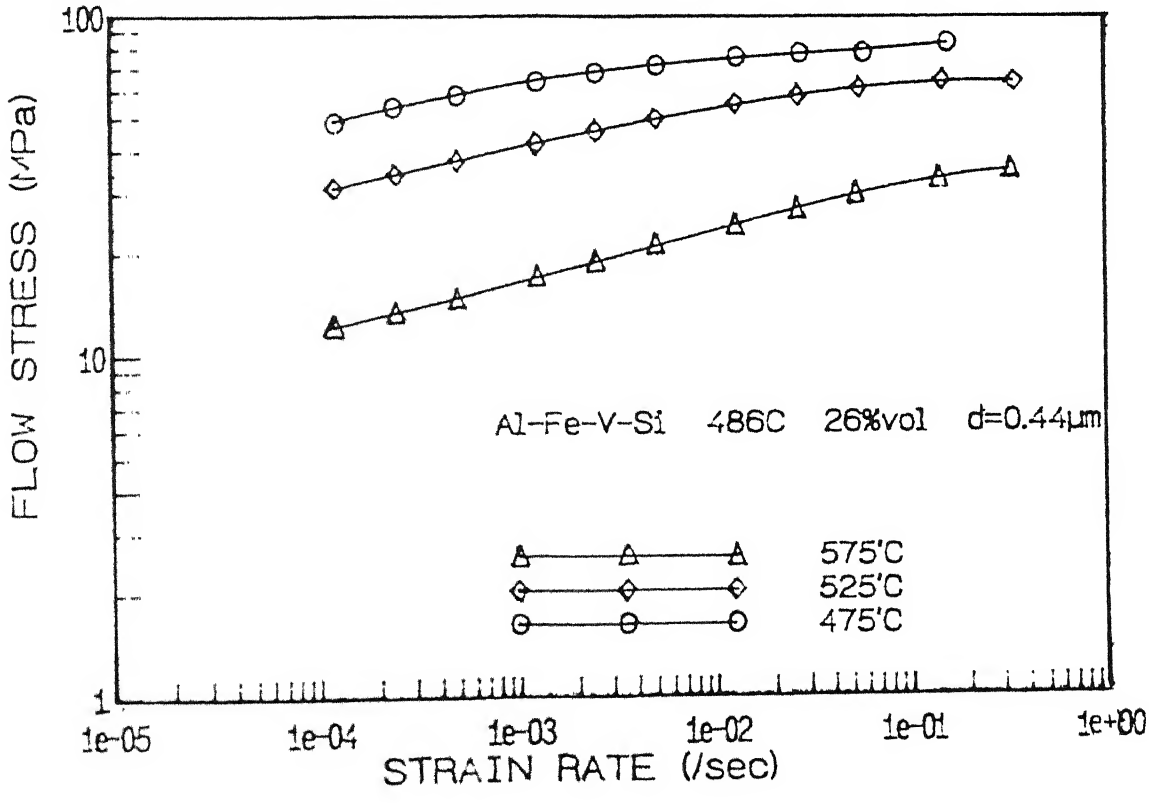

Fig. 4.20 : σ-$\dot{\varepsilon}$ behaviour of Al-Fe-V-Si alloy with 26%vol dispersoid and d=0.44µm

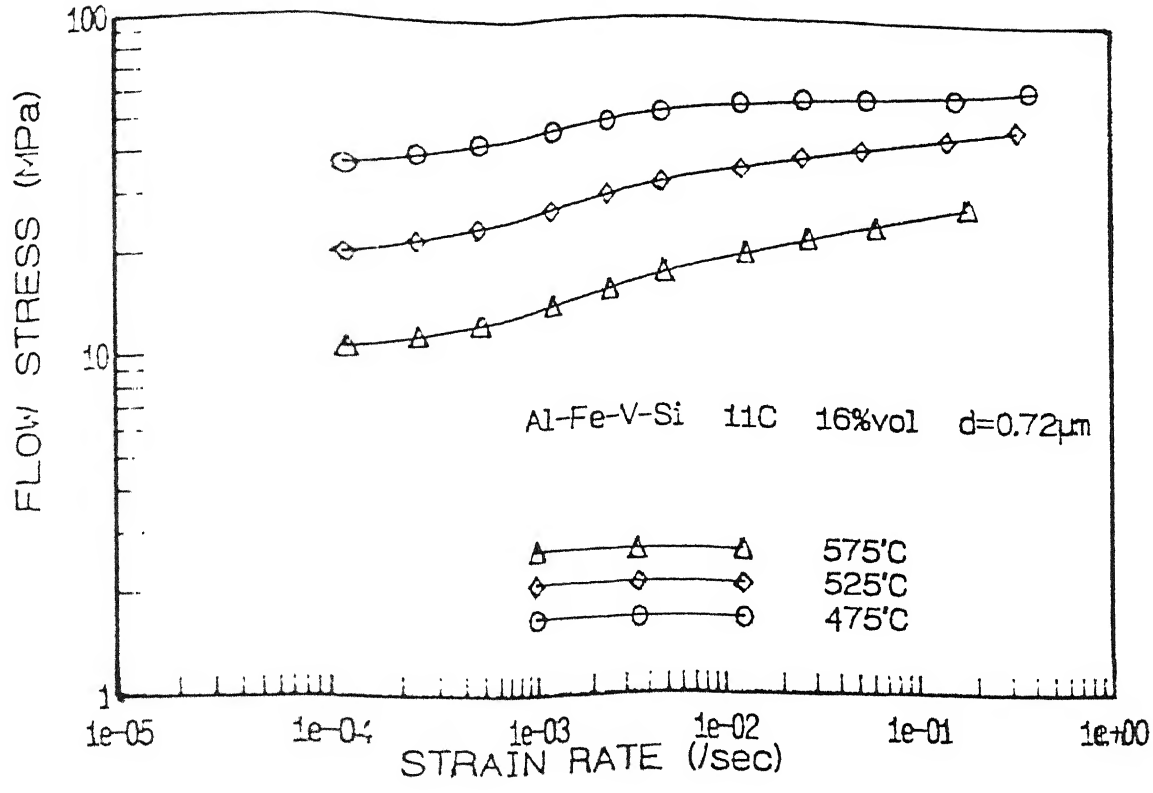

Fig.4.21 : σ-$\dot{\varepsilon}$ behaviour of Al-Fe-V-Si alloy with 16%vol dispersoid and d=0.72µm

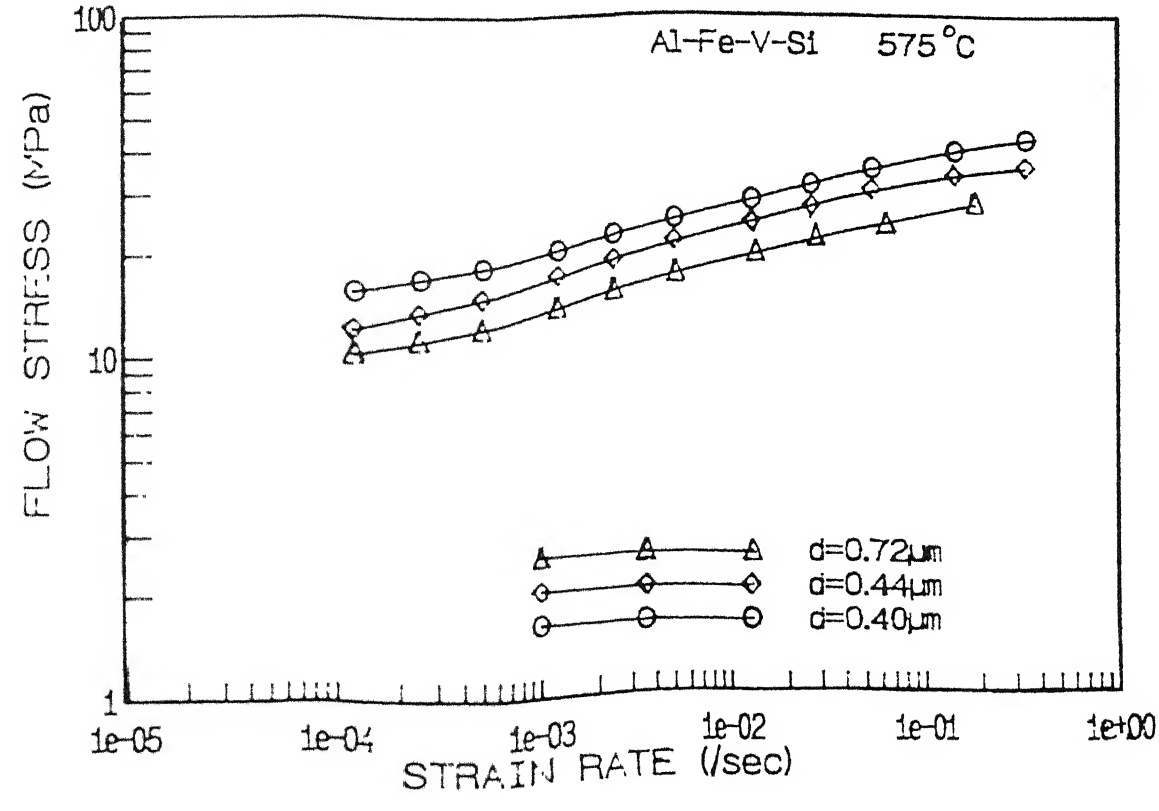

Fig. 4.22 : Comparison of σ-$\dot{\varepsilon}$ behaviour of Al-Fe-V-Si alloys at 575 °C

CHAPTER V

DISCUSSION

The high temperature deformation behaviour of the four alloys shows distinctly two types of trends. Two alloys, Mn modified Al-Zn-Mg-Cu and Al-4% Ti, exhibit high values of m that clearly indicate their superplastic behaviour, whereas the other two alloys, Mo modified Al-Zn-Mg-Cu and Al-Fe-V-Si, show rather low values of m. Hence these four alloys have been classified into two groups which are discussed separately.

5.1 ALLOYS EXHIBITING HIGH m VALUES

5.1.1 STRESS - STRAIN RATE BEHAVIOUR

As regards to the Mn modified Al-Zn-Mg-Cu alloy at 400°C, the $\sigma - \dot{\varepsilon}$ plots show decreasing slope at high strain rate range, especially evident for Mn-120hr and Mn-263hr samples, suggesting the onset of low m region III. At higher temperatures of 450 and 500°C, the $\sigma - \dot{\varepsilon}$ plots show increasing slopes with increasing strain rate for all the grain sizes. The $m - \dot{\varepsilon}$ plots at higher temperatures show only regions I and II and region III seems to be outside the strain rate range experimented. From the maximum m values, tabulated in Table 4.5(a), it is observed that the effect of temperature on it is very distinct. In all the cases, with increase in temperature, the maximum m value of $\sigma - \dot{\varepsilon}$ plot increases signifying the predominance of region II mechanism with increase in temperature. The highest value of m is 0.41 which is a clear indication of superplastic behaviour.

For the Al-4% Ti, the $\sigma - \dot{\varepsilon}$ plots are typically sigmoidal in nature, clearly showing three regions. Their slopes increase with strain rate and then decrease. But region III is

comparatively less prominent in the mechanically alloyed sample (d = 1.0 μm) for which m $\leq$ 0.2 . This value is low compared to the trends shown by the other two grain sizes. Here it is to be noted that the sample has 4 volume percent higher dispersoid content (additional Al_2O_3 and Al_4C_3 dispersoids coming from mechanical alloying process) than the other two. From Table 4.5(b), it is observed that both temperature and grain size (unlike the Mn modified one) have distinct effect on the maximum value of m observed. Maximum m value increases with increase in temperature and also with increase in grain size. The highest value of m observed for this alloy is 0.45 which is even higher than the previously discussed Mn modified Al-Zn-Mg-Cu alloy.

5.1.2 INTERPRETATION OF REGION I IN TERMS OF THRESHOLD STRESS

As discussed in section 3.2.3 and 3.4, the increase in m with the increase in strain rate to a high value characteristic of region II can be interpreted in terms of a threshold stress for superplastic flow. It may be recalled that the constitutive equation for superplastic flow with a threshold stress is given by Eqn. (3.17). If such an equation is applicable, the issue is then to evaluate the best values of σ_o and m that are consistent with the experimental data for each test temperature and grain size. Several σ vs. $\dot{\varepsilon}^m$ plots can be generated with the experimental stress-strain rate data of regions I and II for a series of m values and the one which shows the best linear fit of experimental points should be chosen as the characteristic m for region II flow mechanism. This mode of analysis has been attempted for all the samples (a computer program by means of which such data analysis has been done is given in Appendix B). Typical two results for two alloy samples have been presented in Fig.5.1 and Fig.5.2. In both the cases, best linear fit are obtained in the range m = 0.2 to 0.3. At higher m values, experimental points deviate from linear trend in the low strain rate domain especially for finer grain size and lower temperature, which suggests that the characteristic

m value lies in the range of 0.2 to 0.3 . But this possibility can be ruled out since the characteristic m must be greater than or equal to the experimentally observed maximum m for region II. Thus the manifestation of best linearity of σ vs. $\dot{\varepsilon}^m$ plots with low m values is of little physical significance.

The maximum m for Mn modified Al-Zn-Mg-Cu alloy is 0.41 and that for Al-4% Ti is 0.45 whereas the typically reported value of m for region II of a number of superplastic materials in the literature is 0.50 . Thus it is reasonable to consider an m value of 0.5 as typical of region II flow mechanism. With m=0.5, Eqn. 3.17 reduces to

$$\sigma = \sigma_o + K\dot{\varepsilon}^m \qquad (5.1)$$

For both the alloys, at all temperatures and grain sizes, σ_o is evaluated from the intercept made by the best fit straight line through the experimental points in the linear plot of σ vs. $\dot{\varepsilon}^{0.5}$ and the results are presented in Tables 5.1(a) and 5.1(b) .

Here it is to be noted that when the whole set of grain sizes and temperatures are considered, there are some plots which exhibit reasonable linearity. Nonlinear behavior at low strain rate range is more evident with finer grain size and at lower temperature. But if the characteristic m values were 0.5, then the reason for this deviation from linearity in some cases needs to be assessed. This aspect is discussed in the next section along with its implications.

It is evident from Table 5.1 that σ_o is a strong function of temperature. It drops rapidly with increase in temperature, suggesting that the process causing the threshold barrier is eased out with the thermal energy provided at high temperature. It also seems to drop with the increase in grain size. The temperature and grain size dependence of σ_o is represented by Eqn. 3.13 .

In Figs. 4.7 and 4.11, $\sigma - \dot{\varepsilon}$ plots for various grain sizes have been juxtaposed at a given temperature for Mn modified Al-Zn-Mg-Cu and Al- 4% Ti respectively. Both the alloys show a

crossover of $\sigma - \dot{\varepsilon}$ plots suggesting that the flow stress of specimens of finer grain size is higher than that of coarser grain specimens in region I but the situation is just the opposite in region II. The reason for such a trend was discussed in section 3.3.

Table 5.1(a)

Threshold stress (MPa) for deformation in region II with m = 0.5 for Mn modified Al-Zn-Mg-Cu

Sample	Grain size (μm)	σ_o (MPa) at test temperature °C		
		400	450	500
Mn-as received	0.7	28.6	15.3	9.4
Mn-120hr	1.3	20.8	13.5	7.8
Mn-263hr	2.5	17.1	12.2	6.3

Table 5.1(b)

Threshold stress (MPa) for deformation in region II with m = 0.5 for Al-4%Ti

Sample	Grain size μm	σ_o (MPa) at test temperature °C			
		525	550	575	605
AM-4C (mechanical alloying)	1.0	22	—	10.9	1.9
AT-4	1.3	—	9.2	3.9	1.6
AM-4C	2.6	5.6	—	2.5	0.5

5.1.3 INTERPRETATION OF REGION I BY STRAIN RATE DEPENDENT THRESHOLD STRESS

As illustrated in Figs. 5.1 and 5.2, experimental points show a deviation from linearity in some cases towards lower stress in σ vs. $\dot{\varepsilon}^{0.5}$ plots as the strain rate decreases. Such deviation is more prominent with decreasing temperature and finer grain size as shown in Figs. 5.3 to 5.5. For Mn modified Al-Zn-Mg-Cu alloy, Fig. 5.3 exhibits the effect of temperature for a given grain size at a given temperature and Fig. 5.4 exhibits the effect of temperature for a given grain size. Fig. 5.5 shows similar plots for the Al-4% Ti alloy specimens at various temperatures.

As previously discussed in section 3.5 the deviation from linearity of σ vs. $\dot{\varepsilon}^{0.5}$ plots in the lower strain rate range may be possibly because of a strain rate dependent threshold stress. In that case the overall constitutive equation would be given by Eqn. 3.20. With $m_2 = 0.5$, Eqn. 3.20 reduces to

$$\sigma = K_1 \dot{\varepsilon}^{m_1} + K_2 \dot{\varepsilon}^{0.5} \qquad (5.2)$$

This constitutive equation (which is, however, typical of series type interaction) has three unknown parameters, K_1, K_2, m_1 dividing both sides of Eqn. 5.2 by $\dot{\varepsilon}^{0.5}$, we obtain

$$\left(\frac{\sigma}{\dot{\varepsilon}^{0.5}}\right) = K_2 + K_1 \dot{\varepsilon}^{(m_1 - 0.5)} \qquad (5.3)$$

Given the $\sigma - \dot{\varepsilon}$ data, a series of double linear plots of $\sigma / \dot{\varepsilon}^{0.5}$) vs. $\dot{\varepsilon}^{(m_1-0.5)}$ can be generated for a range of m_1 values. As per Eqn. 5.3, for a certain value of m_1, the plot will be linear over the whole strain rate range with a slope of K_1 and an intercept of K_2. This optimum m can be deduced on the basis of

best fit straight line among those of varying m_1 values. Such plots were generated for m_1 =0.01 to m_1 = 0.20 and the one with the highest correlation coefficient 'r' was identified along with the corresponding values of K_1 ,K_2 and m_1. The optimum values of K_1, K_2 and m_1.with the corresponding value of r for all the samples are tabulated in Table 5.2 (a computer program by means of which such data analysis was done is given in Appendix C).

In Figs. 5.6 to 5.8, constant threshold stress criterion (Eqn. 5.1), strain rate dependent threshold (Eqn. 5.2) criterion and location of experimental points have been juxtaposed for three samples. For generation of constant threshold stress curves (shown as dotted lines), values of σ_o have taken from Table 5.1 and for generation of strain rate dependent threshold curves (shown as solid lines), values of K_1 ,K_2 and m_1 have been taken from Table 5.2. In all the cases strain rate dependent threshold stress criterion shows better compatibility with experimental data than the constant threshold hypothesis. The difference between these two is most prominently visible in the low strain rate range.

Thus it appears that the threshold stress for superplastic flow is strain rate dependent in addition to its dependency on temperature and grain size. The strain rate sensitivity index of the threshold process varies over a narrow range in all cases and a value of $m_1 \approx 0.1$ can be considered as representing the entire set of data irrespective of temperature and grain size of both the alloys.

The value of the correlation coefficient ,r_1, is seen to be grater than 0.99 in all the cases which justifies the mean m_1 as characteristic of the process responsible for the threshold stress. Comparing the K_1 and K_2 values for both the alloys it is observed that both decrease with rise in temperature. It can also be noted from the data of table 5.3 that K_1 and K_2 are grain size dependent at a given temperature. While K_1 decreases with increasing grain size, K_2 varies the opposite way with grain size. Considering the relation between K and grain size (d) in Eqn. 3.18, it can be inferred that the threshold stress process with characteristic strain rate sensitivity of 0.10 has a negative

Table 5.2

Optimum values of m_1, K_1 and K_2 in Eqn. 5.2

Alloy	Sample	d (μm)	Temp (°C)	m_1	K_1	K_2	r
Mn modified Al-Zn-Mg-Cu	Mn-as received	0.07	400	0.08	54.0	81.7	0.9999
			450	0.08	29.4	48.3	0.9999
			500	0.06	15.14	24.5	0.9999
	Mn-120hr	1.3	400	0.11	61.1	128.6	0.9999
			450	0.10	29.9	70.7	0.9999
			500	0.13	23.0	19.7	0.9999
	Mn-263hr	2.5	400	0.13	61.0	287.2	0.9969
			450	0.13	38.1	107.6	0.9999
			500	0.11	16.7	52.0	0.9997
Al - 4% Ti	AM - 4C Mech alloyed	1.0	525	0.05	33.5	23.8	1.0000
			575	0.05	16.0	27.61	0.9998
			605	0.07	3.3	10.0	1.0000
	AT - 4	1.6	550	0.10	21.1	61.0	0.9999
			575	0.12	11.0	47.1	1.0000
			605	0.10	3.0	23.4	0.9996
		2.6	525	0.13	18.3	97.2	0.9999
			575	0.13	7.8	61.2	0.9994
			605	0.06	1.0	30.6	0.9990

TABLE 5.3

Values of K_1 and K_2 in Eqn. 5.2 with m = 0.10 for Al-Zn-Mg-Cu-Mn and Al-4%Ti

Alloy	Sample	d (μm)	Temp (°C)	K_1	K_2	r
Mn modified Al-Zn-Mg-Cu	Mn - as received	0.7	400	66.3	33.3	0.9996
			450	36.1	21.7	0.9998
			500	22.8	7.3	0.9993
	Mn - 120hr	1.3	400	54.8	161.7	0.9999
			450	30.0	70.7	0.9999
			500	17.24	36.5	0.9998
	Mn - 263hr	2.5	400	44.5	367.1	0.9980
			450	27.5	160.4	0.9994
			500	15.0	58.9	0.9997
Al - 4% Ti	AM - 4C Mech alloyed	1.0	525	54.6	31.9	0.9994
			575	25.8	17.1	0.9990
			605	4.4	8.6	0.9997
	AT - 4	1.6	550	21.1	61.0	0.9999
			575	9.0	54.2	0.9999
			605	3.0	23.4	0.9996
	AT - 4C	2.6	525	13.5	117.0	0.9998
			575	5.8	69.6	0.9991
			605	1.4	29.0	0.9987

grain size exponent p, whereas the deformation process with strain rate sensitivity 0.50 has a positive value of p.

The process with a strain rate sensitivity of 0.5 can be identified as the grain boundary sliding mechanism, an integral part of superplastic deformation. The other process with a strain rate sensitivity of 0.10 seems to be an accommodation process (see section 2.2.1.2) which relaxes stress concentration generated by grain boundary sliding so that further sliding may take place. Keeping in mind the low value of m_1, this process may be a dislocation mechanism where the physical rearrangement of matter take place by the movement of dislocations and hence stress concentration is released. Grain boundary migration and local diffusion may be the alternative mechanisms of stress relaxation during grain boundary sliding. The expression of K as given in Eqn.3.18 can be rewritten as

$$K = A\, d^{pm} \exp(Qm/RT) \qquad (5.4)$$

Where A = constant

Q = activation energy

The activation energy of the process can be evaluated from the slope of ln K vs 1/T type Arrhenius plot for a constant grain size whereas the grain size exponent p can be found from the slope of ln K vs ln d plot for a constant temperature. The values of Q and p for K_1 and K_2 are listed in Table 5.4 and 5.5. (note: The values of K_1 and K_2 are taken from Table 5.3)

Table 5.4

Activation energy (Q) of K_1 and K_2 for Al-Zn-Mg-Cu-Mn and Al-4%Ti

Alloy	Sample	Q for K_1 (KJ/mole)	Q for K_2 (KJ/mole)
Mo modified Al-Zn-Mg-Cu	Mn-as received d=0.7 μm	452.0	127.4
	Mn-120hr d=1.3 μm	489.0	125.8
	Mn-263hr d=2.5 μm	457.2	154.2
Al-4%Ti	AM-4C d=1.0 μm	1672.3	180.4
	AM-4 d=1.6 μm	2095.1	206.7
	AT-4C d=2.6 μm	1523.7	188.2

Table 5.5

Grain size exponent (p) of K_1 and K_2 for Al-Zn-Mg-Cu-Mn and Al-4%Ti

Alloy	Temperature °C	p for K_1	p for K_2
Mn modified Al-Zn-Mg-Cu	400	-3.1	3.7
	450	-2.1	3.1
	500	-3.2	2.3
Al - 4% Ti	575	-15.6	2.9
	605	-11.9	2.5

For Al-Zn-Mg-Cu-Mn

average activation energy for K_1 = 466.1 kJ/mole

average activation energy for K_2 = 135.8 kJ/mole

average grain size dependence for K_1 = - 2.8

average grain size dependence for K_2 = 3.0

For Al-4% Ti

average activation energy for K_1 = 1763.5 kJ/mole

average activation energy for K_2 = 192.4 kJ/mole

average grain size dependence for K_1 = 14.3

average grain size dependence for K_2 = 2.7

The grain size dependence of K_1 for Al-4%Ti alloy is anomalously high and so is the activation energy of K_1 for both the materials. The typical value of p for region II is 2-3. Thus for both the materials, grain size exponent p of K_2 is well within the expected range. The grain size dependence of K_1 is, however, higher than that that found out by Murty et al. [22,23] estimated on the basis of threshold stress.

5.1.4 POSSIBILITY OF m = 1 AS REGION II MECHANISM

Although in this investigation, characteristic m value for superplastic deformation was considered to be 0.5, its basis can be justifiably argued since theoretically strain rate sensitivity index of a flow process can be as high as unity. This aspect has been previously discussed in section 3.6. Hence it may be desirable to explore the applicability of a constitutive

equation with m = 1 and appropriate threshold stress that may in general depend on strain rate. The constitutive equation of such a type is

$$\sigma = K_1 \dot{\varepsilon}^{m_1} + K_2 \dot{\varepsilon} \qquad (5.5)$$

Similar to the mode of analysis in section 5.1.3, (σ/ε) vs. $\dot{\varepsilon}^{(m_1-1)}$ plots were generated for m_1 = 0 to 0.5, but no m_1 could give a reasonably good linear fit with the experimental data of any specimen. A typical case is shown in Fig. 5.9 for Mn-263 sample with m_1 = 0 to 0.1. Incidentally, pure diffusion creep as described in Eqn. 2.4 has a m value of unity. But the presence of dispersoids is likely to introduce a threshold stress in the constitutive equation of pure diffusional flow for dispersion strengthened alloys. Then the applicability of the constitutive Eqn 2.4 coupled with a threshold stress may be considered for the data of regions 1 and 2. The following values of the requisite parameters of the constitutive equation are used for this purpose.

lattice parameter = 4.04 Å

D_{o_l} = 1.71 cm^2/sec $\qquad$ $D_{o_{gb}}$ = 0.028 cm^2/sec

Q_l = 34 kCal/mole $\qquad$ Q_{gb} = 19.5 kCal/mole

R = 1.987 Cal/mole/°K

δ_{gb} = 5 Å

Using these values in Eqn. 2.4 along with different values of σ_o, the constitutive equation of pure diffusional flow mechanism for dispersion strengthened materials has been plotted and compared with the experimental curve. But the match between the theoretical and the experimental curves is far from satisfactory. Fig.5.10 is shown as a typical case to affirm that superplastic flow mechanism for fine grained dispersion strengthened materials does not correspond to an m value of unity along with a threshold stress.

5.1.5 POSSIBILITY OF AN INDEPENDENT FLOW MECHANISM AT LOW STRAIN RATE

As discussed previously in chapter 3.8, if the threshold stress is very high then the region III mechanism may interfere with region I (Fig.3.12). To check this possibility some $\sigma - \dot{\varepsilon}$ plots of Al-4%Ti were considered where the region III was clearly visible. On extrapolating the region III portion of AT-4C sample (Fig.4.10) tested at 525 and 575°C back to low strain rate range, it is observed that the extrapolated line can no way intersect the region I portion within the strain rate range experimented. So for Al-4%Ti alloy, it can be affirmed that its low strain rate behavior is not influenced by the region III mechanism. However, this possibility can not not be explored for other alloys due to the non appearance of region III within the strain rate range dealt with.

5.2 ALLOYS EXHIBITING LOW STRAIN RATE SENSITIVITY

Two alloys, Mo modified Al-Zn-Mg-Cu and Al-Fe-V-Si are grouped in this category.

5.2.1 Stress-Strain Rate Behaviour

At 400°C, all the $m - \dot{\varepsilon}$ plots of Mo modified Al-Zn-Mg-Cu alloy show a trough - like trend, i.e., m value decreases with increase in strain rate and then again increases. At 450°C, the slopes of the $\sigma - \dot{\varepsilon}$ plots in all the three cases show insensitivity to strain rate, as a result of which the $m - \dot{\varepsilon}$ plots look more or less flat. At higher temperatures 500 and 550°C, the m values increase with strain rate to about 0.2 and then become constant or show a slight decrease in some cases.

As regards to Al-Fe-V-Si alloys [24], the $m - \dot{\varepsilon}$ plots are either flat or having a small peak at all the test temperatures, i.e., m values increase with strain rate, exhibit a plateau region and then drop ..The highest m value is around 0.15.

At a given temperature, the $\sigma - \dot{\varepsilon}$ plots for varying

grain sizes and dispersoid content are compared for two alloys in Fig. 4.18 and 4.22. These plots look nearly parallel to each other unlike the cross-over trend shown by the other group of higher m alloys. Another important observation is that the $\sigma - \dot{\varepsilon}$ plots shift to lower flow stress as the grain size increases, suggesting a negative value of grain size exponent p throughout the strain rate range. Among the Al-Fe-V-Si alloys, two have almost identical grain sizes of 0.40 μm and 0.44 μm, yet their σ-$\dot{\varepsilon}$ plots are significantly different. This behaviour may be attributed to the fact that although their grain sizes are similar, they have widely different dispersoid content (36 volume pct. for d=0.40 μm and 26 volume pct. for d=0.44 μm). Apart from the temperature and grain size, the dispersoid content seems to affect the σ-$\dot{\varepsilon}$ behaviour. Thus while analyzing the stress-strain rate behaviour of Al-Fe-V-Si at a constant temperature, the dispersoid content should be considered along with the grain size.

These two types of alloys have ultrafine microstructures amenable to superplasticity. On the other hand creep resistance can also be expected through the presence of fine dispersoids which inhibit dislocation motion at elevated temperatures. As discussed in section 3.9, such cases of low m behaviour can be interpreted from two very different viewpoints. Firstly, it might be a case of suppressed superplasticity where region II is eclipsed by high magnitude of threshold stress on one hand and early onset region III on the other. Thereby, region II is restrained from attaining its high characteristic m value. Secondly, it might be a case of normal plasticity, i.e., dislocation creep.

The experimental data for these two alloys are analyzed from both of these viewpoints in an endeavour to find a way to distinguish between these two possibilities.

5.2.2 INTERPRETATION IN TERMS OF SUPERPLASTICITY

Similar to the analysis of the high rate sensitivity materials as in section 5.1.2, σ vs. $\dot{\varepsilon}^{m}$ plots were

generated for m = 0.1 to m = 0.5. Two typical results of such analysis are shown in Fig. 5.11 and 5.12. Best linearity, as per the regression analysis, is observed for m = 0.2. At higher m values the plots deviate from linearity in the low strain rate range especially at lower temperatures. The typical m value of 0.5 is considered for the interpretation of data in terms of a constant threshold stress for superplastic deformation. The correlation coefficient was in the range of 0.92 to 0.97 for m = 0.5. The calculated values of σ_o and K (as per Eqn. 5.1) by this analysis are tabulated in Tables 5.6 and 5.7. Typical σ vs. $\dot{\varepsilon}^m$ plots for the two alloys are shown in Fig. 5.13 and 5.14 at different temperatures.

For both the alloys, the activation energy deduced from the temperature dependence of K is close to that for Q_{gb}. Another important observation is that both σ_o and K have a negative grain size exponent p.

In view of the nonlinear nature of the plots especially at lower temperatures, the data are further analyzed in terms of a strain rate dependent threshold stress as in section 5.1.3. The optimum values of K_1 ,K_2 ,m_1 and corresponding values of r are shown in Table 5.8.

Table 5.6(a)

Threshold stress (MPa) for Mo modified Al-Zn-Mg-Cu alloy with m = 0.5

Sample	σ_o (MPa) at test temperature		
	450	500	550
Mo-as received	35.4	27.9	15.5
Mo-120hr	34.2	23.1	13.0
MO-500hr	31.3	21.6	12.4

Table 5.6(b)

Threshold stress (MPa) for Al-Fe-V-Si with m = 0.5

Sample	σ_o (MPa) at test temperature °C		
	475	525	575
16 vol pct. d=0.72μm	35.9	20.3	10.2
26 vol pct. d=0.44μm	46.2	27.0	12.2
36 vol pct. d=0.40μm	59.7	29.1	16.2

Table 5.7 (a)

Values of K with m = 0.5 for Mo modified Al-Zn-Mg-Cu

Sample	K at test temperature °C			Activation energy kJ/mole
	450	500	550	
Mo-as received	421.7	161.8	54.9	198.2
Mo-120hr	224.3	151.5	53.3	139.4
Mo-500hr	182.8	108.0	57.1	111.6

Table 5.7 (b)

Value of K with m = 0.5 for Al-Fe-V-Si alloy

Sample	K at test temperature °C			Activation energy kJ/mole
	475	525	575	
16 vol pct. d=0.72μm	246.0	149.5	88.8	105.8
26 vol pct. d=0.44μm	359.2	287.1	115.9	115.4
36 vol pct. d=0.40μm	683.1	283.9	101.8	196.6

For the Mo modified alloy, the average m_1 is 0.05, whereas that for Al-Fe-V-Si is 0.11. The K_1 and K_2 values corresponding to the respective average m_1 values are given in Table 5.9 (a) and (b).

It is seen from the data in Table 5.9 that K_1 and K_2 decrease with the rise in temperature for both the alloys. But due to the scatter in the data in some cases the effect of grain size is not well defined, although the implicit trend seems to suggest a negative value of p. Here it is to be noted that the grain size exponent of K is also negative (Table 5.7) when the threshold stress is considered to be independent of strain rate. Making use of the temperature dependent K_1 and K_2 values, The activation energy has been evaluated in each case and the resulting data are listed in Tables 5.10 (a) and (b).

In Figs. 5.5 and 5.6, the computed stress-strain rate data based on constant threshold stress and strain rate dependent threshold stress concepts are compared with the experimental data for two materials. The data calculated on the basis of strain rate dependent threshold stress is seen to correlate better with the experimental data.

Table 5.8

Optimum values of m_1, K_1 and K_2 in Eqn. 5.2 for Al-Zn-Mg-Cu-Mo and Al-Fe-V-Si

Alloy	Sample	Temp. (°C)	m_1	K_1	K_2	r
Mo modified Al-Zn-Mg-Cu	Mo- as received	450	0.08	82.87	34.14	1.0000
		500	0.06	46.02	52.99	1.0000
		550	0.03	19.85	29.84	1.0000
	Mo - 120hr	450	0.09	81.15	6.77	1.0000
		500	0.06	39.70	63.17	1.0000
		550	0.02	15.22	48.85	1.0000
	Mo 500hr	450	0.07	60.46	48.43	1.0000
		500	0.05	33.88	60.50	1.0000
		550	0.02	15.59	41.21	0.9999
Al-Fe-V-Si	11C 16 vol% d = 0.72μm	475	0.09	81.89	33.70	0.9997
		525	0.12	58.30	18.34	0.9999
		575	0.10	24.73	34.42	1.0000
	480C 26 vol% d = 0.44μm	475	0.11	132.48	27.47	0.9993
		525	0.12	91.97	26.60	0.9999
		575	0.13	39.02	21.49	1.0000
	486C 36 vol% d = 0.40μm	475	0.12	190.66	9.00	0.9998
		525	0.12	87.55	6.39	1.0000
		575	0.09	34.54	43.38	1.0000

Table 5.9(a)

K_1 and K_2 values for Mo modified Al-Zn-Mg-Cu with m = 0.05

Sample	Temp. °C	K_1	K_2	r
Mo - as received	450	59.41	212.4	0.9998
	500	41.42	77.93	1.0000
	550	24.08	9.76	0.9999
Mo - 120 hr	450	52.54	187.97	0.9995
	500	35.68	87.78	1.0000
	550	20.84	14.78	0.9997
Mo - 500 hr	450	48.88	121.50	0.9999
	500	33.87	60.50	1.0000
	550	21.22	9.83	0.9994

Table 5.9(b)

K_1 and K_2 values for Al-Fe-V-Si with m = 0.11

Sample	Temp °C	K_1	K_2	r
460 C 16 vol% d = 0.72μm	525	52.73	39.62	0.9998
	575	27.31	24.13	1.0000
460 C 26 vol% d = 0.44μm	475	130.44	84.07	0.9993
	525	83.03	64.65	0.9998
	575	31.93	47.78	0.9999
486 C 36 vol% d = 0.40μm	475	171.80	96.60	0.9997
	525	79.06	42.23	1.0000
	575	41.95	15.86	0.9999

Table 5.10(a)

Activation energy (Q) with m = 0.5 for Al-Zn-Mg-Cu-Mo

Sample	Q for K_1 (kJ/mole)	Q for K_2 (kJ/mole)
Mo-as received	868.1	294.8
Mo-120hr	890.5	243.6
Mo-500hr	803.9	240.8

Average activation energy for K_1=854.3 kJ/mole

Table 5.10(b)

Activation energy (Q) with m = 0.5 for Al-Fe-V-Si

Sample	Q for K_1 (kJ/mole)	Q for K_2 (kJ/mole)
26 vol pct. d=0.44μm	653.6	58.0
36 vol pct. d=0.40μm	660.9	185.8

5.2.3 INTERPRETATION IN TERMS OF DISLOCATION CREEP BEHAVIOUR

As these two alloys show low strain rate sensitivity, which is a characteristic of dislocation controlled creep, their stress-strain rate behaviour is also analyzed from the point of view of creep type of behaviour.

With reference to the Fig. 5.11 and 5.12, the σ-$\dot{\varepsilon}^m$ plots for various values of m show best linearity, as per the regression analysis, for m = 0.2. On the other hand, it is to be noted that the maximum m value for Mo modified Al-Zn-Mg-Cu alloy is around 0.22 and that for Al-Fe-V-Si is 0.16. Thus it is quite reasonable to consider the characteristic m value for creep deformation to be 0.2 for both the alloys. Furthermore the region III of superplastic materials is usually identified as the dislocation creep region with a typical m value of 0.2.

The threshold stress for creep is found from the intercept of the regression line through the experimental points on the σ vs. $\dot{\varepsilon}^m$ plots. such plots for the two alloys at different temperatures are shown in Figs. 5.17 and 5.18. The values of σ_o thus obtained are presented in Tables 5.11(a) and (b) along with the corresponding correlation coefficient r and the activation energy of the process responsible for threshold process.

In spite of some scatter in the data for the Mo modified alloy, the threshold process for both the materials appears to have a negative grain size exponent. The values of K with m = 0.2 are shown in Tables 5.12(a) and (b) along with the activation energy.

It is seen from these data that K for the Mo modified Al-Zn-Mg-Cu alloy is nearly independent of grain size as it is the case in dislocation creep normally. But K for Al-Fe-V-Si alloy shows a negative grain size exponent.

5.2.4 COMMENTS ON THE OPERATIVE FLOW MECHANISM

Among the two approaches for the interpretation of flow behaviour of low m alloys, the choice cannot be made by only looking at the fit of the constitutive equation with the experimental data as quantified by the correlation coefficient r in Table 5.9 (for strain rate dependent threshold stress concept) and Table 5.11 (for dislocation creep behaviour), since in both the cases usually r> 99%. So in order to discriminate between these two options, there is a need to consider the associated parameters, such as the activation energy and grain size

dependence for the mechanisms involved.

As regards to the high m alloys, at a given temperature, the cross-over of $\sigma - \dot{\varepsilon}$ plots for various grain sizes can be substantiated by the observation that K_1 has a negative value of p while K_2 has a positive value (as shown in Table 5.5). On the other hand, in the analysis of the low m materials, assuming it to be a case of suppressed superplasticity, p for K_1 is again negative. But in contrast to the high m materials, p for K_2 is negative. If the analysis based on a constitutive equation for superplastic flow with a threshold stress is applicable to Mo modified Al-Zn-Mg-Cu and Al-Fe-V-Si alloys (as analyzed in section 5.2.2 with $m_2 = 0.5$), then the grain size exponent p of K_2 would be expected to be positive like that for two other superplastic materials. This is because the grain boundary sliding, an integral part of the superplastic mode of deformation, is easier for finer grains. Thus the characteristic of deformation behaviour of this group of alloys in terms of the constitutive equation with $m_2 = 0.5$ results in a negative grain size exponent for K_2, which is not consistent with the superplastic flow mechanism. Rather, the other approach, i.e., interpretation in terms of dislocation creep behaviour appears more appropriate.

Table 5.11 (a)

Creep threshold stress (σ_o) with m = 0.2 for Al-Zn-Mg-Cu-Mo

Sample	Temp °C	σ_o (MPa)	r	Q (kJ/mole)
Mo as-received	450	24.5	.9969	39.36
	500	18.1	.9999	
	550	10.8	.9901	
Mo-120hr	450	22.7	.9970	49.65
	500	14.6	.9992	
	550	13.7	.9855	
Mo-500hr	450	10.8	.9996	51.32
	500	8.1	.9964	
	550	7.3	.9912	

Average activation energy for threshold process = 46.7 kJ/mole

Table 5.11 (b)

Creep threshold stress (σ_o) with m = 0.2 for Al-Fe-V-Si

Sample	Temp °C	σ_o (MPa)	r	Q (kJ/mole)
16 vol pct. d=0.72μm	475	23.7	.9924	87.92
	525	10.2	.9983	
	575	4.3	.9998	
16 vol pct. d=0.72μm	475	27.7	.9858	82.24
	525	13.2	.9875	
	575	5.6	.9995	
16 vol pct. d=0.72μm	475	32.2	.9963	74.30
	525	16.3	.9992	
	575	7.7	1.0000	

Average activation energy for threshold process = 81.5 kJ/mole

Table 5.12 (a)

Values of K with m = 0.2 for Mo modified Al-Zn-Mg-Cu

Sample	K at test temperature °C			Activation energy kJ/mole
	450	500	550	
Mo as received	90.5	56.1	25.5	304.2
Mo-120hr	81.1	55.3	29.1	246.3
Mo-500hr	69.6	50.0	28.1	217.5

Average activation energy for K = 256.0 kJ/mole

Table 5.12(b)

Value of K with m = 0.2 for Al-Fe-V-Si alloy

Sample	K at temperature °C			Activation energy kJ/mole
	475	525	575	
16 vol pct. d=0.72μm	83.1	62.1	36.7	209.2
26 vol pct. d=0.44μm	122.2	80.1	47.6	242.4
36 vol pct. d 0.40μm	200.1	91.9	49.1	362.7

Average activation energy for K = 271.1 kJ/mole

The deformation mechanism for the Mo modified alloy might be identified with the dislocation creep process since dislocation creep has a very weak grain size dependence ($p \approx 0-1$). But, the negative grain size exponent of K of the Al-Fe-V-Si alloys differs from the constitutive equation for the dislocation creep mechanism. The negative value of p for K in Al-Fe-V-Si seems to suggest the retention of the grain boundary strengthening effect at elevated temperature, which might be due to the presence of dispersoids at the grain boundaries. This type of grain boundary strengthening effect resembles the Hall-Petch relation [26, 27] applicable to low temperature behaviour, but this relation has a lower grain size exponent (= - 0.5) than that observed in the Al-Fe-V-Si alloys.

The rationalization of this behaviour may be done in terms of the reinforcement effect introduced by the high content (upto 0.36 volume fraction) of intermetallic dispersoids

in the Al-Fe-V-Si alloys. Such a large content of intermetallic dispersoids might as well enable this material to behave like a particle reinforced metal-matrix composite. The observation of 'the increase in flow stress with the drop in grain size' should rather be interpreted as 'the increase in flow stress with the increase in dispersoid content' (as the higher volume fraction yields finer grain size). the composite reinforcement effect through the load sharing by the fine intermetallic particles is probably responsible for the observation of the *apparent* negative grain size exponent of the flow process of the Al-Fe-V-Si alloys. Thus, for this alloy, the observed increase in strength with volume fraction of dispersoids at all the temperatures and strain rates is probably a consequence of this composite strengthening effect rather than the grain size effect.

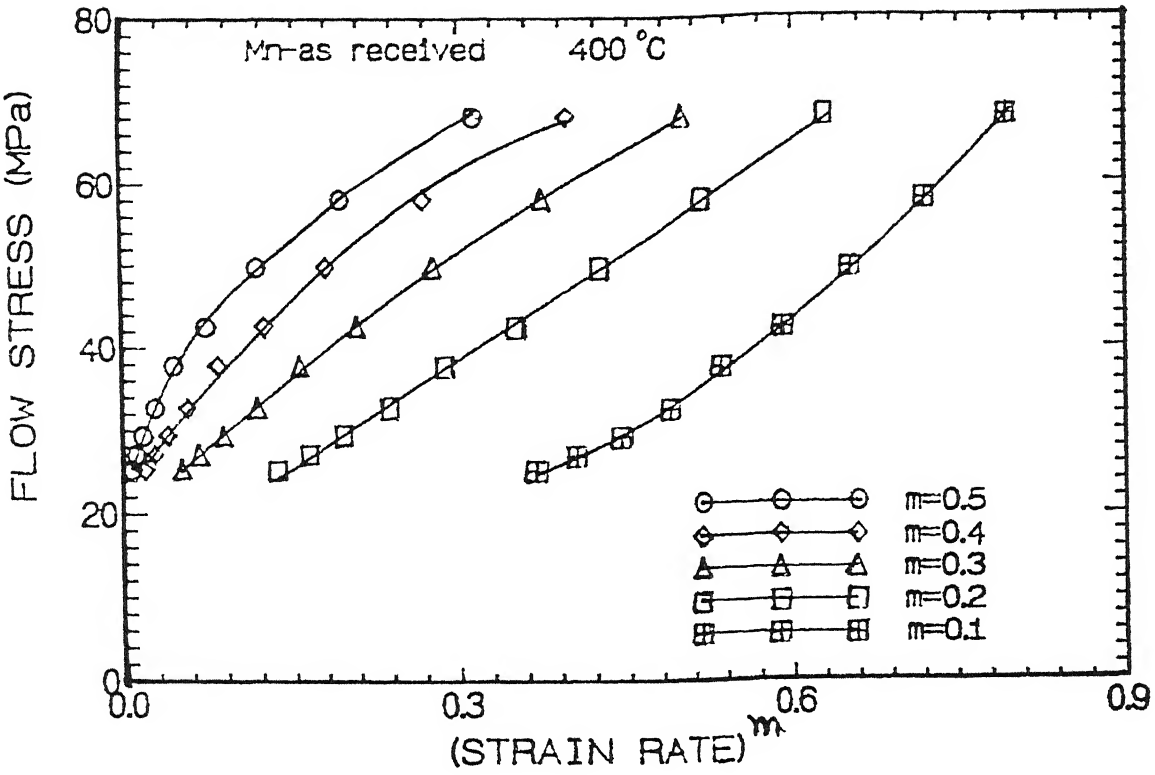

g. 5.1 : σ-$\dot{\varepsilon}^m$ behaviour of Mn modidied alloy in as received condition at 400 °C

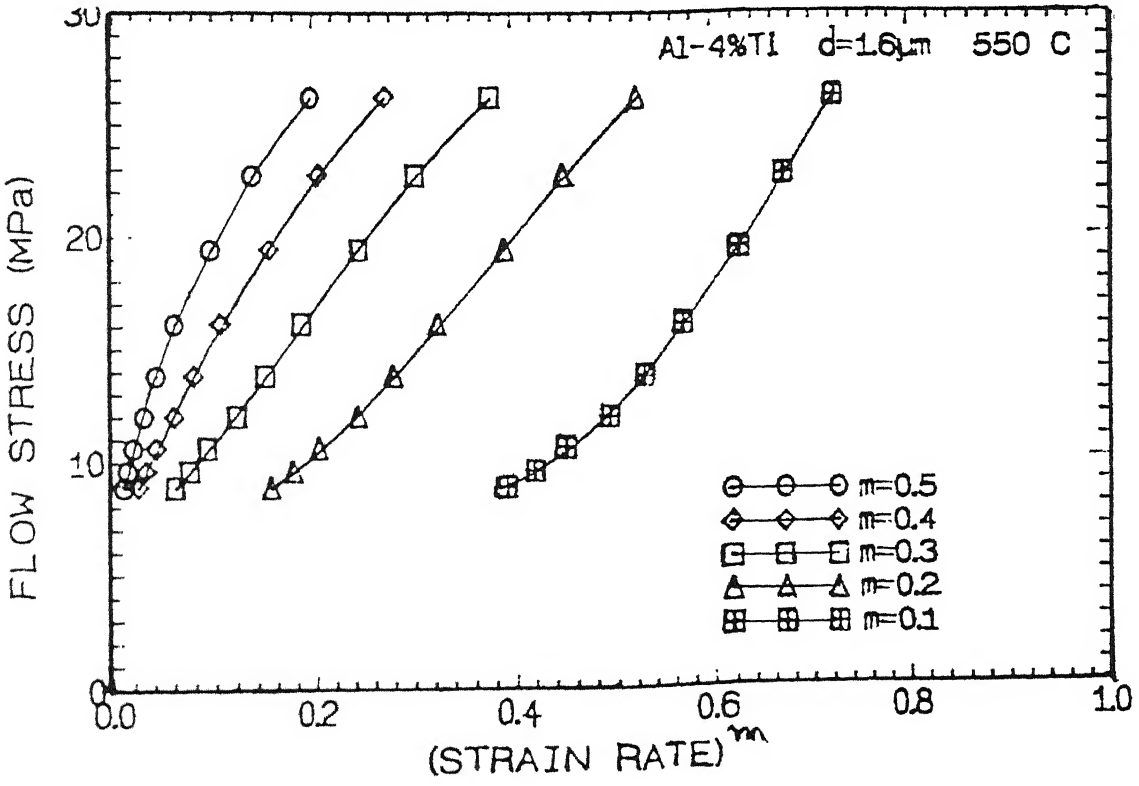

Fig. 5.2 : σ-$\dot{\varepsilon}^m$ behaviour of Al-4%Ti alloy with d=1.6μm at 550 °C

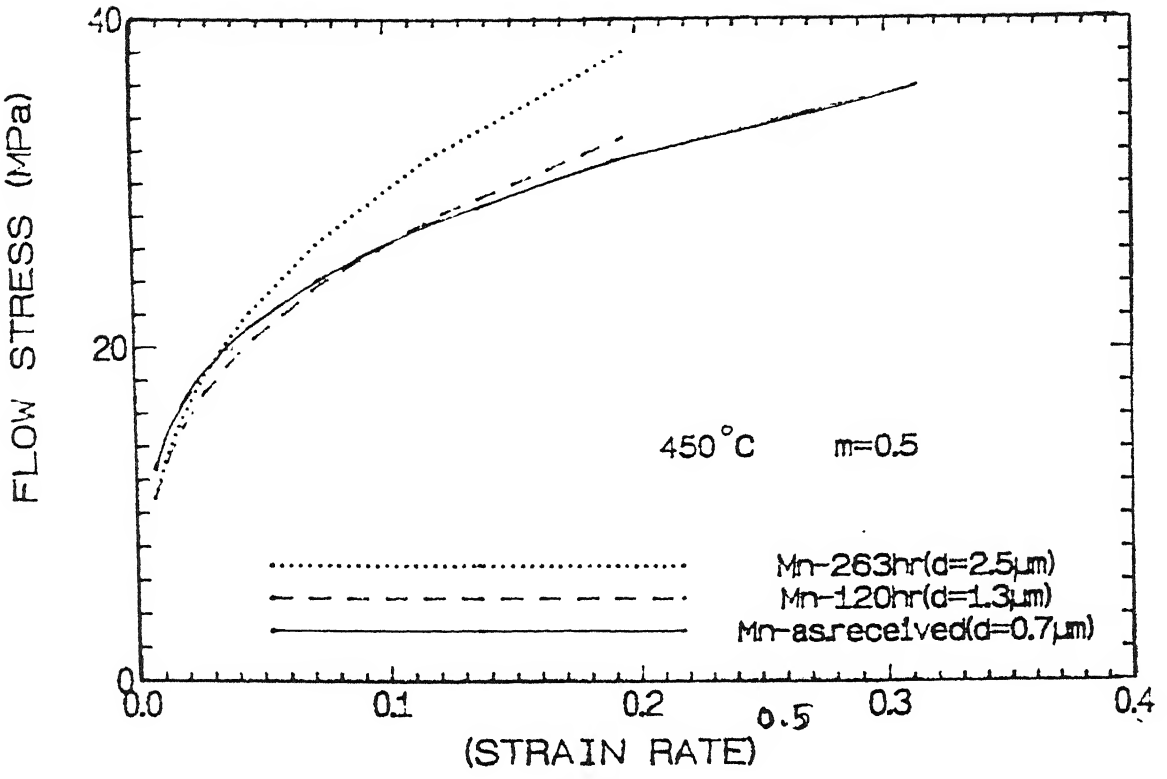

Fig. 5.3 : σ-$\dot{\varepsilon}^{0.5}$ behaviour of various Mn modified alloys at 450°C with m=0.5

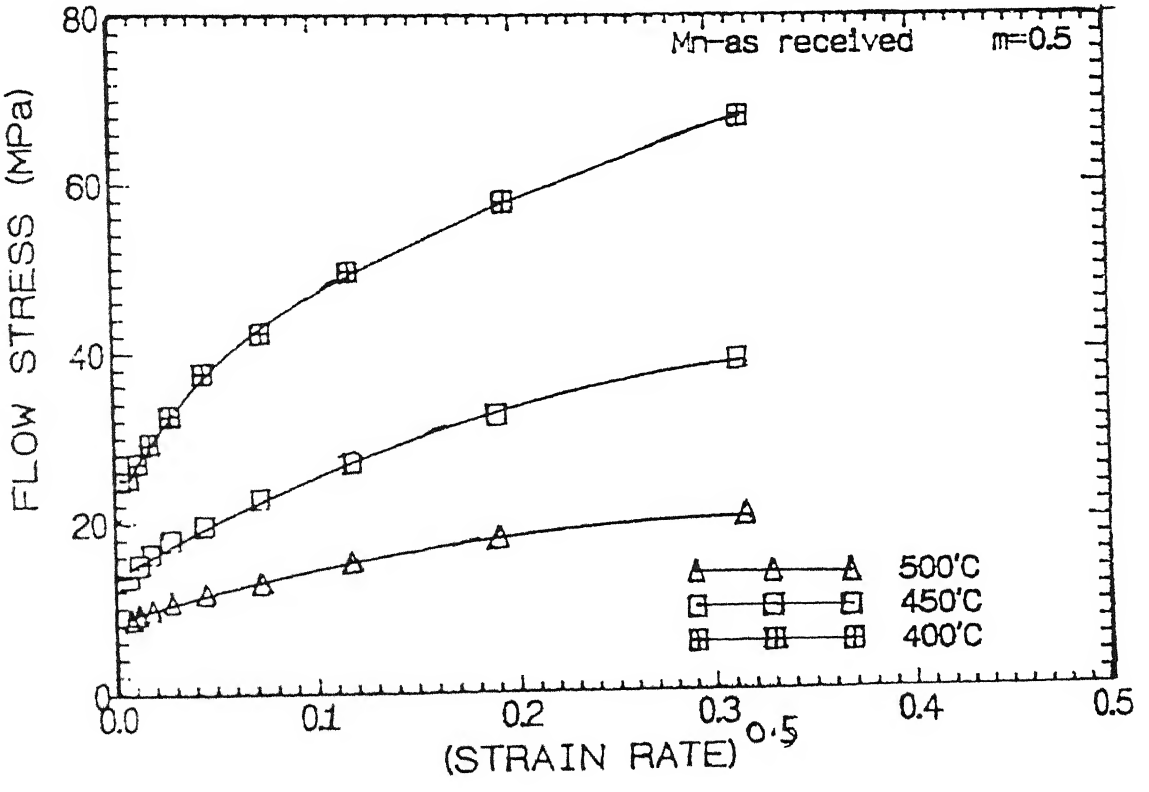

Fig. 5.4 : σ-$\dot{\varepsilon}^{0.5}$ behaviour of Mn-as received alloy (d=0.7μm) with m=0.50

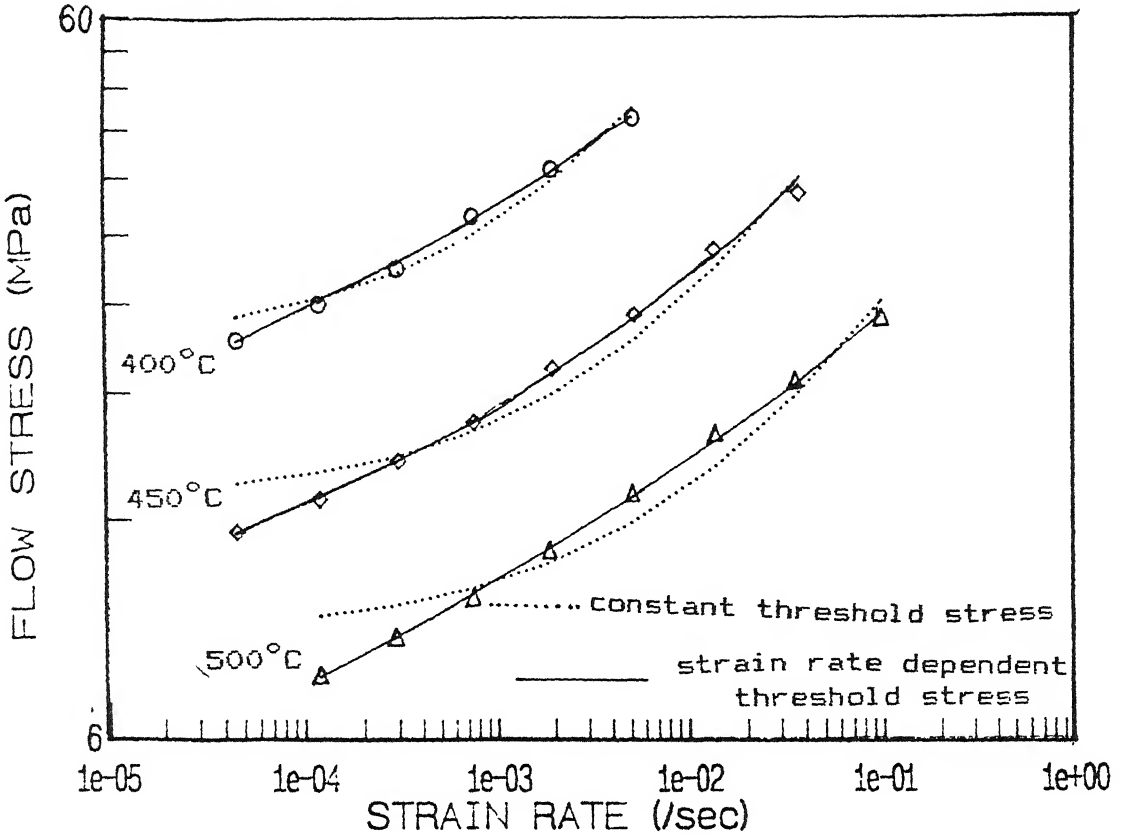

Fig. 5.7 : Comparison of constant threshold and strain rate dependent threshold stress concepts for Mn-120hr alloy with d=1.3 μm

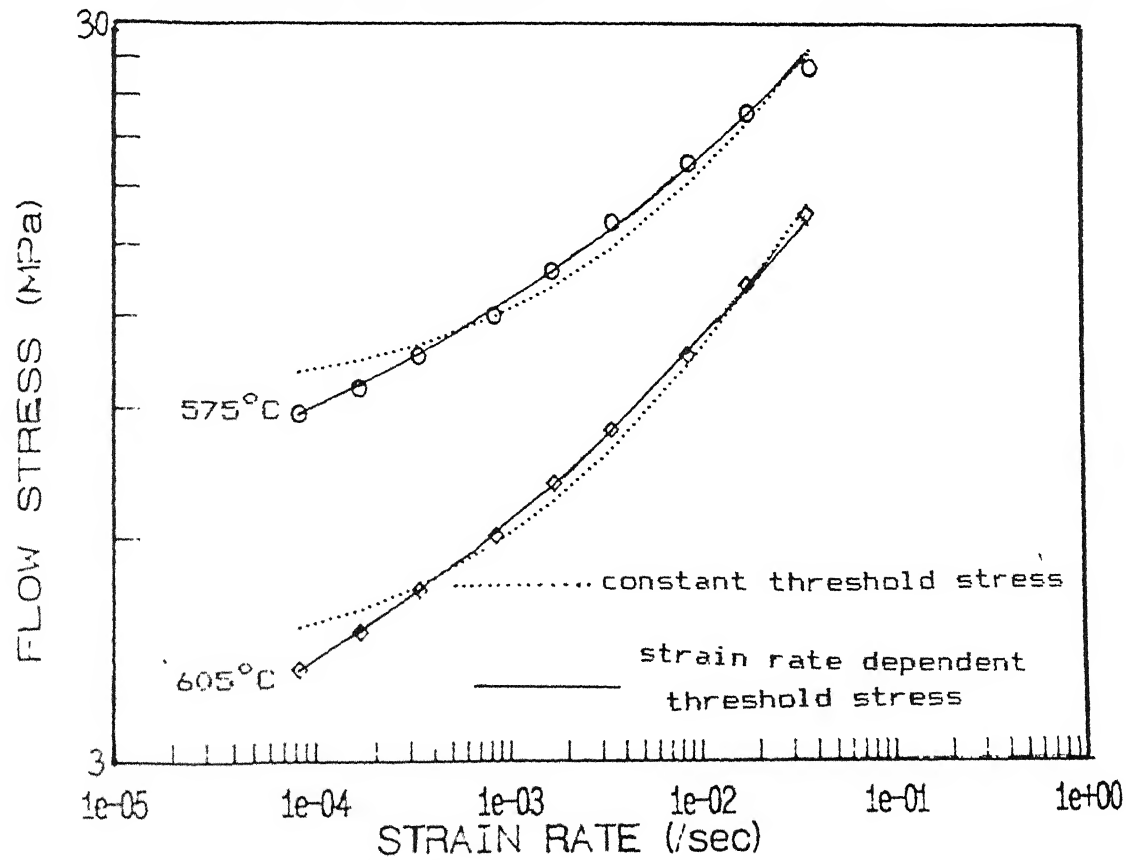

Fig. 5.8 : Comparison of constant threshold and strain rate dependent threshold stress concepts for Al-4%Ti alloy with d=1.6 μm

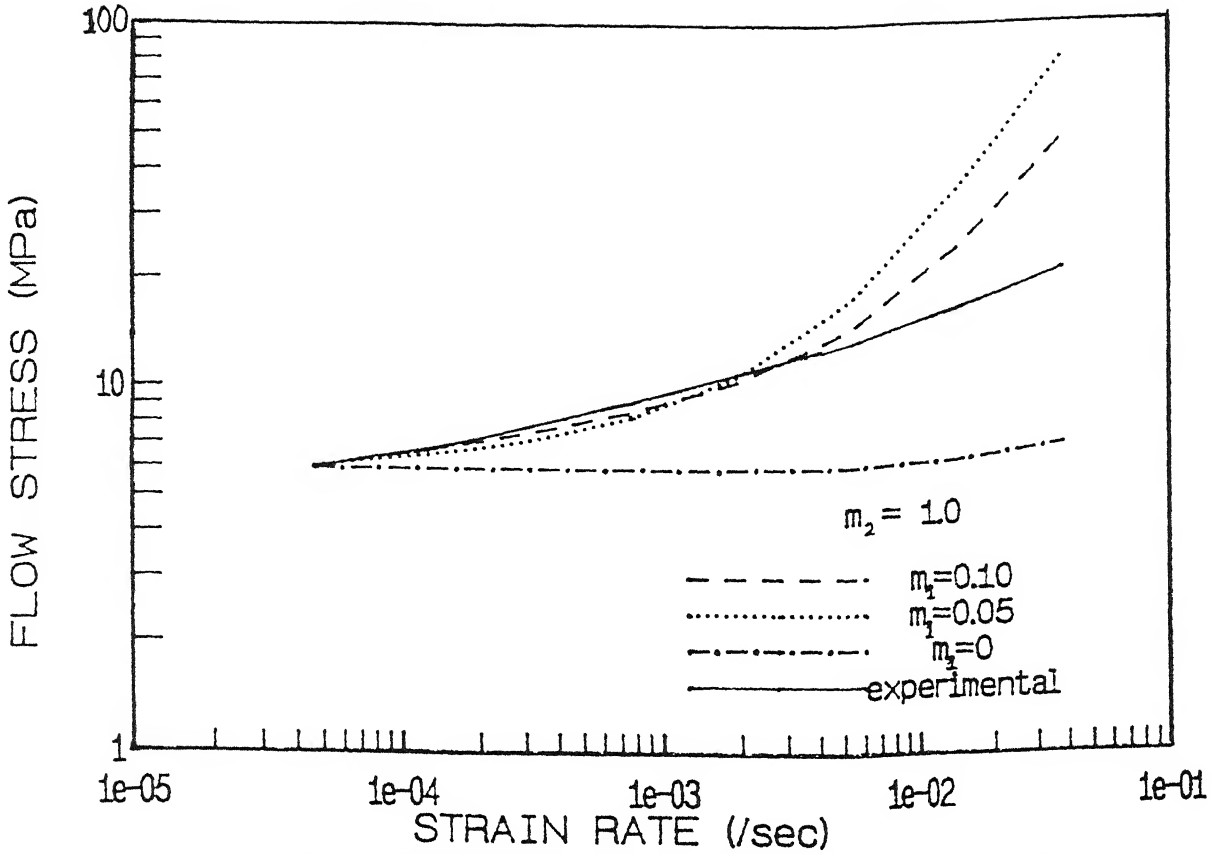

5.9 : Matching of a deformation mechanism having m_2=1.0 with the experiment ta shown with various assumed values of m_1 (material is Mn-263hr at 500°C)

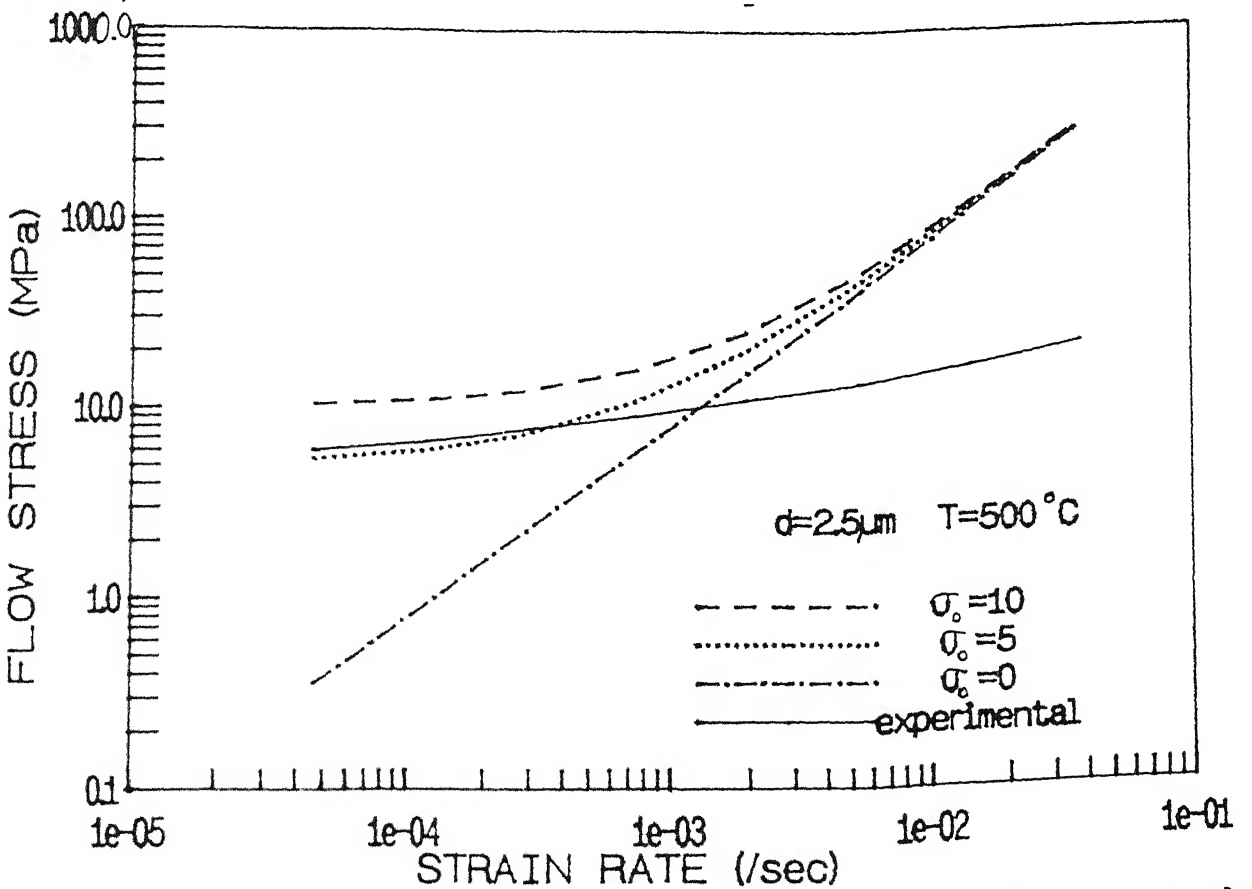

5.10: Comparison of threshold stress(MPa) incorporated Nabarro-Herring

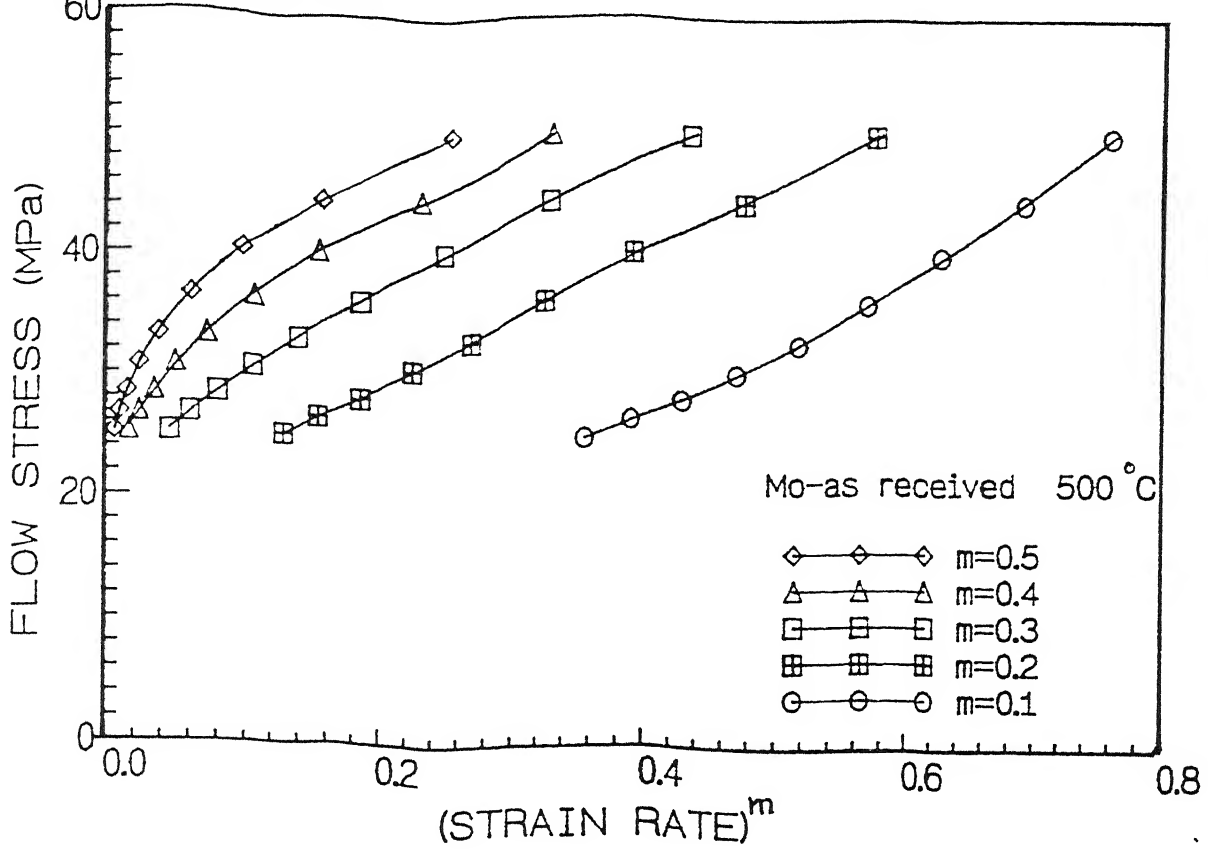

g. 5.11 : σ-$\dot{\varepsilon}^m$ behaviour of Mo modified alloy in as received condition at 500

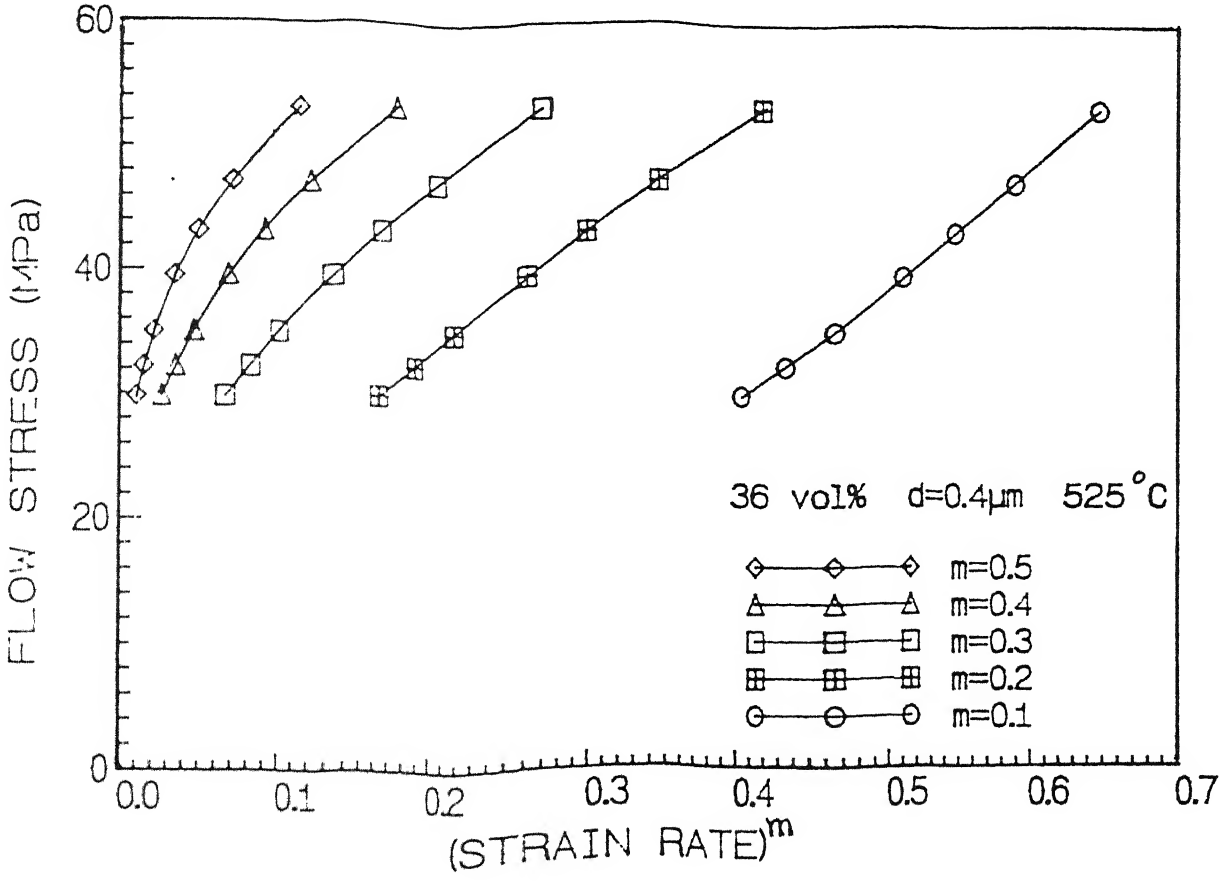

Fig. 5.12 : σ-$\dot{\varepsilon}^m$ behaviour of Al-Fe-V-Si alloy at 525 °C

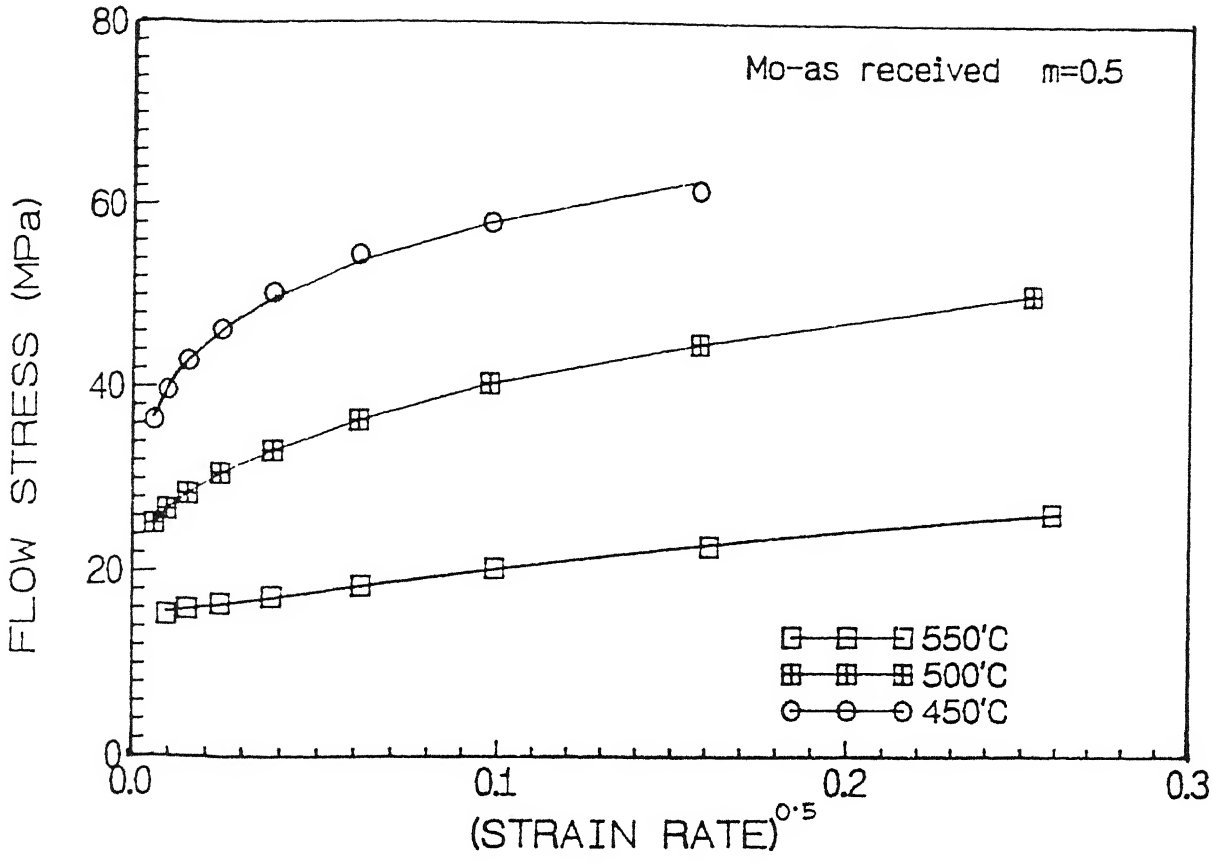

g.5.13 : σ-$\dot{\varepsilon}^{0.5}$ behaviour of Mo modified alloy in as received condition at 525

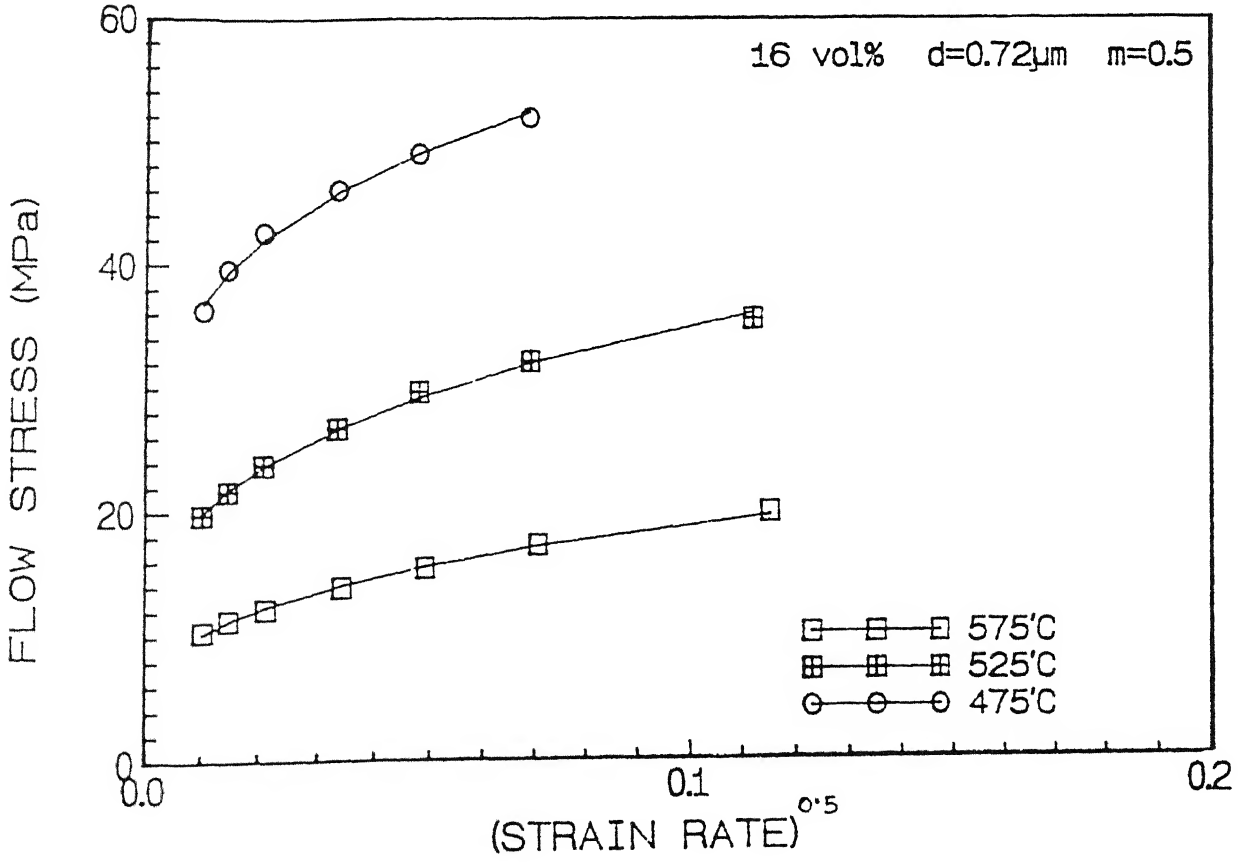

Fig 5.14 : σ-$\dot{\varepsilon}^{0.5}$ behaviour of Al-Fe-V-Si alloy

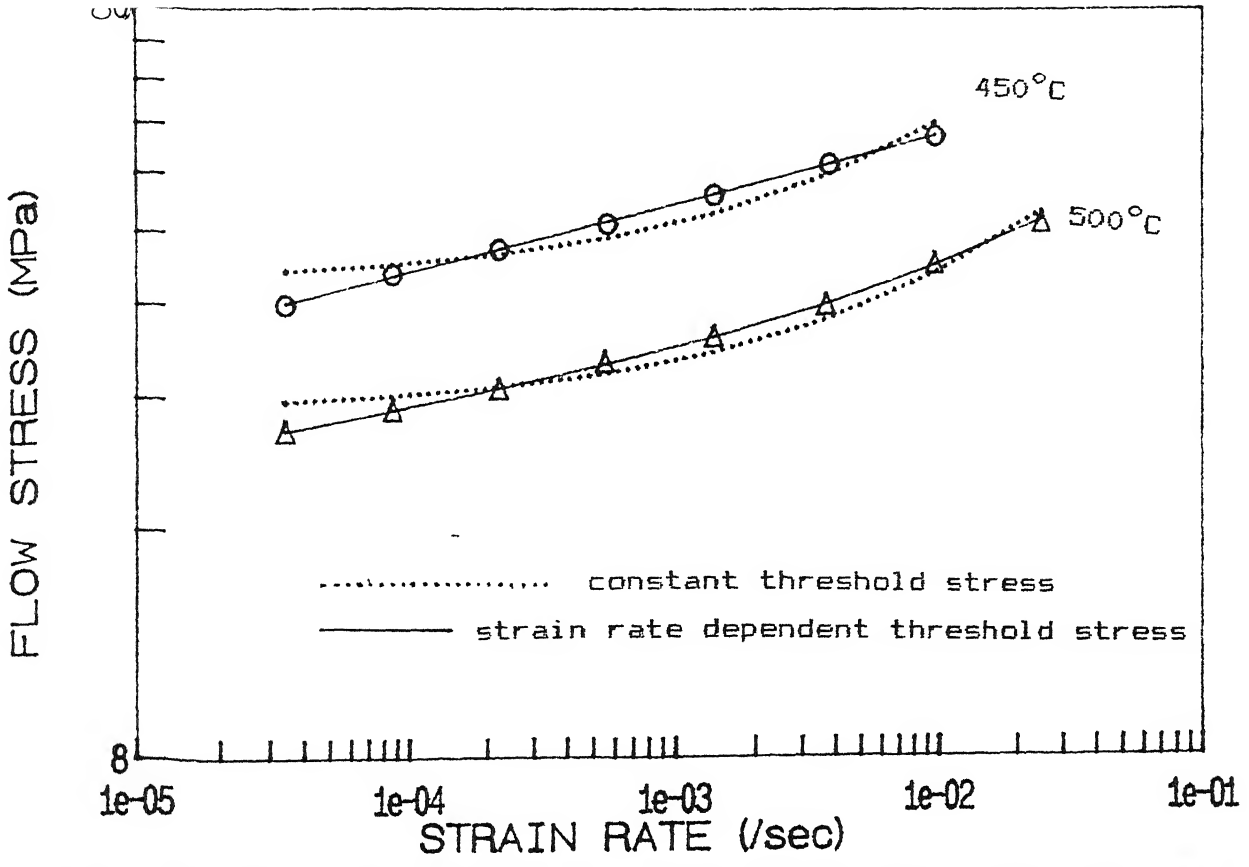

Fig. 5.15: Comparison of constant threshold stress and strain rate dependent threshold stress concepts with the experimental data for Mo-120hr sample

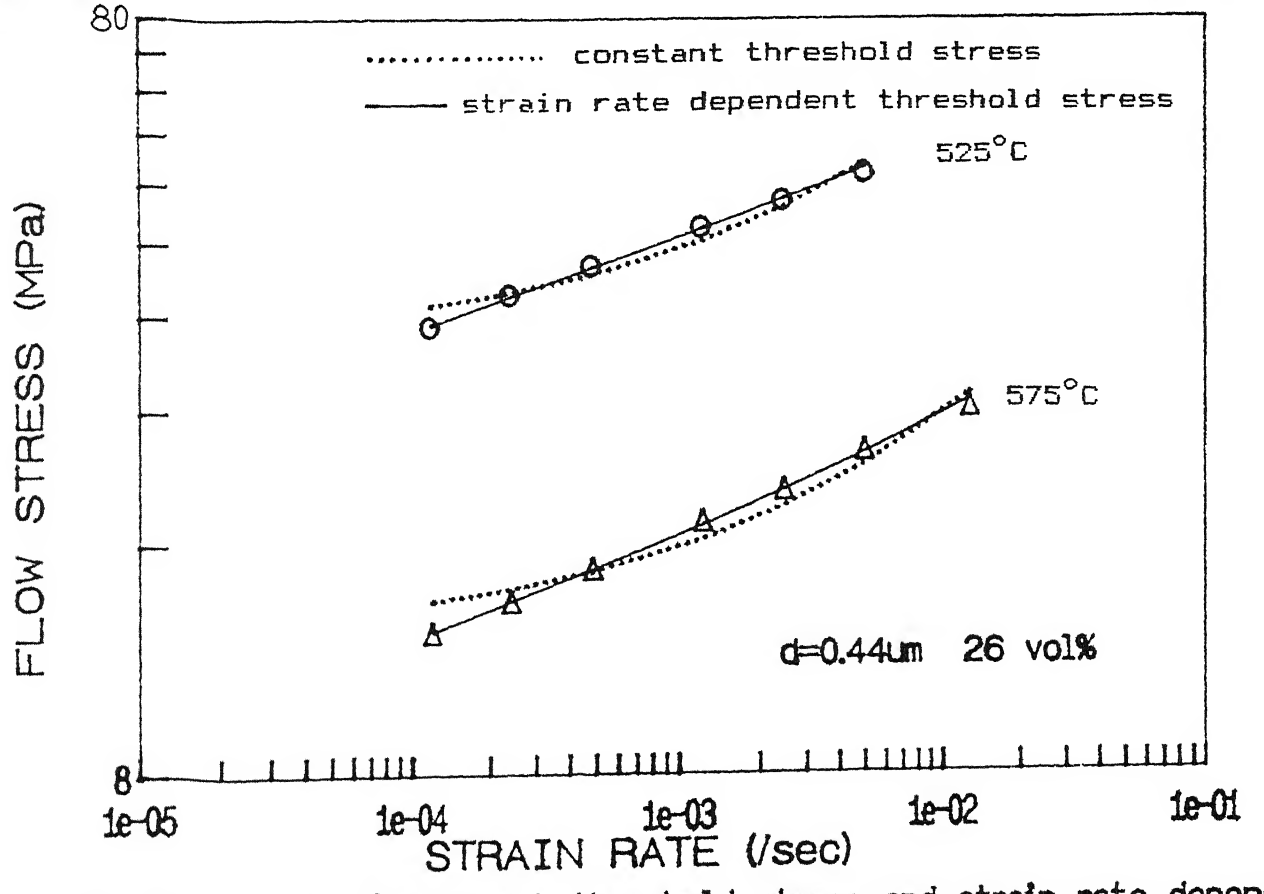

Fig. 5.16: Comparison of constant threshold stress and strain rate dependent

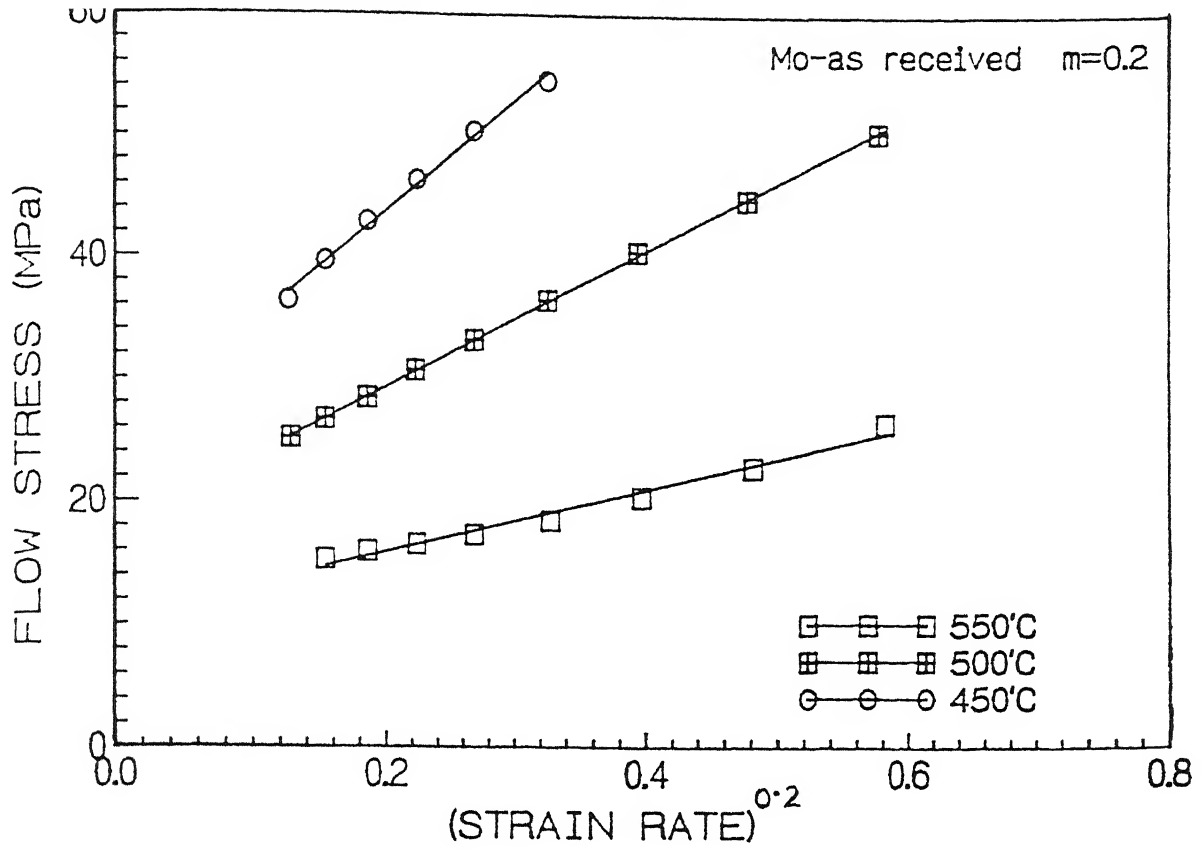

g.5.17 : σ-$\dot{\varepsilon}^{0.2}$ behaviour of Mo modified alloy in as received condition at 525

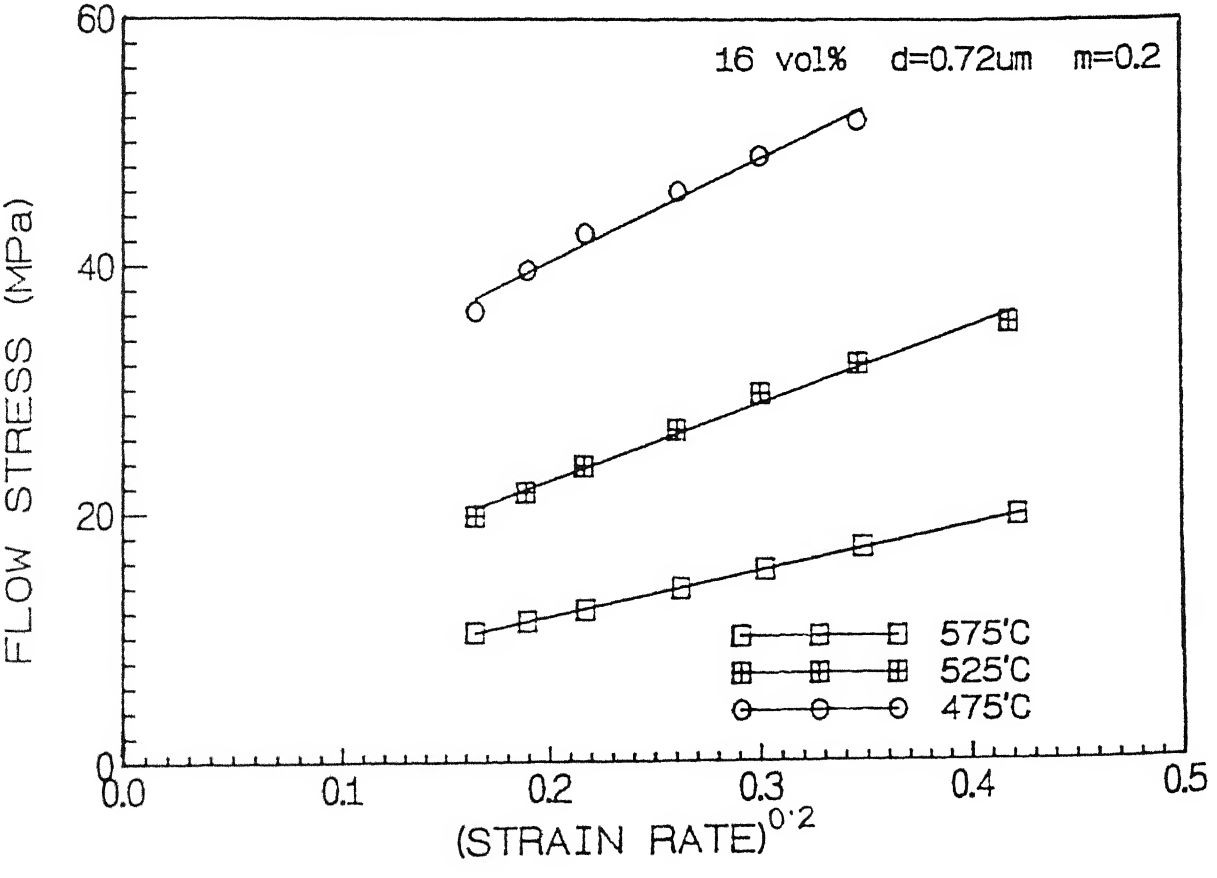

Fig.5.18 : σ-$\dot{\varepsilon}^{0.2}$ behaviour of Al-Fe-V-Si alloy

CHAPTER VI
SUMMARY AND CONCLUSIONS

1. Rapidly solidified P/M route processed Al alloys with fine grain size and intermetallic dispersoids exhibit distinctly two types of elevated temperature deformation behaviour (high and low rate sensitivity). Among the alloys considered, Mn modified Al-Zn-Mg-Cu and Al-4%Ti alloys are of the first category and Mo modified Al-Zn-Mg-Cu and Al-Fe-V-Si the second category. Differential strain rate tests were carried out in this investigation on two materials, viz., Mn modified and Mo modified Al-Zn-Mg-Cu alloys and the literature data were used for the other two alloys.

2. The flow mechanisms for their high temperature deformation were assessed by the process of evaluating the experimental constitutive equations and comparing them with those for the applicable mechanisms.

3. The stress-strain rate data (for a given temperature and grain size) of the first category of alloys conform to a constitutive equation with a mildly strain rate dependent threshold stress coupled with a term of higher strain rate sensitivity ($m = 0.5$). The characteristic m value for such a strain rate dependent threshold stress is 0.10 for both the alloys. The grain size exponent of the threshold process is ≈ 3, whereas that for the superplastic flow mechanism ($m = 0.5$) is ≈ -3.

4. The data of lower m materials were analyzed from two different viewpoints, viz., superplasticity and normal dislocation creep (with $m = 0.2$) both with

threshold stress.

(a) In the first type of analysis (with m=0.5),both constant threshold stress and strain rate dependent threshold stress concepts were checked. The characteristic m value of the threshold process for Mo modified Al-Zn-Mg-Cu is 0.05 and that for Al-Fe-V-Si is 0.11. The grain size exponent p is negative in both the cases. The negative value of p for the mechanism with m=0.5 is not consistent with the mechanism of superplastic flow in these materials.

(b) In the second type of analysis with m=0.2, the dislocation creep constitutive equation coupled with a threshold stress was used. While the grain size exponent p is negative for the threshold process for both the alloys, it is independent of grain size for Mo modified one and negative for Al-Fe-V-Si. The dislocation creep constitutive equation is applicable to the flow process for Mo modified Al-Zn-Mg-Cu but not so satisfactorily in the other case. The negative grain size exponent may be attributed to composite strengthening in the Al-Fe-V-Si alloy.

REFERENCES

1. N. Grant, "Rapid Solidification of Metallic particles ", AIME Conference procedings, High Strength Powder Metallurgy of Aluminium Alloys, ed. by M.J.Kockzak and G.J.Hildeman, Feb., 1982, P.3

2. C.G.Levi and R.Mehrabian, " Heat flow During Rapid Solidification of undercooled metal droplets ", Met Trans A.,Vol.13A, 1982, P.221

3. R.Mehrabian, "Rpid Solidification", International Metals Reviews, vol.27, no.4, 1982, P.185

4. J.E.Bird, A.K.Mukherjee and J.E.Dorn, "Quantitative relation between properties and microstructure", ed. D.G.Brandon and A.Rosen, Iseraeli Univ. pres, Jerusalem, 1969, P.255-341.

5. M.F.Ashby and R.A.Verrall, "Diffusion accommodated flow and superplasticity", Acta Met., vol.21, 1973, P.149

6. A.Ball and M.M.Hutchison, "Superplasticity in the Aluminium-Zinc euctoid", Metal Sc.J., vol.3, 1969, No.1

7. A.K.Mukherjee, "High Temperature Creep", Treatise on Material Sc. & Tech., vol.6, Academic press, N.Y., 1975, P.164

8. A.K.Mukherjee, "The rate controlling mechanicsm in superlasticity", Mat.Sc. & Engg., vol.8, 1971, P.83

9. E.Orowan, in Symposium on internal stress in metals and alloys, London, Institute of metals, 1948, P 451

10. J.W.Martin, "Micromechanism in particle hardened alloys", Cambridge Univ.Press, Cambridge, 1980

11. G.S.ANsell and J.Weertman, Trans. AIME, vol.215, 1959, P838

12. L.M.Brown and R.K.Ham, "Dislocation particle interactions", Strengthening methods in crystals, chapter 2, Ed. Kelly & Nicholson, Applied Sc. Pub. ,1971

13. R.Lagneborg, "Bypassing of dislocations past particles by climb mechanism", Scripta Met., vol. 7, No. 6, 1973, P 605

14 E.Arzt and M.F.Ashby, "Threshold stress in materials containing dispersoid particles", Scripta Met., vol 16, 1982, P 1285

15 V.K.Kockx, Philosophical Magazine, vol.13, 1966, P.541

16. E.Arzt and J.Schroder, "Weak beam studies of dislocation dispersoids interactions in ODS superalloys", Scripta Met., vol. 19, 1985, P. 1129

17. D.J.Strolovitz et al., "Diffusionally modified dislocation particle elastic interaction", Acta Met., vol. 32, No. 7, 1984, P.1079

18. E.Arzt and D.S.Wilkinson, "Threshold stress for dislocation climb over hard particles, the effect of an attractive interaction", Acta Met., vol.34, No.10, 1986, P.1893

19 J.Rosler and E.Arzt, "A new model based creep equation for dispersioned strengthened materials", Acta Met., vol.38, No.4, 1990, P.671

20. K.A.Hay and R.T.Pascoe, "Interdependent processes in high temperature deformation", J. of Mat. Sc., vol.9, 1974, P.1285

21. R.S.Misra and G.S.Murty, "Stress strain rate behavior of superplastic Zinc-Aluminium eutectoid alloy", J. Mat. Sc., vol.23, 1988, P.593

22. G.S.Murty and M.J.Koczak, "Investigation of region I of a superplastic Al-Zn-Mg-Cu-Mn alloy", Mat. Sc. & Engg., vol.96, 1987, P.117.

23. G.S.Murty and M.J.Koczak, "Superplastic behavior of an Al-4wt%Ti alloy processed by the powder metallargy route", Mat. Sc. & Engg., vol.100, 1988, P.37

24. G.S.Murty and M.J.Koczak, "Rate sensitivity in the high temperature deformation of dispersion strengthened Al-Fe-V-Si alloys", J. of Mat. Sc., vol.24, 1989, P.510

25. J.Wolfenstine, G.Gonzalez-Doncel and O.D.Sherby, "Deformation behavior under constant structure of creep resistance Al-Fe alloys", J. of Mat. Sc. Letters, vol.9, 1990, P.410

26. E.O.Hall, Proceedings of physics society of London, vol.643, 1951, P.747

27. N.J.Petch, London J. of Iron and Steel Indistry, vol.173, 1953, P25

APPENDIX A

```
c*************************************************************************
c       This is a program to analyse differential strain rate change test
c       data under compression from MTS machine to obtain  σ - ε̇
c       and  m - ε̇      data
c*************************************************************************
c       chv=time taken by cross head in sec for 10mm movement(as set in the
c         machine window)
c       load1=load taken in kg at the initial point of each cross head velocity
c       load2=load taken in kg at the final point of each cross head velocity
c
c       deformation (as measured by def(i)) =deformation of the sample im mm
c                                            upto the last point of each cross
c                                            head velocity level
c                                       #NOTE: deformation at each stage should
c                                              be measured from the initial
c                                              gage length
c
c       l=instantaneous gage length in mm
c       d-sig% =percent increase in stress for strain rate hardening
c       tsr=true strain rate
c       eps=true strain
c
c*************************   mts f   ***************************************
        implicit real*4(a-h,o-z)
        dimension v(25),def(0 26),s1(25),s2(25),gl(0 26),a(0:26)
     1  ,tsr(25),eps(25),sh(25),srs(25),sig1(25),sig2(25),tsrm(25)
        open(unit=20,file='mts out')
        write(6,10)
10      format(5x,'give initial gage length(mm),dia(mm) &
     1  no  of data points')
        read(*,*)gli,d,n
        write(20,20)gli,d,n-1
20      format(5x,'initial gage length=',f5 2,10x,
     1  'initial dia=',f5.2,10x,/,25x,'no.of data set=',i2,////)
        write(6,30)
30      format(5x,'give chv(sec/10mm),load1 & load2 in kg,
     1  deformation in mm')
            do 40 i=1,n
            read(*,*)v(i),s1(i),s2(i),def(i)
40          continue
        def(0)=0
        a(0)=3.14*d**2/4.
        gl(0)=0
        d1=3 14*d**2*gli/4.
            do 50 i=1,n-1
            gl(i)=gli-def(i)
            a(i)=d1/gl(i)
            tsr(i)=10/(v(i)*gl(i))
            tsrm(i)=20/((v(i)+v(i+1))*gl(i))
            eps(i)=(def(i)-def(i-1))*100./gl(i)
            sig1(i)=9.8*s1(i)/a(i-1)
            sig2(i)=9.8*s2(i)/a(i)
            dsig=sig2(i)-sig1(i)
            sh(i)=dsig*100./sig1(i)
            srs(i)=alog(s1(i+1)/s2(i))/alog(v(i)/v(i+1))
50          continue
        write(20,60)
60      format(2x,'CHV',6x,'LOAD1',5x,'LOAD2',3x,'L',5x,
     1  'EPS%',7x,'D-SIG%',4x,'TSR',3x,'STRESS',3x,'m')
        write(20,70)
70      format(1x,'sec/cm',5x,'kg',9x,'kg',4x,
     1  'mm',24x,'/sec',4x,'MPa',//)
            do 100 i=1,n-1
            write(20,80)v(i),s1(i),s2(i),gl(i),eps(i)
     1      ,sh(i),tsr(i),sig2(i),srs(i)
80          format(1x,e7 2,2x,f6.1,4x,f6 1,2x,f5.2,2x,e7.2,4x,
     1      f6.2,2x,e8.2,1x,f6 2,2x,f4.3)
100         continue
        stop
        end
```

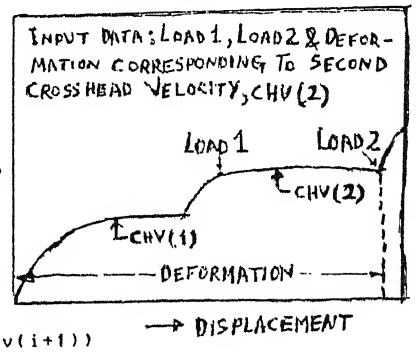

APPENDIX B

```
c*************************************************************************
c       This is a program to generate σ vs. ε̇^m  data for a series of values
c       of m, the corresponding threshold stress and correlation coefficient
c       for the constitutive equation  In the output, the first data-column
c       is ε̇^m  and the second is σ
c*************************  thm f  ***************************************
c       c=threshold stress (MPa)
c       K=slope
c       r=correlation coefficient
c*************************************************************************
        double precision x(20),xm(20),y(20),a,b,c,r,d,f
        double precision sumx,sumy,sumx2,sumy2,sumxy
        real k
        open(unit=20,file='thm out')
        write(6,10)
10      format('give initial & final values of m,increment of m,
     1  no  of data')
        read(*,*)p1,p2,p3,n
        write(6,30)
30      format('give strain rate & flow stress(MPa)')
              do 35 i=1,n
              read(*,*)x(i),y(i)
35            continue
        j=ifix((p2-p1)/p3+1 0)
        write(20,60)j
60      format(i2)
        do 150 l=1,j
           sumx=0.0
           sumx2=0.0
           sumy=0 0
           sumy2=0 0
           sumxy=0 0
                 do 100 i=1,n
                 xm(i)=x(i)**p1
                 sumx=sumx+xm(i)
                 sumx2=sumx2+xm(i)*xm(i)
                 sumy=sumy+y(i)
                 sumy2=sumy2+y(i)*y(i)
                 sumxy=sumxy+xm(i)*y(i)
100              continue
           a=n*sumxy-sumx*sumy
           b=n*sumx2-sumx*sumx
           d=n*sumy2-sumy*sumy
           f=sumy*sumx2-sumx*sumxy
           r=a/sqrt(b*d)
           c=f/b
           k=a/b
           write(20,110)l,n,p1,c,k,r
110        format(i2,/,i2,/,'m=',f3 2,',','c=',f5.1,',','K=',f6.1,
     1     ',','r=',f6.4)
                 do 200 i=1,n
                 write(20,120)xm(i),y(i)
120              format(e8 3,2x,f7.3)
200              continue
           p1=p1+p3
150        continue
        stop
        end
```

APPENDIX C

```
c*************************************************************************
c       This is a program to calculate the optimum value of m1 (from a series
c       of m1 values) for a given value of m2 and hence the optimum values of
c       K1 and K2 corresponding to those values of m1 and m2, all obeying the
c       constitutive equation                    σ = K1 ε̇^m1 + K2 ε̇^m2
c
c       This program also computes the correlation coefficient of
c     (σ/ε̇^m2) vs. ε̇^(m1 - m2)    plot for each value of m1 and gives,
c
c       for a given strain rate, the % difference between the experimental
c       value of stress and the stress calculated by the above constitutive
c       eqn. In the output, for each value of m1, the first data-column
c       is ε̇^(m2-m1) the second is (σ/ε̇^m2) and the third is the %difference
c
c*****************************  BT F  ************************************
      real m,k1,k2
      double precision x(20),xm(20),y(20),ym(20),ys(20),dif(20)
      double precision sumx,sumy,sumx2,sumy2,sumxy,a,b,c,d,r,f
      open(unit=20,file='bt out')
      write(6,25)
25    format('give fixed value of m2')
      read(*,*)m
      write(6,10)
10    format('give initial & final values of m1,increment of m1,
     1 and no. of data')
      read(*,*)p1,p2,p3,n
      write(6,30)
30    format('give strain rate & flow stress')
                do 35 i=1,n
                read(*,*)x(i),y(i)
35              continue
           do 55 i=1,n
           ym(i)=y(i)/(x(i)**m)
55         continue
      j=ifix((p2-p1)/p3+1.0)
      write(20,60)j
60    format(i3)
         do 150 k=1,j
         sumx=0.0
         sumx2=0.0
         sumxy=0.0
         sumy=0.0
         sumy2=0.0
              do 100 i=1,n
              xm(i)=x(i)**(p1-m)
              sumx=sumx+xm(i)
              sumx2=sumx2+xm(i)*xm(i)
              sumxy=sumxy+xm(i)*ym(i)
              sumy=sumy+ym(i)
              sumy2=sumy2+ym(i)*ym(i)
100           continue
         a=n*sumxy-sumx*sumy
         b=n*sumx2-sumx*sumx
         d=n*sumy2-sumy*sumy
         f=sumy*sumx2-sumx*sumxy
         r=a/sqrt(b*d)
         k2=f/b
         k1=a/b
         write(20,110)k,n,p1,r,k1,k2
110      format(i3,/,i2,/,'m1=',f4.3,',','r=',f6.4,
     1   ',','K1=',f7.3,',','k2=',f9.3)
              do 200 i=1,n
              ys(i)=k1*x(i)**p1+k2*x(i)**m
              dif(i)=(y(i)-ys(i))*100.0/y(i)
              write(20,120)xm(i),ym(i),dif(i)
120           format(e8.3,2x,f8.3,4x,f8.4,'%')
200           continue
         p1=p1+p3
150      continue
      stop
      end
```